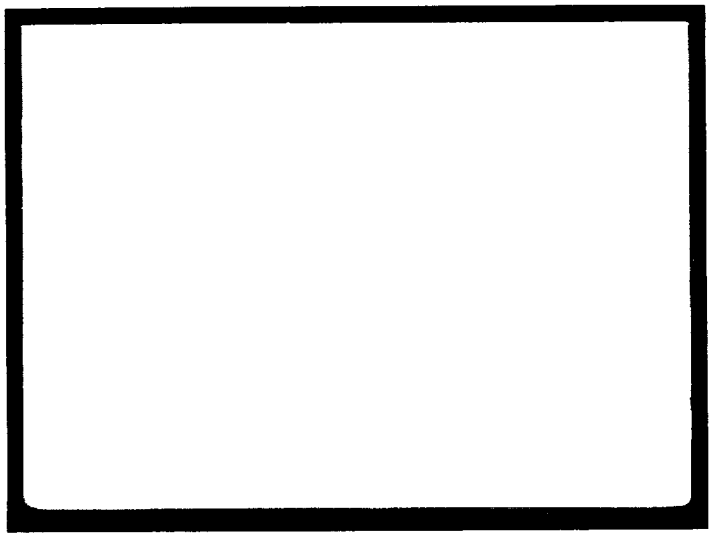

GPO PRICE $ _____

CFSTI PRICE(S) $ _____

Hard copy (HC) 3.00

Microfiche (MF) 1.00

ff 653 July 65

FACILITY FORM 602

N66 32555
(ACCESSION NUMBER)

12
(PAGES)

CR-76800
(NASA CR OR TMX OR AD NUMBER)

(THRU)

1

(CATEGORY)

RESEARCH INC.

SANTA BARBARA, CALIFORNIA

Report 65-9566-7

Final Summary Report

for

AEROBEE 150A
ROLL LOCK-IN STUDY

November 1965

Contract No. NAS 5-9566

Prepared by

James E. Brunk

ALPHA RESEARCH, INC.
1266 Coast Village Road
Santa Barbara, California

for

NASA Goddard Space Flight Center
Greenbelt, Maryland

Copy 17

FOREWARD

This report was prepared under NASA contract NAS 5-9566, by Alpha Research, Inc. The contract was monitored by Mr. J. T. Lawrence, Sounding Rocket Branch, Goddard Space Flight Center.

The principal investigator for this contract was Mr. James E. Brunk. The effort was carried out from April 1965 through November 1965.

ABSTRACT

The near-resonant motion of the Aerobee 150A, a four-finned sounding rocket vehicle with liquid-propellant sustainer and solid-propellant booster, is investigated. Pitch-roll coupling and roll lock-in are shown to be greatly influenced by induced rolling moments resulting from both aerodynamic sources and lateral configurational asymmetry. The near-resonant motion is further complicated by the presence of an aerodynamic side moment, which can be considered as a Magnus-type moment dependent upon the aerodynamic roll angle.

The various mechanisms which can produce roll lock-in or extended resonance are discussed, and the probable effect of these motions on the roll rate and angle of attack are described. It is shown that both the orientation and magnitude of the various asymmetries are important in determining the possibility of lock-in or extended resonance.

In most instances the near-resonant motion can be simulated by the linear solution for the trim angle of attack vector, in conjunction with an exact analysis of the rolling moments. Using p/ω as a dependent variable, the trim angle of attack and roll equations can be combined into a single first-order non-linear differential equation with time-varying coefficients. The solution to this equation has been obtained numerically using only a desk-type calculator, and some typical results are presented.

The effects of aerodynamic and inertial non-linearities on the pitch-yaw-roll motion are studied by use of a special circular motion theory. It is shown that when the amplification factor derived from the linear equations

of motion becomes infinite, a condition which can result from a positive side moment, there correspond steady-state circular motion solutions at angles of attack on the order of 20 degrees. A lateral displacement of the center of gravity and center of pressure of about 0.1 inch will provide roll equilibrium during a large angle of attack steady-state circular motion.

TABLE OF CONTENTS

		Page
Foreward		ii
Abstract		iii
Nomenclature		ix
I.	INTRODUCTION	1
II.	VEHICLE CHARACTERISTICS	7
III.	GENERAL DISCUSSION OF THE ROLL LOCK-IN PROBLEM	10
IV.	QUASI-STEADY ANALYSIS OF THE NEAR-RESONANT MOTION OF SOUNDING ROCKET VEHICLES	17
V.	APPLICATION OF CIRCULAR MOTION THEORY	21
VI.	CONCLUSIONS AND RECOMMENDATIONS	26
References		29
Appendix A	Vehicle Physical Characteristics and Nominal Trajectory Data	31
Appendix B	Aerodynamic Data for Aerobee 150A	33
Appendix C	Linear Solution for the Trim Angle of Attack	35
Appendix D	Rolling Moments Due to Lateral Asymmetry	43
Appendix E	Derivation of an Equation for p/ω	45
Appendix F	Circular Motion Theory	48

LIST OF FIGURES

Figure	
1	Trim Amplification Factor and Phase Angle
2	Aerobee 150A Configuration
3	Comparison of Induced Rolling Moments for Several Sounding Rocket Vehicles
4	Comparison of Aerodynamic Side Force Characteristics for Two Sounding Rocket Vehicles
5	Roll, Pitch, and Side Moment Characteristics of the Aerobee 150A at Nominal Resonance Conditions
6	Relation Between Aerodynamic Induced Rolling Moment and Trim Orientation
7	Relation Between Aerodynamic Induced Rolling Moment and Rolling Moment Due to Lateral Asymmetry
8	Numerical Evaluation of $C_{\ell_\alpha} + C_{\ell_{\delta\bar{\delta}}}$ as a Function of p/ω for Four Lateral Asymmetry Conditions
9	Ratio of Side Moment Coefficient to Pitching Moment Coefficient, $C_{SM_\alpha} / C_{M_\alpha}$, for Infinite Amplification Factor
10	Variation of Side Moment Coefficient With Aerodynamic Roll Angle
11	Non-Rolling Trim Orientations for Positive Side Moment at Resonance as a Function of Lateral Asymmetry Orientation
12	Variation of the Nominal Spin Rate Parameter, p_T/ω, With Time
13	Variation of the Coefficients of p/ω and $\dot{(p/\omega)}$ With Time

Figure

14	Variation of the Pitching Moment Derivative, Normal Force Derivative, and Damping Parameter With Time
15	Numerical Solution for p/ω as a Function of Time
16	Effect of a Side Moment on the C_{m_o} Required for Trim
17	Required Lateral Asymmetry for a Steady-State Circular Motion
18	Aerobee 150A-B_2 - Weight Versus Time
19	Aerobee 150A-B_2 - Center of Gravity and Moments of Inertia Versus Time
20	Aerobee 150A-B_2 - Velocity and Dynamic Pressure Time Histories
21	Aerobee 150A-B_2 - Altitude and Mach Number Time Histories
22	Aerobee 150A - Nominal Spin History
23	Aerobee 150A - Rolling Moment Derivatives C_{ℓ_δ} and C_{ℓ_p} Versus Mach Number
24	Aerobee 150A - Drag Coefficient Versus Mach Number
25	Aerobee 150A-B_2 - C_N vs $\vec{\alpha}$, Mach Number 2.53
26	Aerobee 150A-B_2 - C_N vs $\vec{\alpha}$, Mach Number 3.50
27	Aerobee 150A-B_2 - C_N vs $\vec{\alpha}$, Mach Number 4.85
28	Aerobee 150A-B_2 - C_N vs $\vec{\alpha}$, Mach Number 6.80
29	Aerobee 150A-B_2 - C_m vs $\vec{\alpha}$, Mach Number 2.53
30	Aerobee 150A-B_2 - C_m vs $\vec{\alpha}$, Mach Number 3.50
31	Aerobee 150A-B_2 - C_m vs $\vec{\alpha}$, Mach Number 4.85
32	Aerobee 150A-B_2 - C_m vs $\vec{\alpha}$, Mach Number 6.80

Figure

33 Aerobee 150A-B_2 $C_{y'}$ vs $\vec{\alpha}$

34 Aerobee 150A-B_2 $C_{n'}$ vs $\vec{\alpha}$

35 Aerobee 150A-B_2 - Normal Force Center of Pressure

36 Aerobee 150A-B_2 - Side Force Center of Pressure

37 Aerobee 150A-B_2 - Stability Margin Versus Mach Number

38 Aerobee 150A-B_2 - Normal Force Derivative Versus Mach Number

39 Aerobee 150A-B_2 - Pitch Damping Derivative Versus Mach Number

40 Body Axes Showing Direction and Sense of Forces and Moments

41 Nomenclature for Rolling Moments Due to Lateral Asymmetry

42 Inertial and Fixed-Plane Axes

43 Coordinate Axes With Respect to the Velocity Vector

44 Nomenclature for Finned Rocket in Circular Motion

45 Circular Motion Solutions for Nominal Resonance Conditions

NOMENCLATURE

a	=	thrust lateral misalignment
C_D	=	drag coefficient
C_{ℓ_δ}	=	rolling moment coefficient due to fin cant
C_{ℓ_p}	=	$\partial C_\ell \Big/ \partial \frac{pd}{2V}$, roll damping derivative
C_{ℓ_i}	=	aerodynamic induced rolling moment coefficient
$C_{\ell_{\Delta\bar{g}}}$	=	rolling moment coefficient due to lateral asymmetry
C_{ℓ_a}	=	rolling moment coefficient due to thrust asymmetry
$C_{n'}$	=	yawing moment coefficient for plane normal to angle of attack plane
C_{n_o}	=	body-fixed yawing moment due to asymmetry
$C_{n_{\pi/2}}$	=	fixed-plane non-spin-dependent yawing moment at $\vec{\alpha} = \pi/2$
$C_{n_{p_{\pi/2}}}$	=	fixed-plane Magnus moment at $\vec{\alpha} = \pi/2$
$C_{n_{\dot{\alpha}}}$	=	fixed-plane circular motion damping derivative
C_N	=	normal force coefficient
C_{N_α}	=	normal force derivative
C_m	=	pitching moment coefficient (angle of attack plane)
C_{m_o}	=	body-fixed pitching moment coefficient due to asymmetry
$C_{m_{\pi/2}}$	=	fixed-plane pitching moment coefficient at $\vec{\alpha} = \pi/2$
C_{M_α}	=	aeroballistic pitching moment derivative

C_{m_f}	=	$\partial C_m / \partial \frac{qd}{2V}$, fixed-plane pitch damping derivative
C_{M_q}	=	$\partial C_m / \partial \frac{qd}{V}$, pitch damping derivative, linear theory
C_{SM_α}	=	side moment coefficient
$C_{y'}$	=	side force coefficient for plane normal to angle of attack plane
C_{y_0}, C_{y_p}	=	body-fixed lateral force coefficients due to asymmetry
d	=	body diameter
H	=	damping parameter (see Appendix C)
i	=	$\sqrt{-1}$
I	=	transverse moment of inertia
I_x	=	axial moment of inertia
I'	=	$I / \rho s d^3$
I_x'	=	$I_x / \rho s d^3$
K_3	=	magnitude of trim vector
ℓ	=	aerodynamic reference length (1.25 feet, full scale)
m	=	vehicle mass
M	=	aerodynamic overturning moment parameter (see Appendix C)
M_s	=	aerodynamic side moment parameter (see Appendix C)
p	=	axial spin or roll rate
p_T	=	theoretical roll rate
P	=	$(p\ell/V)(I_x/I)$
q	=	dynamic pressure

q	=	angular velocity with respect to y' fixed-plane axis
r	=	angular velocity with respect to z' fixed-plane axis
s	=	dimensionless distance
S	=	aerodynamic reference area (1.23 square feet, full scale)
t	=	time
T	=	Magnus moment parameter (see Appendix C)
V	=	total velocity
v	=	lateral velocity in direction of body-fixed y axis
w	=	lateral velocity in direction of body-fixed z axis
x, y, z	=	body-fixed axes
x, y', z'	=	fixed-plane axes
X, Y, Z	=	inertial reference axes
$\Delta \bar{y}$	=	lateral displacement of center of gravity and center of pressure
$\vec{\alpha}$	=	total angle of attack
α^*	=	angle of attack at which C_{ℓ_α} reverses sign
β	=	angle of sideslip
δ	=	angle between trim vector and φ_{CP}
δ	=	fin cant angle
ϵ	=	thrust misalignment
ξ	=	$\frac{V + iw}{V}$, complex angle of attack
η	=	angular orientation of thrust misalignment

θ	=	Euler angle defining fixed-plane axes
ψ	=	Euler angle defining fixed-plane axes
φ	=	roll orientation angle for body-fixed trim
Φ	=	aerodynamic roll angle
ρ	=	air density
ω	=	undamped linear pitch natural frequency

subscripts

o	=	steady-state

superscripts

$\dot{}$	denotes differentiation with respect to time
$\wedge$	denotes non-dimensional angular velocity

I. INTRODUCTION

A continuing problem in the design of unguided canted-fin sounding-rocket vehicles is the avoidance of undesirable motions as the result of the vehicle approaching or passing through pitch-roll resonance. The problem is made more severe by the fact that the pitch and roll frequencies usually become coincident during a portion of the flight where the aerodynamic forces and moments can be large.

Sounding Rocket Motion At and Near Resonance

The angle of attack motion of a sounding rocket at resonance is virtually independent of the disturbances at launch and low altitudes, and can be represented in most cases by a linear solution for the magnitude of the trim angle of attack. It is also a matter of record that the spin rate of a canted fin sounding rocket approaches equilibrium at altitudes below the altitude range where resonance is likely to occur. Thus, the symmetric rocket has a spin history through resonance which depends only upon time-wise variations in the roll-driving and roll-damping moments, and aerodynamic lag effect[1].

The slightly unsymmetrical rocket experiences a wide variety of resonance phenomena depending upon the type of asymmetry present, and its magnitude and orientation. These asymmetries manifest themselves in two ways; first through initiating a trim angle of attack, and secondly by introducing non-linear aerodynamic effects and couplings.

The amplification of the trim angle of attack at resonance, irrespective of changes in the rolling motion, has received considerable attention. Whitlock, Reference 2, has compared steady-state and six-degrees-of-freedom analyses of pitch-roll resonance for a long slender sounding rocket for the case of unperturbed steady-state roll. For this case, it is shown that the steady-state linear theory reasonably predicts the resonant motion.

Effect of Aerodynamic Induced Rolling Moment

The motion of a rolling finned rocket in trimmed flight becomes more complicated when rolling, pitching, and yawing moments dependent upon angle of attack and roll orientation are introduced. The existence and effects of such moments were first described by Nicolaides[3]. Such moments have a periodic variation with the aerodynamic roll angle, ϕ, defined as the angle between the angle of attack plane and a fixed plane on the rocket, such as one containing a fin. A rotationally symmetric rocket with n similar fins has a symmetry angle of $2\pi/n$, and therefore the moments can usually be expressed as a Fourier sine series

$$\sum_{k=1}^{\infty} \sin n k \phi$$

With the introduction of aerodynamic induced roll moment, the complexity of the resonant motion greatly increases. We must now consider the orientation of the trim angle of attack as well as its magnitude. Strong interactions exist between the rolling motion and the near-circular angle-of-attack motion associated with trimmed flight. As a consequence, the phenomenon described by Nicolaides as lock-in is likely to occur when the angle of attack plane is slowly rotating through a region of negative induced rolling moment.

These regions cannot be avoided, since the phase shift in the angle-of-attack plane between $p = 0$ and $p = \omega$ is greater than the symmetry angle if the rocket has three or more fins.

Roll Lock-In

A discussion of lock-in is hampered by the lack of a general definition. The original analyses of Nicolaides[3] and also Murphy[4] consider the case of pure circular motion, where the roll rate and nutation rate are coincident. In this case, a stable variation of induced rolling moment ($C_{\ell_p}\left(\frac{\partial C_{\ell_\alpha}}{\partial \phi}\right) > 0$ at $\phi_{\alpha_{K-IN}}$) results in a lock-in between the roll and nutation motions and a pure lunar* motion.

In the case of the sounding rocket, the nutation vector is absent and the circular motion rate of the rocket in trimmed flight is just the spin rate. The angular orientation of the angle of attack plane is given by the phase angle for the angle of attack vector. In the absence of induced rolling moments, the phase angle will vary as illustrated in Figure 1, with an approximate 90-degree shift occurring at resonance.

For the sounding rocket, two interpretations of lock-in are possible. On the one hand, we can say that lock-in corresponds to lunar motion. This can be made a precise definition by requiring that the aerodynamic roll angle, ϕ, at some point approach a constant value in a stable manner. Note that resonance conditions are not required by this definition.

A second and less precise lock-in definition implies that the roll and pitch natural frequencies will be approximately equal for some period of time. The distinction between the pitch natural frequency, used here, and the nutation

---

* So described because the same side of the vehicle always faces the velocity vector.

frequency used in the original Nicolaides definition is important. The basis for the second lock-in definition for sounding rocket vehicles is the observation that for resonant conditions a negative induced rolling moment can extend the resonant period in such a manner that the spin rate and pitch natural frequency are approximately equal or appear to be locked-in. This type of lock-in can be better described as extended resonance. This apparent lock-in results from the shape of the curve of the phase angle versus the spin-to-natural-frequency ratio, and can be explained by the fact that if the phase angle is maintained near 90 degrees, the ratio p/ω will remain near unity. This occurrence is likely when the rocket encounters a large negative gradient in the variation of the total rolling moment with aerodynamic roll angle at or near resonance. It is important to note that while extended resonance results in a slowly changing aerodynamic roll angle, it does not imply a constant aerodynamic roll angle as in the first definition.

Neither lock-in definition indicates the gross effect to the roll or angle of attack motion. This must be determined for each individual case. But more important, extended lock-in may either increase or decrease the angle of attack and aerodynamic loads which would have been encountered without lock-in. In addition, lock-in may significantly reduce the spin rate at very high altitudes, even though the angle of attack motion is acceptable.

Other Factors Affecting Lock-In

The problems of lock-in and extended resonance are made even less tractable by changing air density and velocity, and variations in the aerodynamic coefficients with Mach number during the resonant period.

The greatest complication to the determination of sounding rocket lock-in behavior arises from the existence of two or more periodic rolling

moments, which need not be in phase. Such a complication immediately arises when there is a lateral offset between the center of gravity and center of pressure. This asymmetry induces an angle-of-attack dependent rolling moment with a roll period of 2π, and a phase angle dependent upon the angular orientation of the asymmetry. With the presence of both the aerodynamic induced rolling moment and the rolling moment due to lateral asymmetry, lock-in can occur at any aerodynamic roll angle.

The phase relationship between the aerodynamic induced roll and the roll due to lateral asymmetry is extremely important. First, the phase relationship can affect the magnitude of the rolling moments at lock-in, thus either prolonging or shortening the period of lock-in. Second, depending upon the aerodynamic roll angle at lock-in, the aerodynamic side moment* can be either positive or negative. This is extremely significant. The side moment modifies the aerodynamic damping, which in turn determines the magnitude of the trim amplification factor. At resonance the magnitude of the amplification factor is limited only by the amount of aerodynamic damping; hence, it is possible for the trim to increase catastrophically if the side moment is positive and decreases the aerodynamic damping to near zero. On the other hand, lock-in in a region of negative side moment may decrease the trim angle of attack.

Scope of Present Investigation

The present roll lock-in investigation has been accomplished for the purpose of obtaining a better overall understanding of the near resonance motion of sounding rocket vehicles, and the Aerobee 150A in particular. This

---

* The side moment is the non-spin-dependent Magnus moment resulting from aerodynamic roll and angle of attack.

has been achieved by both a qualitative review of the roll lock-in problem, and by development of simplified equations of motion.

Although the present effort is preceeded by analyses of the Aerobee 150, Aerobee 150A, and Aerobee 350, References 5 through 9, the foregoing have lacked generality in that References 5, 6, and 9 do not consider the rolling moment due to lateral center of gravity - center of pressure asymmetry, and References 7 and 8 do not include the effect of the aerodynamic side moment. Both of these factors have a pronounced effect on the resonant motion.

The basic approach used herein is to combine the linear solution for the trim angle of attack with the exact non-linear roll equation. Such an approach permits the various possibilities for lock-in and extended resonance to be examined both qualitatively and quantitatively.

Finally, large angle of attack resonant motions are examined by use of a special circular motion theory, which is capable of including non-linear pitch-yaw dynamics.

II. VEHICLE CHARACTERISTICS

The Aerobee 150A

The Aerobee 150A is a four-finned two-stage unguided sounding rocket vehicle currently being launched by the National Aeronautics and Space Administration. The sustainer is an Aerobee 4,100-pound sea-level liquid-propellant thrust engine, and the booster is an Aerojet 2.5 KS - 18,000 type solid propellant rocket with 18,600-pound sea-level thrust. The booster rocket is drag separated from the sustainer section 2.5 seconds after launch. The Aerobee 150A configuration with separated booster is depicted in Figure 2. The physical characteristics of the vehicle, and nominal trajectory data are described in Appendix A.

Based on wind tunnel values for C_{ℓ_δ} and C_{ℓ_p} and a fin-cant angle of 0.21 degrees, nominal spin resonance occurs at approximately t = 37.0 seconds, Mach number 3.5, 62,000 feet altitude, and with the roll and pitch rate equal to 5.95 radians per second.

Aerodynamics of the Aerobee 150A

Basic aerodynamic data for the Aerobee 150A, as obtained from wind tunnel tests[10], are presented in Appendix B. The normal force coefficient, stability margin, and pitch damping data are typical for sounding rocket vehicles.

The aerodynamic data most significant to the roll lock-in problem are the induced rolling moment and induced side moment. Figure 3 shows a com-

parison of the induced rolling moment coefficient versus angle of attack for several sounding rocket vehicles. These data are for aerodynamic roll angles of 30 and 22.5 degrees, corresponding to three- and four-finned rockets, respectively. The aerodynamic roll angle used throughout this report is defined in the sketch on page 39. For the comparison of induced rolling moments, it can be seen that the Aerobee 150A has the lowest angle of attack for induced rolling moment sign reversal, approximately 8 degrees total angle of attack. Because of the importance of the angle of attack for rolling moment sign reversal, this angle is designated α^*. Below the cross-over angle of attack, all of the configurations exhibit negative induced rolling moment coefficients for the aerodynamic roll angles shown.

The trends of two different theoretical predictions for the induced rolling moment are shown in Figure 3 for comparison. These data have not been corrected to the Aerobee 150A configuration, but are nevertheless representative. The theoretical approach of Reference 11, which considers the effect of the body vortices as well as the potential flow, predicts a positive induced rolling moment which increases with angle of attack in a cubic manner. The induced rolling moments computed in Reference 11, which are for triangular planform fins, do not show the negative rolling moment at small angles of attack. In Reference 12, a theoretical prediction of the induced roll is made for rectangular planform fins, assuming that the Mach cone from one of the tips does not intersect the surface of the other two normal fins. This analysis, which does not consider the effects of separation or body-vortices, shows that negative induced rolling moments exist at small angles of attack.

Side force data for the Aerobee 150A and another four-finned sounding rocket are presented in Figure 4. It will be noted that the side force does not exhibit a sign reversal with increasing angle of attack. However, the center

of pressure of the side force falls well forward of the fins at some Mach numbers and angles of attack, such that the side moment can in some instances reverse sign with changing angle of attack. The variations in the side moment, although not well understood, appear to lead to sign reversal points which are completely independent of those for the induced rolling moment. In the region of resonance, the side moment for ϕ = 22.5 degrees is negative at all angles of attack greater than about 2.5 degrees.

In order that the relationships between the pitching moment, side moment, and rolling moment be clearly seen, the variation of each of these moment coefficients with angle of attack is plotted in Figure 5 for an aerodynamic roll angle of 22.5 degrees. The Mach number and center of gravity are representative of resonance conditions.

III. GENERAL DISCUSSION OF THE ROLL LOCK-IN PROBLEM

Initiation of Roll Lock-In

In practically all cases, roll lock-in is initiated with a build-up of induced rolling moments (either from aerodynamic effects or lateral asymmetry) in a sense opposite to the direction of spin. Thus, for a rocket with fins canted for positive roll, the induced rolling moments preceeding lock-in are usually negative. In the discussion which follows, we will consider only the case where the rocket fins are canted for positive roll.

The basic mechanism for initiation of roll lock-in can be seen by considering the trim angle of attack and its orientation, since prior to resonance the launching transients have damped out. The orientation of the trim angle of attack is determined by the orientation of the vehicle asymmetries and by a phase shift which is dependent upon the ratio of the roll and pitch frequencies, p/ω (see Figure 1). With increasing p and decreasing ω the corresponding phase shift causes the aerodynamic roll angle, ϕ, to increase, positively, throughout the flight. Thus, the only mechanism which can cause ϕ to remain constant, i.e. locked-in, is a reduction in the spin rate, which in turn requires a negative rolling moment. The negative rolling moment must be provided by the induced rolling moments, since at the initiation of lock-in $C_{\ell_\delta}\delta \approx C_{\ell_p} \frac{pd}{2V}$.

Roll Lock-In With Aerodynamic Induced Rolling Moment

The initiation of lock-in, when only the aerodynamic induced rolling moment is present, can be seen more clearly by examining a plot of the induced rolling moment versus the aerodynamic roll angle, Figure 6. The curve shown is for a specific angle of attack, which is less than α^*. Superimposed is the orientation of the trim angle of attack for an arbitrary asymmetry. Also depicted is the phase shift in the trim angle of attack for increasing values of $f'(\omega)$. These data were computed from the linearized motion theory described in Appendix C.

For the present example, two possibilities exist for lock-in with $f'(\omega) = 1$. First, lock-in may occur at some $\Phi < 45$ degrees. As can be seen, f_{α} can increase to the order of 0.85 with only a small change in Δf. Second, lock-in may occur at a Φ slightly greater than 90 degrees, where f_{α} is approximately unity. Obviously, the latter cannot occur as long as the vehicle has a lock-in in the first region.

Whether or not roll lock-in occurs depends upon the magnitude of the non-rolling trim, the variation of the aerodynamic induced rolling moment with angle of attack, and the trim amplification. The latter, of course, depends greatly upon the aerodynamic damping as $f'(\omega)$ approaches unity.

In most instances a vehicle will break out of the first lock-in region, because the trim angle of attack will increase beyond α^*, and the sign of the induced rolling moment will reverse. However, for small asymmetries a vehicle can stay locked-in at $\Phi < 45$ degrees for a significant period of time. Such a case is described in a subsequent section of this report.

It is important to note from the preceeding example that the exact behavior of the aerodynamic roll angle, Φ, cannot be readily determined.

Although qualitatively it is easy to see that ϕ may be at least slowly changing in a region of negative induced roll, it is not clear that $\dot{\phi}$ can be held constant, or $\dot{\phi}$ maintained near zero. Thus, a precise determination of lock-in requires solution of the equations of motion.

Unfortunately, it is not possible to develop a simplified equation of motion to describe the behavior of the aerodynamic roll angle; hence other methods must be selected for determining the exact nature of the motion under near-resonant conditions.

Although the initiation of lock-in is difficult to describe in simple analytic terms, the conditions under which the induced rolling moment can no longer sustain a lock-in condition can be approximated.

For $\alpha < \alpha^*$ the maximum aerodynamic induced rolling moment is known, and we can assume that it occurs at $\phi_i = 22.5 + n(90)$, where $n = 0, 1, 2$, etc. Hence, the worst condition would be where the initial trim is such that the lock-in angle, ϕ, corresponds to $\phi_i = 22.5 + n(90)$. Break-out will begin when the spin rate satisfies the inequality

$$\left| C_{\ell_\delta} \delta + C_{\ell_{p^2}} \frac{pd}{2V} \right| < \left[C_{\ell_{\phi_i}} (\alpha^*) \right]_{max} \quad , \alpha < \alpha^*$$

At angles of attack greater than α^* the induced rolling moment increases steadily with angle of attack for all values of the angle of attack which are of interest. Thus, the maximum aerodynamic induced rolling moment can be specified only if the angle of attack history is known. The trim angle of attack history can be determined from a linear solution of the equations of motion (see Appendix C), providing p/ω is known or assumed. One logical choice is to assume $p/\omega = 1$, a condition near which lock-in will usually occur.

The break-out requirement now becomes approximately

$$\left| C_{\ell_\delta}\,\delta + C_{\ell_p}\,\frac{pd}{2V} \right| > \left| \left[C_{\ell_{i_{\bar{q}_i}}} \left(\vec{\alpha}_{trim},\ p/\omega = 1 \right) \right] \right| \quad , \quad \alpha > \alpha^*$$

The above inequality can be evaluated as a function of time to determine the conditions under which break-out can be assured.

The above approach is the basis for the roll lock-in analyses described in References 7 and 8. The usefulness of the break-out criterion hinges on the assumption of $p/\omega = 1$ and the simplification of the roll dynamics to equilibrium conditions. As will be shown subsequently, these assumptions can lead to considerable error.

Roll Lock-In With Aerodynamic Induced Rolling Moment and Rolling Moment Due to Lateral Asymmetry

The analytic form of the rolling moment due to lateral displacement of the center of gravity and aerodynamic center of pressure is described in Appendix D. The relationship between the aerodynamic induced rolling moment and the rolling moment due to lateral asymmetry is depicted in Figure 7. The rolling moment due to lateral asymmetry is depicted for several orientations of the center of pressure with respect to the longitudinal principal axis. For ease of visualization, these are illustrated as offset centers of gravity.

Significantly, the sum of the two induced rolling moments is maximum for only one orientation of the lateral asymmetry. For example, with $\alpha > \alpha^*$, the maximum negative induced rolling moment occurs with the center-of-gravity location designated number four. This condition, as can be seen from the diagram, corresponds to a non-rolling trim located at ϕ = 247.5 degrees.

The lateral asymmetry can also be oriented such that the aerodynamic induced rolling moment and the rolling moment due to lateral asymmetry are opposed at resonance. More generally, the regions where the combined rolling moments are negative can correspond to any ϕ, providing that suitable orientations of the lateral asymmetry are specified.

To determine the actual magnitude of the two induced rolling moments, the angle of attack must be considered, since both induced rolling moments are angle-of-attack dependent. For a specific configuration, the sum of the two induced rolling moments changes rapidly through the resonance region, because there are changes in both the magnitude of the angle of attack and its orientation. This effect is best illustrated by numerical examples. Figure 8 shows the variation of $C_{\ell_\alpha} + C_{\ell_{\alpha_A}}$ with ϕ for four lateral asymmetry orientations, a center of gravity - center of pressure displacement of 0.25 inches, and a non-rolling trim angle of attack of 0.14 degrees. In each of these examples, the non-rolling trim lies in the plane of the lateral asymmetry (as indicated in the sketch accompanying the figure), and the rolling moment due to lateral asymmetry has a maximum positive value at resonance. These numerical examples show that near resonance, the total rolling moment can be positive irrespective of the aerodynamic induced rolling moment, if the rolling moment due to lateral asymmetry has a positive maximum at resonance.

Effect of the Side Moment

The side-moment coefficient C_{SM_α} has a pronounced effect on the non-rolling trim amplification for near-resonant conditions. The relationship between the trim amplification factor and the side moment coefficient can be seen from the development of the linear theory for the trim angle

of attack, Appendix C. Inspection of equation (C-11) shows that the trim amplification becomes infinite at resonance when

$$\frac{H - \frac{I_x}{I} r}{\sqrt{-M}} + \frac{M_\delta}{M} = 0 \qquad (1)$$

where

$$\frac{M_\delta}{M} = \frac{C_{\delta M_\alpha}}{C_{M_\alpha}}$$

is the ratio of the side-moment coefficient to pitching moment coefficient. The values of $C_{\delta M_\alpha} / C_{M_\alpha}$ which satisfy equation (1) for the Aerobee 150A are presented in Figure 9 as a function of time. At the nominal resonance time, 37.0 seconds, the ratio $C_{\delta M_\alpha} / C_{M_\alpha}$ has a value of only 0.117, and at later times in the flight the values of this ratio are even less.

Since the amplification factor is infinite for negative values of $C_{\delta M_x} / C_{M_x}$, it is clear that $C_{\delta M_\alpha}$ leads to catastrophic yaw when $C_{\delta M_\alpha}$ is positive.

Because the side moment coefficient, $C_{\delta M_x}$, is periodic with roll orientation, catastrophic yaw can occur only for certain values of the roll orientation angle. Figure 10 shows, qualitatively, the variation of $C_{\delta M_\alpha}$ with ϕ at Mach number 3.5. Thus, catastrophic yaw requires that the aerodynamic roll angle at lock-in fall in the regions $45 < \phi < 90$, $135 < \phi < 180$, $225 < \phi < 270$, or $315 < \phi < 360$ degrees.

To determine the angle of attack at which catastrophic yaw might commence, it is necessary to consider the non-linear variation of C_n with angle of attack, from which the secant slope (and hence $C_{\delta M_\alpha}$) is derived. If we select a lock-in angle corresponding to one of the ϕ's where the side moment has a positive maximum, then a critical angle of attack can be defined

as the angle of attack where the secant slope of C_n satisfies equation (1). At t = 37 seconds the critical value of the secant slope is 2.51, and the corresponding critical angle of attack is 5.5 degrees. This can be interpreted as meaning that catastrophic yaw will have commenced at some angle of attack less than 5.5 degrees.

Because the side moment effect can so easily lead to catastrophic yaw conditions, it is important to see which asymmetries and non-rolling trim orientations result in the lock-in angles where the side moment is positive. These boundaries can be established in an approximate manner by considering only those lock-in conditions which result from lateral asymmetry rolling moments.

The critical non-rolling trim orientations for each lateral asymmetry are depicted in Figure 11. It is easily seen that the probability of catastrophic yaw for a vehicle with random asymmetries is something less than 25 per cent.

IV. QUASI-STEADY ANALYSIS OF THE NEAR-RESONANT MOTION OF SOUNDING ROCKET VEHICLES

Development of a First-Order Differential Equation for Near-Resonant Motion

In the preceeding sections, a qualitative analysis of the roll lock-in regions was achieved by considering the orientations and magnitudes of the contributing aerodynamic coefficients and asymmetries. However, it is desirable to have an analytic method for description of near-resonant motions which may exhibit lock-in characteristics. Preferably, such a method should be less complex than the solution of the six-degrees-of-freedom equations, and should also provide insight as to why the lock-in has occurred.

Because the near-resonant motion of a sounding rocket involves primarily pitch-roll coupling between the trim angle of attack and the induced rolling moments, it seems appropriate to consider a motion solution involving only these factors. The magnitude and orientation of the trim can be obtained from the usual linearized equation of motion, while the induced rolling moments can be expressed in terms of the angle of attack and its orientation with respect to the vehicle fin planes and asymmetries.

To accomplish this marriage, it is necessary to find a dependent variable which is common to both the angle of attack dynamics and the roll dynamics. Such a variable is the ratio, p/ω, where ω is the undamped natural pitch frequency.

The equations relating p/ω to the magnitude and orientation of the trim angle of attack are derived in Appendix C, while Appendix D contains the equations relating the angle of attack to the rolling moment due to lateral

asymmetry. Finally, the derivation of a first-order non-linear differential equation for $\dot{p}$ is presented in Appendix E. This derivation is accomplished by appropriate modification of the roll differential equation.

For convenience, the $\dot{p}/\omega$ differential equation is re-presented below.

$$\left[\quad\right] = \left[\quad\right] \tag{2}$$

where

$$\left[\quad\right] = f(K_3)\sin 4\phi$$

$$\left[\quad\right] = \frac{\Delta\bar{y}}{\ell}\left[C_{N_\alpha}(K_3)\sin\quad\right]$$

$$\left[\quad\right] + \Delta\ell$$

$$\left[\frac{K_3}{(K_3)_{p=0}}\right]$$

$$\left[\quad\right] - \Delta\ell$$

The angle of attack parameters $K_3/(K_3)_{p=0}$ and $\Delta\ell$ are given in terms of $\dot{p}/\omega$ by equations (C-11) and (C-12). The $\dot{p}/\omega$ terms in equation (2) contain time-varying coefficients which can be evaluated independently of the solution for $\dot{p}/\omega$. This greatly simplifies the numerical solution of equation (2). It will be noted that all of the coefficients on the left-hand side of (2) can be determined directly from a nominal spin history, p_T versus time, and the variation of the pitch natural frequency with time.

Numerical Results

Some solutions of equation (2) have been obtained by numerical integration, using a desk-type calculator. The calculations are based on a fin cant angle of 0.21 degrees, which produces a ρ_T/ω variation with time, as illustrated in Figure 12. The time-varying coefficients of ρ/ω in equation (2) are plotted in Figure 13. The time-varying aerodynamic coefficients C_{M_α} and C_{N_α}, and the damping parameter $H = \frac{I_x}{I} T/\sqrt{-M}$ are plotted in Figure 14. The dependence of C_{ℓ_δ} and $C_{\delta M_\alpha}$ on angle of attack was determined from Figure 5. The non-linearity in C_{M_α} was not considered.

In the first calculation, Case I, only the aerodynamic induced rolling moment was included. The asymmetry was assumed to be due entirely to aerodynamic misalignment with $\sqrt{C_{m_o}^2 + C_{n_o}^2} = 0.15$. The asymmetry was oriented such that the non-rolling trim was at $\Phi = 11$ degrees. In Case I a lock-in was obtained for about 3 seconds, as depicted in Figure 15. The value of Φ at lock-in was about 93 degrees, and the trim angle of attack reached a maximum value of about 4.5 degrees just prior to break-out.

The second calculation, Case II, included a 0.1-inch lateral displacement of the center of gravity and center of pressure. The trim angle of attack was assumed to be due to aerodynamic misalignment with $\sqrt{C_{m_o}^2 + C_{n_o}^2} = 0.15$. The non-rolling trim was oriented at $\Phi = 0$, while the lateral center of pressure was given an orientation $\Phi_{cp} = 90$ degrees.

The solution for ρ/ω in Case II is also depicted in Figure 5. This case is somewhat unusual in that the phase angle, $\Delta\Phi$, has not changed more than 20 degrees out to $t = 50$ seconds, which is approximately 13 seconds after nominal resonance. Although the aerodynamic roll angle, Φ,

has not become constant, the rate of increase of $\dot{\phi}$ is extremely small. This type of motion could be classified as an extended resonance; however, it should be noted that p/ω is significantly less than unity.

In Case II the trim angle of attack increases very slowly, attaining a magnitude of only 2.84 degrees at t = 50 seconds. This is less than the maximum trim for Case I, where lock-in occurred for only a short period. The reason for the slow build-up of trim in Case II is that p/ω is well below unity, which effect reduces the amplification factor. In Case II, where both induced rolling moments are present, only slight reduction in the total rolling moment occurs as the angle of attack approaches α^*. Therefore, break-out cannot occur as readily as in the case where only the aerodynamic induced rolling moment is present.

Case II serves to show that the assumption of p/ω = 1 (as used in References 7 and 8) is not always valid for determination of the break-out conditions. For example, in cases where p/ω is approximately constant, but not equal to unity, the trim angle of attack solution will be sufficiently in error as to negate any boundaries based on $p/\omega = 1$.

V. APPLICATION OF CIRCULAR MOTION THEORY

The near-resonant angle-of-attack motion of a sounding rocket vehicle is nearly circular, because it is comprised of the slowly varying trim vector, which rotates at the spin rate. Circular-type motions can receive special treatment through the use of perturbation theory. The advantage of a special circular motion analysis is that the aerodynamic and inertial moments can be considered in their more exact non-linear form, and the effect of the non-linear side moment can be determined more precisely.

The side moment acts in much the same manner as a Magnus moment, and thus can act as a driving mechanism for a sustained large angle-of-attack motion. When the angle of attack becomes large, the pitching and yawing moments resulting from the asymmetries become insignificant, and the linear solutions for the trim angle of attack are no longer valid.

Linear Trim Solution With Side Moment Coefficient

The linear solution for the trim angle of attack at resonance is given in Appendix C as

$$(K_3)_{RES} = \frac{C_{m_\delta}}{C_{M_\alpha}} \left[\frac{1}{\left[H - \frac{I_x}{I} T \right] \Big/ \sqrt{-M}} + \frac{M_s}{M} \right] \tag{3}$$

where

The coefficients C_{M_α} and $C_{\delta M_\alpha}$ are secant slopes, and can be evaluated at various angles of attack. From equation (3) and the aerodynamic data in Figures 5 and 13, an evaluation has been made of the C_{m_0} required for various trim angles of attack. The analysis includes the non-linear variation of C_{M_α}, as well as the effect of aerodynamic roll angle. The results are plotted in Figure 16 for two aerodynamic roll angles where C_{M_α} is positive. For the maximum values of $C_{\delta M_\alpha}$ (ϕ = 67.5 degrees) the C_{m_0} required for trim drops to zero at an angle of attack slightly greater than 6 degrees. However, C_{m_0} reaches a maximum at an angle of attack of only 4.0 degrees, so that all trim solutions at larger angles of attack are unstable. When the side-moment coefficient is reduced by a factor of two (ϕ = 52.5 degrees), the angle of attack for maximum C_{m_0} increases to only about 5.0 degrees.

Thus, for lock-in roll orientations where the side moment is positive, the linear solutions for the trim angle of attack are valid only at very small angles of attack.

Lunar Circular Motion Solutions With Side-Moment Coefficient

The non-linear circular motion solutions at nominal resonance conditions (τ = 37 seconds, Mach number 3.5) are presented in Figure 45. The derivation of the equations and the method of obtaining the solutions is completely discussed in Appendix F.

Inspection of Figures 16 and 45 shows that the angles of attack at which the linear trim solutions become invalid correspond very closely with the angles of attack at which the unstable circular motion solutions are obtained.

For example, with ϕ = 67.5 degrees, the linear trim solution becomes unstable at about 4 degrees, while the corresponding unstable circular motion solution occurs at 5 degrees angle of attack. The stable circular motion solution for ϕ = 67.5 degrees occurs at an angle of attack of about 22.5 degrees. Therefore, between 4 degrees and 22.5 degrees angle of attack the motion is in a transient state.

For ϕ's where the side moment is less than maximum, the angles of attack corresponding to the unstable trim and unstable circular motion solutions increase, while the stable circular motion solutions decrease.

Rolling Moment Requirements for Steady-State Circular Motion

For each lunar circular motion solution, there corresponds specific values of $\bar{z}$, $\bar{t}$, and $\bar{r}$. For ϕ to remain constant the roll equation must also be satisfied. The requirements for constant ϕ are approximately equivalent to requiring a zero value for total induced rolling moment, i.e.

$$C_{\ell_i}(\bar{t}) + C_{\ell_{\Delta z}}(\bar{\phi}) = 0 \qquad (4)$$

For the purposes of an example, it is convenient to select an orientation of the plane of lateral asymmetry such that $\delta = \pi/2$. This assumption simplifies the rolling moment due to lateral asymmetry at resonance, and we obtain

$$C_{\ell_{\Delta z}} = -\frac{\Delta \bar{z}}{\ell}\left[C_{N_\alpha}(\bar{\alpha}) \sin\delta\right] = \frac{\Delta \bar{z}}{\ell} C_{N_\alpha}(\bar{\alpha})$$

and as before

$$C_{\ell_i} = C_{\ell_{i_{\bar{z}=22.5}}}(\bar{\alpha}) \sin 4\bar{\phi}$$

The amount of lateral asymmetry required to maintain roll equilibrium is, therefore

$$\frac{\Delta y}{l} = -\frac{\left[\quad \right]}{C_{N_\alpha}} \qquad (5)$$

Values of $\Delta y / l$ are plotted in Figure 7 as a function of α and ϕ for both transient and steady-state circular motions. The amount of lateral asymmetry required to maintain steady-state circular motion is seen to be only slightly greater than $\Delta y / l = 0.01$ or about 0.15 inches. Thus, the probability of a sustained large angle-of-attack motion is quite large if the rocket locks in at an aerodynamic roll angle where the side moment is positive.

Additional Remarks

It should be noted that a steady-state large angle of attack circular motion does not require that the aerodynamic roll angle be constant, but merely slowly varying. Also, at a given time in the trajectory lunar circular motion can exist for a wide range of roll rates. This can be seen from the relationship

$$p = \dot{\psi} \cos \alpha$$

which defines lunar motion. It will be noted that a change in the roll rate, p, does not necessarily infer that the aerodynamic roll angle is changing, because there may be a corresponding change in $\dot{\psi} \cos \alpha$. A change in the angle of attack plane rotation, $\dot{\psi}$, is easily brought about by a change in the side moment, as can be seen from equation (F-21).

Extreme caution should be exercised, therefore, in any attempt to solve the roll lock-in problem by use of positive rolling moments at resonance,

because if the trim angle of attack is sufficiently large to introduce a side moment, a large angle-of-attack lunar-type motion may still occur.

Further, it can be shown that the circular motion solutions for near-lunar motions are almost the same as for lunar motion.

The above facts emphasize the need for considering the non-linear effects associated with near-resonant motion. However, the complications are too great to permit a general type of analysis to be made.

VI. CONCLUSIONS AND RECOMMENDATIONS

Conclusions

(1) Roll lock-in phenomena are shown to originate primarily from two induced rolling moments: a) an aerodynamic induced rolling moment dependent upon angle of attack and the orientation of the angle-of-attack plane with respect to the fin planes, and b) an angle-of-attack dependent rolling moment resulting from lateral displacement of the center of gravity and aerodynamic center of pressure. These rolling moments, together with the trim angle of attack produced by aerodynamic, vehicle, and thrust asymmetries, initiate the anomalous motion which occurs near resonance.

(2) Several roll lock-in type motions can occur near resonance. These can be divided between motions which are truly locked-in, in which case the aerodynamic roll angle approaches a constant value, or motions in which the ratio p/ω is slowly varying or nearly constant for an extended period of time. The duration of the lock-in or extended resonance depends upon the orientation and magnitude of the asymmetries as well as all of the aerodynamic and flight parameters.

(3) The amplification of the non-rolling trim angle of attack increases with an extended resonance or lock-in, due to the decrease in aerodynamic damping with increasing altitude. The amplification factor is further influenced by the magnitude and sense of the aerodynamic side moment as well as by the proximity to unity of the spin-to-natural-frequency ratio, p/ω.

(4) Positive values of the aerodynamic side moment can greatly decrease the effective aerodynamic damping of near-resonant motions, and produce very large angle-of-attack coning motions. The existence of a roll orientation where the side moment is positive requires that the aerodynamic roll angle at resonance or lock-in fall in the angular sector $45 < \phi < 90$, or sectors which are spaced 90 degrees from this sector. This requires that the resonant angle of attack exceed α^*; or at small angles of attack, that lateral asymmetry be present to produce an induced rolling moment which can oppose the aerodynamic induced rolling moment.

(5) When all of the factors affecting roll lock-in and/or extended resonance are considered simultaneously, it becomes impractical to determine upper bounds on the magnitude of the vehicle asymmetries, since the resonant motion behavior is just as critical with respect to the angular orientation of the individual asymmetries.

(6) In most instances, the near-resonant motion of a sounding rocket vehicle can be closely approximated by considering the linear solution for the trim angle of attack in conjunction with the exact non-linear equation of motion for roll. Using ϕ as a dependent variable, these two modes can be combined into a single first-order non-linear differential equation with time-varying coefficients which can be easily solved without the use of a digital computer. This technique should be extremely useful for investigating specific vehicle configurations, flight trajectories, and asymmetries.

(7) When the resonant angle of attack becomes large in conjunction with the side moment being positive, the non-linear nature of the pitch-roll dynamics precludes the use of the linear theory for predicting the angle of attack motion. This type of problem can be investigated by the use of the special circular motion theory developed in this report.

Recommendations

(1) Dynamic wind tunnel tests should be conducted to determine the effect of angle-of-attack plane rotation on the aerodynamic forces and moments. Since highly non-linear variations of the rolling moment, side force, and side moment are measured statically, it is very likely that similar effects occur dynamically, that is, with angle-of-attack plane rotation. Such tests could be accomplished by the use of a bent rotating sting, which could provide the necessary simulation of the coning motion.

(2) Additional six-degrees-of-freedom motion calculations should be accomplished to determine the exact motion of a sounding rocket vehicle under the influence of combined aerodynamic induced rolling moment and rolling moment due to lateral asymmetry. These calculations should also include non-linear aerodynamic side-moment coefficients, and should explore the effects of different aerodynamic damping coefficients for planar and circular motion.

REFERENCES

1. Parsons, W. D., "Roll-Rate Lag of Rockets Accelerating in the Upper Atmosphere," AIAA Journal of Spacecraft and Rockets, Volume 2, Number 2, pp. 271-272.

2. Whitlock, Charles H., "Comparison of Steady-State and Six-Degree-of-Freedom Analyses of Pitch-Roll Resonance Conditions for a Long Slender Sounding Rocket," NASA TN D-1816, June 1963.

3. Nicolaides, J. D., "Two Nonlinear Problems in the Flight Dynamics of Modern Ballistic Missiles," IAS Report 59-17, January 1959.

4. Murphy, Charles H., "Free Flight Motion of Symmetric Missiles," BRL Report No. 1216, July 1963.

5. Maun, E. K., "Aerobee 150 Roll Lock-In Study - Development of a Roll Lock-In Criterion," Space-General Corporation Report 785FR-3, Contract NAS 5-9060, July 1965.

6. Sollow, P. H., "Aerobee 150 Roll Lock-In Study - Roll Lock-In Susceptibility Study Using the SGC 6-Degree-of-Freedom Trajectory Simulation Computer Program," Space-General Corporation Report 785FR-2, Contract NAS 5-9060, July 1965.

7. Price, D. A., Jr., "Final Report For the Aerobee 150A Roll Lock-In Study," Contract NAS 5-9061, Lockheed Missiles and Space Company.

8. Price, D. A., Jr., "Final Report for Aerobee 350 Roll Lock-In Study," Contract NAS 5-9061, Lockheed Missiles and Space Company.

9. Sollow, P. A., "Roll-Yaw Coupling Study - Aerobee 350," Space-General Corporation Final Report 379RC-2, Volumes 1, 2, and 3, Contract NAS 5-3313, December 1964.

10. Lawrence, J. T., "Aerobee 150A Aerodynamic Data From NOL Wind Tunnel Tests," NASA Goddard Space Flight Center Report X-671-64-47, February 1964.

11. Spahr, Richard J., "Contribution of the Wing Panels to the Forces and Moments of Supersonic Wing-Body Combinations at Combined Angles," NACA Technical Note 4146, January 1958.

12. Twiss, P. M. and L. J. Beecham, "Wind Tunnel Investigation of Rolling Moments Due to Combined Roll and Yaw of Cruciform Winged Projectiles at Supersonic Speeds," RAE Technical Note No. G. W. 41, July 1949, Confidential.

13. Space-General Corporation Letter SGC 5135:M0140, 24 October 1963.

14. Brunk, J. E., "The Dynamics and Aerodynamics of Self-Sustained Large Angle of Attack Body Spinning Motions," Alpha Research, Inc. Report 63-1158-1, AFOSR-4596, February 1963.

APPENDIX A.

Vehicle Physical Characteristics and Nominal Trajectory Data

The Aerobee 150A configuration investigated in the present study is depicted in Figure 2, and consists of an ogive-nose payload, extension, and sustainer sections. This configuration is designated B-2 in Reference 10. Data for the vehicle with its solid propellant rocket booster attached are not presented here.

Weight, center of gravity, and moment of inertia data as a function of time are presented in Figures 18 and 19.

The sustainer motor has a burning time of 51.5 seconds, and the sustainer thrust is given by

$$\text{sustainer thrust} = 4728 - 628 \frac{P_{ATMOSPHERE}}{P_{SEA\ LEVEL}}$$

Nominal trajectory data based on an 87-degree launch angle at sea level are depicted in Figures 20 and 21. Burn-out occurs at approximately 6.2 Mach number at 125,000 feet.

The nominal spin history is presented in Figure 22. This is based on a fin cant angle of 0.21 degrees. The variations of C_{ℓ_δ} and C_{ℓ_p} with Mach number for zero angle of attack are presented in Figure 23, and were obtained from Reference 13.

Based on the above, nominal spin resonance occurs near t = 37.0 seconds, Mach number 3.5, and 62,000 feet, with the roll and pitch rates equal to 5.95 radians per second.

APPENDIX B.

Aerodynamic Data for Aerobee 150A

The vehicle drag curve, from Reference 13, is repeated here as Figure 23.

The static and dynamic characteristics of the Aerobee 150A in pitch and roll were obtained from tests at the U. S. Naval Ordnance Laboratory, White Oak, Maryland, Reference 10. Static test data consisting of normal force, pitching moment, side force, and yawing moment, and induced rolling moment were obtained at three roll orientations (ϕ = 0, 25, 45 degrees), and at Mach numbers 2.53, 3.50, 4.85, and 6.80. Only data for configuration B-2 are presented here.

Because the data were obtained at combined angles of attack and sideslip and reduced with respect to body axes, it was necessary to transform all of the lateral force and moment data to obtain the force and moment coefficients in the angle of attack plane (designated here as C_N and C_m) and the forces and moments in the symmetry plane normal to the angle of attack plane (designated here as C_y and C_n). The latter quantities are referred to as the side force and side moment, respectively, and are treated as Magnus-like coefficients in the aerodynamic analyses.

The resulting plots of C_N, C_m, C_y, and C_n versus angle of attack for each of the test Mach numbers are presented in Figures 25 through 34. The side force and yawing moment are shown only for ϕ = 22.5, while C_N and C_m are shown for ϕ's of 0, 22.5, and 45 degrees. The centers of pressure for the normal force and side force are illustrated in Figures 35 and 36. The stability margin and normal force derivative versus Mach number are depicted in Figures 37 and 38.

Pitch damping data, $C_{M_q} + C_{M_{\dot{\alpha}}}$, are presented as a function of Mach number in Figure 39. These data are based on the flight center of gravity corresponding to each Mach number.

APPENDIX C.

Linear Solution for the Trim Angle of Attack

The equation of motion for a slightly unsymmetrical rocket at small angle of attack can be expressed in non-rolling coordinates as[4]

$$\ddot{\xi} + \cdots + \cdots \dot{\xi} - \left[\cdots + \cdots \left(P T + M_s \right) \right] \tilde{\xi} = \cdots A e^{i \Phi} \qquad \text{(C-1)}$$

where

$\tilde{\xi} = \xi + i \eta$ ($\sim$ indicates non-rolling axes)

$\cdots = \cdots / 2m \left[C_{L_\alpha} - k_t^{-2} \left(C_{M_q} + C_{M_{\dot{\alpha}}} \right) \right]$

$\cdots = \left(\cdots \rho^2 / 2I \right) C_{M_\alpha}$

$\cdots = \left(\cdots \frac{\rho^2}{2m} \right) k_t^{-2} C_{SM_\alpha}$

$\cdots = \cdots \rho \ell / 2m \left[C_{L_\alpha} + k_a^{-2} C_{M_{p\alpha}} \right]$

$\cdots = \cdots \rho / 2m \left[k_t^{-2} \left(C_{m_0} + i C_{n_0} \right) + \left(P \frac{I}{I_x} - 1 \right) \left(C_{\gamma_0} - i C_{\gamma_0} \right) \right]$

$P = \left(\rho \ell / V \right) \left(\frac{I_x}{I} \right)$

$k_t = \sqrt{I / m \ell^2}$

$k_a = \sqrt{I_x / m \ell^2}$

$\mathcal{L} = \int_0^s \mathcal{L}' \, ds$ and $s = 1/\ell \int_{t_0}^{t} V \, dt$

$\mathcal{L}' = \rho \ell / V$

In the above equation, jet damping and the effects of axial acceleration are not considered. The body axes and direction and sense of the forces and moments are shown in Figure 40.

The particular solution of (C-1) is

$$\xi = K_1 e^{i\varphi_{10}} e^{(\lambda_1 + i\varphi_1')\alpha} + K_2 e^{i\varphi_{20}} e^{(\lambda_2 + i\varphi_2')\alpha} + K_3 e^{i\varphi_{30}} e^{i\varphi} \qquad \text{(C-2)}$$

In the work which follows, it is the undamped trim vector $K_3 e^{i\varphi_{30}} e^{i\varphi}$ which is of interest. It should be noted that $\xi = K_3 e^{i\varphi_{30}}$ describes the trim vector with respect to the body axes, whereas $e^{i\varphi}$ orientates the body axes with respect to the non-rolling coordinate system. The particular solution gives

$$K_3 e^{i\varphi_{30}} = \frac{-iA}{(\varphi')^2 P(\varphi) + M - i(\varphi' H - PT - M_s)} \qquad \text{(C-3)}$$

Ratio of Rolling Trim to Non-Rolling Trim. Substituting $p = 0$ into (C-3), we obtain

$$\left(K_3 e^{i\varphi_{30}}\right)_{p=0} = \frac{\left(\frac{\rho S \ell}{2m} k_x^{-2} C_{m_0} + C_{Z_0}\right) - i\left(\frac{\rho S \ell}{2m} k_x^{-2} C_{m_0} - C_{Y_0}\right)}{M} \qquad \text{(C-4)}$$

which for $C_{y_0} = C_{z_0} = 0$ reduces to

$$\left| K_3 e^{i\varphi_{30}} \right|_{p=0} = \frac{C_{n_0} - i\, C_{m_0}}{C_{m_\alpha}}$$

Noting that the absolute value of the quotient of two complex numbers $x_1 + i y_1$ and $x_2 + i y_2$ can be expressed as

$$\left| \frac{x_1 + i y_1}{x_2 + i y_2} \right| = \sqrt{\frac{x_1^2 + y_1^2}{x_2^2 + y_2^2}}$$

we obtain the ratio of the rolling trim to non-rolling trim as

$$\frac{K_3}{(K_3)_{p=0}} = \left| \frac{K_3 e^{i\varphi_{30}}}{K_3 e^{i\varphi_{30}}} \right|_{p=0} = \sqrt{\frac{M^2 \left\{ \left[\bar{C}_{n_0} - \left(\frac{PI}{I_x} - 1 \right) C_{z_0} \right]^2 + \left[\bar{C}_{m_0} + \left(\frac{PI}{I_x} - 1 \right) C_{y_0} \right]^2 \right\}}{\left\{ \left[(\Phi')^2 - P(\Phi') + M \right]^2 + \left[\Phi' H - PT - M_s \right]^2 \right\} \left\{ \left[\bar{C}_{n_0} + C_{z_0} \right]^2 + \left[\bar{C}_{m_0} - C_{y_0} \right]^2 \right\}}} \qquad \text{(C-5)}$$

where

$$\bar{C}_{m_0} = C_{m_0} \frac{\rho V^2}{2m} k_t^{-2}$$

$$\bar{C}_{n_0} = C_{n_0} \frac{\rho V^2}{2m} k_t^{-2}$$

For the special case of $C_{y_0} = C_{z_0} = 0$, equation (C-5) reduces to

$$\frac{K_3}{(K_3)_{p=0}} = \left| \frac{K_3 e^{i\varphi_{30}}}{K_3 e^{i\varphi_{30}}} \right|_{p=0} = \sqrt{\frac{M^2}{\left[(\Phi')^2 - P(\Phi') + M \right]^2 + \left[\Phi' H - PT - M_s \right]^2}} \qquad \text{(C-6)}$$

Orientation of Trim Vector. The orientation of the trim vector* is determined by noting that $K_3 e^{i\varphi_{30}}$ is of the form

$$K_3 e^{i\varphi_{30}} = \frac{x_1 + iy_1}{x_2 + iy_2}$$

such that we can express φ_{30} as

$$\varphi_{30} = \tan^{-1}\left[\frac{x_2 y_1 - x_1 y_2}{x_1 x_2 + y_1 y_2}\right]$$

The orientation of the non-rolling trim is therefore

$$(\varphi_{30})_{p=0} = \tan^{-1}\left[\frac{-\bar{C}_{m_0} + C_{y_0}}{C_{n_0} + C_{\ell_0}}\right] \qquad \text{(C-7)}$$

The orientation of the rolling trim with respect to the non-rolling trim can be expressed as

$$\varphi_{30} - (\varphi_{30})_{p=0} = \tan^{-1}(\varphi_{30}) - \tan^{-1}(\varphi_{30})_{p=0}$$

The difference of the arc tangents can be eliminated by use of the identity

$$\tan\left[\varphi_{30} - (\varphi_{30})_{p=0}\right] = \frac{\tan\varphi_{30} - \tan(\varphi_{30})_{p=0}}{1 + \left[\tan\varphi_{30}\right]\left[\tan(\varphi_{30})_{p=0}\right]}$$

and we obtain finally that

$$\Delta\varphi = \varphi_{30} - (\varphi_{30})_{p=0} = \tan^{-1}\left[\frac{\Phi' H - PT - M_s}{(\Phi')^2 - P(\Sigma) + M}\right] \qquad \text{(C-8)}$$

* Note that $K_3 e^{i\varphi_{30}}$ is with respect to body-fixed axes.

The orientation of the trim vector with respect to the body axes is obtained by noting that

$$\xi = K_3 e^{i\varphi_{30}} = \frac{w + iv}{V}$$

$$\therefore \quad \varphi_{30} = \tan^{-1} \frac{v}{w} \tag{C-9}$$

The trim vector is plotted in the following sketch.

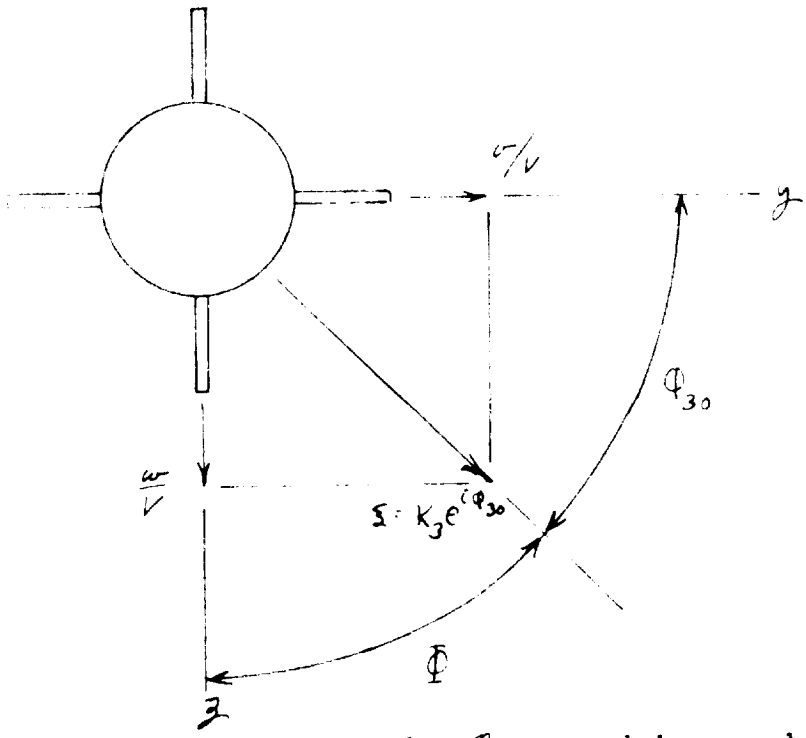

The correspondence of trim orientation angle, φ_{30} , and the aerodynamic roll angle, Φ , is illustrated in the above sketch for the case where the body axes y and z are aligned with the fins.

Equations for the Trim Amplification and Trim Orientation in Terms of the Parameter p/ω. Noting that $\varphi' = pl/v$ and defining the pitch natural frequency, ω, according to the relation

$$\frac{\omega l}{v} = \sqrt{-M} \tag{C-10}$$

we can by substitution and re-arranging obtain (C-6) and (C-8) in the following useful forms.

$$\frac{K_1}{(K_1)_f} = \left[\left(1 - \frac{I_x}{I}\right)^2 + \left[\frac{(p/\omega)\left(H - \frac{I_x}{I}T\right)}{\sqrt{-M}} + \frac{M_s}{M}\right]^2\right]^{-\frac{1}{2}} \tag{C-11}$$

$$\Delta\varphi = \tan^{-1}\left[\frac{(p/\omega)\left(H - \frac{I_x}{I}T\right)}{\sqrt{-M}} + \frac{M_s}{M}}{(p/\omega)^2\left(1 - \frac{I_x}{I}\right) - 1}\right] \tag{C-12}$$

Resonance. For zero damping, the resonance criterion from equation (C-3) is simply

$$(\varphi')^2 - F(\varphi') + M = 0 \tag{C-13}$$

or from (C-2) we can show that

$$pl/v = \varphi_1' \quad \text{or} \quad pl/v = \varphi_2'$$

Statically stable rockets can experience resonance only when $pl/v = \varphi_1'$, the nutation rate, since the precession rate is opposite to the direction of the axial

spin. Equation (C-13) can be re-written to obtain

$$\left(\frac{p}{\omega}\right)^2 \left(1 - \frac{I_x}{I}\right) = 1 \qquad \text{(C-14)}$$

which is the usual resonance criterion for aerodynamically stable rockets. It follows that $I_x/I < 1$, which is not difficult to satisfy for sounding rockets. It will also be noted that for $I_x/I \ll 1$ the resonance condition is very nearly equivalent to $p/\omega = 1$.

Trim Angle of Attack at Resonance. Combining the resonance criterion given by equation (C-14) with equations (C-6) and (C-8), we obtain

$$\left(\frac{K_3}{K_1}\right)_{p=\omega, \text{ resonance}} = \frac{\left[H - \frac{I_x}{I} r\right]}{\sqrt{1 - \frac{I_x}{I}}\sqrt{-M}} + \frac{M_s}{M} \qquad \text{(C-15)}$$

$$\left[\Delta\varphi\right]_{\text{resonance}} = \tan^{-1}(-\infty) = -(\pi/2) \qquad \text{(C-16)}$$

Another quantity which is of interest at resonance is the derivative of $\Delta\varphi$ with respect to p/ω. Thus, from (C-12) we obtain

$$\frac{d\,\Delta\varphi}{d(p/\omega)} = -\left\{ \frac{(p/\omega)^2\left(1 - \frac{I_x}{I}\right)\frac{\left(H - \frac{I_x}{I} r\right)}{\sqrt{-M}} + \frac{\left(H - \frac{I_x}{I} r\right)}{\sqrt{-M}} + 2\,(p/\omega)\left(1 - \frac{I_x}{I}\right)\frac{M_s}{M}}{\left[(p/\omega)^2\left(1 - \frac{I_x}{I}\right) - 1\right]^2 + \left[(p/\omega)\frac{\left(H - \frac{I_x}{I} r\right)}{\sqrt{-M}} + \frac{M_s}{M}\right]^2} \right\} \qquad \text{(C-17)}$$

For $\phi(\omega) \approx 1$ and $I_x / I << 1$, equation (C-17) reduces to

$$\frac{\partial \Delta\phi}{\partial \phi(\omega)} \approx \frac{-2}{\frac{\left(H - \frac{I_x}{I} T\right)}{\sqrt{-M}} + \frac{M_s}{M}} \qquad \text{(C-18)}$$

APPENDIX D.

Rolling Moments Due to Lateral Asymmetry

Rolling moments are produced by lateral aerodynamic and thrust asymmetry as well as by inclination of the principal axes with respect to the body reference axes. Since the body axes may be specified to be the principal axes, only the aerodynamic and thrust asymmetries need be considered here.

The thrust asymmetry will have a roll period of 2π, while the aerodynamic lateral asymmetry can have several roll periods, the most likely of which are π and 4π. A roll period of π, for example, could correspond to the two fins in one plane being larger by the same amount. However, for the purposes of this study, sufficient generality is achieved by assuming that the aerodynamic lateral asymmetry has a period of 2π. Further, a single lateral center of pressure will be assumed, applicable both to the normal force and side force, and in addition we let $C_{y_0} = C_{z_0} = C$.

The lateral displacement of the center of gravity and center of pressure is designated $\Delta\bar{y}$, while the thrust line offset is designated a. The orientations of the center of pressure and thrust line are defined by angles ϕ_{cp} and η, respectively. The orientation of the lateral asymmetries with respect to the body reference axes, which are in the fin planes, is depicted in Figure 41.

From Figure 41 it can be seen that the rolling moment due to lateral aerodynamic asymmetry can be expressed as

$$\left(\frac{qS}{d}\right)\left[\left(C_{N_\alpha} K_3\right)\sin\delta + C_{y'}\left(\Phi, K_3\right)\cos\delta\right] \qquad \text{(D-1)}$$

and that

$$\qquad \text{(D-2)}$$

In equation (D-1)

$$\left(K_3\right)_{p=0}$$

$$\qquad \text{(D-3)}$$

or

Thus, the rolling moment due to thrust is a slowly varying function of time, while the rolling moment due to aerodynamic lateral asymmetry varies with C_{N_α}, K_3, $C_{y'}$, and Φ.

APPENDIX E.

Derivation of an Equation for p/ω

An equation for p/ω, where ω is the undamped natural pitch frequency, can be obtained from the basic roll equation

$$\frac{I_x}{q S \ell} \dot{p} = \frac{M_x}{q S \ell} = C_{\ell_\delta} \delta + C_{\ell_p} \frac{p d}{2V} + C_{\ell_i} + C_{\ell_{\delta_g}} + C_{\ell_a} \qquad \text{(E-1)}$$

In the work which follows, it is assumed that the nominal rocket trajectory is unaffected by changes in the roll rate, even though the roll rate may depart significantly from the nominal roll performance.

Since for rockets like the Aerobee 150A, roll equilibrium is reached sometime prior to resonance, it is convenient to define a theoretical spin rate p_T, which is a function of time. By definition, the variation in p_T will be restricted to changes in the roll coefficients C_{ℓ_δ} and C_{ℓ_p} with Mach number, and to roll rate lag effect. Therefore, we can account for the time-wise variations in the theoretical spin rate by introducing $\dot{p}_T$, as follows:

$$\frac{I_x}{q S \ell} \dot{p}_T = C_{\ell_\delta} \delta + C_{\ell_p} \frac{p_T d}{2V}$$

which can be re-arranged to

$$C_{\ell_p}\left(\frac{d}{2V}\right) = \frac{\frac{I_x}{q S \ell} \dot{p}_T - C_{\ell_\delta} \delta}{p_T} \qquad \text{(E-2)}$$

Substituting (E-2) into (E-1), we obtain

$$\left(\frac{I_x}{q S \ell}\right) \dot{p} - \left(\frac{I_x}{q S \ell}\right)\left(\frac{p}{p_T}\right)\dot{p}_T = C_{\ell_\delta}\,\delta\left(1 - \frac{p}{p_T}\right) + C_{\ell_\alpha} + C_{\ell_{\Delta\bar{y}}} + C_{\ell_a} \tag{E-3}$$

To obtain an equation in terms of p/ω we note that

$$\left(\frac{p}{\omega}\right)^{\cdot} = \frac{\omega\dot{p} - p\dot{\omega}}{\omega^2} = \dot{p}/\omega - (p/\omega)\frac{\dot{\omega}}{\omega} \tag{E-4}$$

and re-arranging, we obtain

$$\dot{p} = \omega\left(\frac{p}{\omega}\right)^{\cdot} + (p/\omega)\dot{\omega} \tag{E-5}$$

By use of (E-5) we can re-write (E-3) as

$$\left(\frac{I_x}{q S \ell}\right)\left[\omega\left(\frac{p}{\omega}\right)^{\cdot} + (p/\omega)\dot{\omega} - (p/\omega)\frac{\dot{p}_T}{(p_T/\omega)}\right] = C_{\ell_\delta}\,\delta\left[1 - \frac{(p/\omega)}{(p_T/\omega)}\right]$$
$$+ C_{\ell_\alpha}\left[(p/\omega), \vec{\alpha}_0\right] + C_{\ell_{\Delta\bar{y}}}\left[(p/\omega), \vec{\alpha}_0\right] + C_{\ell_a} \tag{E-6}$$

This is a first-order differential equation in (p/ω) with time-varying coefficients. It is also non-linear because of the terms $C_{\ell_\alpha}(p/\omega, \vec{\alpha}_0)$ and $C_{\ell_{\Delta\bar{y}}}(p/\omega, \vec{\alpha}_0)$. It should be noted that the time-varying coefficients $\left(\frac{I_x}{q S \ell}\right)\omega$, $\left(\frac{I_x}{q S \ell}\right)\dot{\omega}$, $\left(\frac{I_x}{q S \ell}\right)\frac{\dot{p}_T}{p_T/\omega}$, $C_{\ell_\delta}\,\delta$, $\frac{C_{\ell_\delta}\,\delta}{(p_T/\omega)}$, and C_{ℓ_α} can all be determined from nominal trajectory data and linear aerodynamic derivatives.

To see more clearly the implications of the non-linear terms $C_{\ell_z}(p/\omega, \vec{\alpha}_o)$ and $C_{\ell_{\Delta\bar{y}}}(p/\omega, \vec{\alpha}_o)$, we expand them in the following form:

$$C_{\ell_z}(p/\omega, \vec{\alpha}_o) = f(K_3)\sin 4\Phi$$

$$C_{\ell_{\Delta\bar{y}}}(p/\omega, \vec{\alpha}_o) = -\frac{\Delta\bar{y}}{\ell}\left[C_{N_\alpha}(K_3)\sin\delta + C_{Y_\beta}(\Phi, K_3)\cos\delta\right]$$

where

$$\delta = \left[(\Phi_{30})_{p=0} - \Phi_{CP}\right] + \Delta\Phi$$

$$K_3 = (K_3)_{p=0}\left[\frac{K_3}{(K_3)_{p=0}}\right]$$

$$\Phi = \left[\pi/2 - (\Phi_{30})_{p=0}\right] - \Delta\Phi$$

The quantities $(K_3)_{p=0}$, $(\Phi_{30})_{p=0}$, and Φ_{CP} depend primarily upon the initial magnitude and orientation of the asymmetries; hence the inclusion of $\vec{\alpha}_o$ (the non-rolling trim angle of attack) in $C_{\ell_z}(p/\omega, \vec{\alpha}_o)$ and $C_{\ell_{\Delta\bar{y}}}(p/\omega, \vec{\alpha}_o)$. The quantities $\frac{K_3}{(K_3)_{p=0}}$ and $\Delta\Phi$ are non-linear functions of (p/ω) and the vehicle parameters, and are given by equations (C-11) and (C-12). Thus, we see that C_{ℓ_z} and $C_{\ell_{\Delta\bar{y}}}$ can be expressed entirely in terms of (p/ω), the magnitude and orientation of the asymmetries, and the time-varying vehicle and aerodynamic parameters.

APPENDIX F.

Circular Motion Theory

In this appendix, the exact non-linear equations of motion are developed for a symmetrical rocket. These equations consider the three rotational degrees of freedom. Finally, closed-form solutions are obtained for the case of near-circular motion.

When a triad described by axes , , has an angular velocity, , with respect to an inertial system, and further, when mass and moment of inertia are constant, Newton's Second Law of Motion can be expressed as

$$\vec{M} = [I]\dot{\vec{\omega}} + \vec{\omega} \times [I]\vec{\omega} \qquad \text{(F-1)}$$

where

$M = (\quad \quad)$

$\omega = (\quad \quad)$

For mass rotational symmetry, and a principal axis

$$[I] = \begin{bmatrix} I_x & 0 & 0 \\ 0 & I & 0 \\ 0 & 0 & I \end{bmatrix}$$

(F-1) can be re-written as

$$\vec{M} = \begin{bmatrix} I_x & 0 & 0 \\ 0 & I & 0 \\ 0 & 0 & I \end{bmatrix} \begin{bmatrix} \dot{p} \\ \dot{q} \\ \dot{r} \end{bmatrix} + \begin{bmatrix} \Omega_x \\ \Omega_y \\ \Omega_z \end{bmatrix} \times \begin{bmatrix} p \\ q \\ r \end{bmatrix} \begin{bmatrix} I_x & 0 & 0 \\ 0 & I & 0 \\ 0 & 0 & I \end{bmatrix} \qquad \text{(F-2)}$$

The angular velocity of the triad is described by its component angular velocities with respect to the x , y , z axes, which are

$$\begin{aligned} \Omega_x &= \dot{\varphi} - \dot{\psi} \sin\theta \\ \Omega_y &= \dot{\psi} \cos\theta \sin\varphi + \dot{\theta} \cos\varphi \\ \Omega_z &= \dot{\psi} \cos\theta \cos\varphi - \dot{\theta} \sin\varphi \end{aligned} \qquad \text{(F-3)}$$

These are derived from the Euler angle definitions of Figure 42. The above equations are general, and are not restricted to any Ω .

The selection of Ω to give a fixed-plane coordinate system has particular advantages, and simplifies the study of large angle of attack motions at high rates of spin.

Therefore, it is convenient to select Ω such that y is initially in the XY plane, and stays there, i. e., $\varphi \equiv \dot{\varphi} \equiv 0$. This leads to the set of fixed-plane axes x , y' , z' in Figure 42. With $\varphi \equiv \dot{\varphi} \equiv 0$, equations (F-3) become

$$\begin{aligned} \Omega_x &= -\dot{\psi} \sin\theta \\ \Omega_y &= \dot{\theta} \\ \Omega_z &= \dot{\psi} \cos\theta \end{aligned} \qquad \text{(F-4)}$$

and further, we have

$$p = \dot{\phi} - \dot{\psi} \sin\theta$$

$$q = \dot{\theta} \qquad \text{(F-5)}$$

$$r = \dot{\psi} \cos\theta$$

where the quantity $\dot{\phi}$ represents the roll of the missile with respect to the x, y, z coordinates. Substituting equations (F-4) into equation (F-2), we obtain

$$L = I_x \dot{p} \qquad \text{(F-6)}$$

$$M = I\ddot{\theta} + pr I_x + I r^2 \tan\theta \qquad \text{(F-7)}$$

$$N = I\dot{r} - p\dot{\theta} I_x - I r\dot{\theta} \tan\theta \qquad \text{(F-8)}$$

Equation (F-6) is just the roll equation, which can be treated separately.

To use equations (F-7) and (F-8) for the pitch-yaw dynamics, we must next expand the aerodynamic moments M and N. Since equations (F-7) and (F-8) are in terms of θ and r, we would prefer to use these quantities and their derivatives as our aerodynamic variables. To establish the aerodynamic moments in terms of θ and r it is necessary to select a direction for the aerodynamic velocity vector.

Selecting the aerodynamic velocity vector along the z axis, as in Figure 43, provides a simple correspondence between the total angle of attack, $\vec{\alpha}$, and the Euler angle θ, i.e. $\vec{\alpha} = \pi/2 + \theta$. Likewise, it can be seen that

the rotation of the angle of attack plane is simply $\dot{\psi}$ or $r/\cos\theta$. Further, the moment M is just the overturning moment, and the moment N the side moment or effective Magnus moment.

Aerodynamic Coefficients. The aerodynamic coefficients can be expected to depend upon at least θ, r, $\dot{\theta}$, $p\theta$, pr, $p\dot{\theta}$. We will also assume that all of the coefficients have some variation with θ.

Since it is desired to have aerodynamic expressions which can be generalized to any particular range of angle of attack, and since equations (F-7) and (F-8) contain θ in trigonometric form anyway, we arbitrarily describe the angle of attack dependence of the static aerodynamic overturning and Magnus moments by functions of the form

$$\left[C_{(\quad)}\right]\sin\vec{\alpha} \qquad \text{(F-9)}$$

and note that

$$\sin\vec{\alpha} \quad \cos\theta$$

Further, we have the useful relationship that

$$(C_{(\quad)})_{\vec{\alpha}=\pi/2} = \left[\frac{d(C_{(\quad)})}{d\alpha}\right]_{\vec{\alpha}=0} \qquad \text{(F-10)}$$

The static aerodynamic coefficients to be considered are therefore equivalent to the aeroballistic derivatives C_{M_α}, $C_{N_{p\alpha}}$, and C_{SM_α}.

The dynamic derivatives of interest are $C_{m_{\dot\theta}} = C_{m_q}$, C_{n_r}, $C_{m_{\dot\alpha}}$, $C_{n_{\dot\beta}}$, C_{n_p} and $C_{n_{p\dot\theta}}$, where each may be some function of θ. Because of our primary interest in near-circular motions ($\dot\theta \to 0$), the contributions of $C_{m_{\dot\alpha}}$ and $C_{n_{p\dot\theta}}$ should be negligible, and hence we will not consider these derivatives further. The contributions from C_{m_q} and $C_{n_{p\nu}}$ should likewise be small, because the spin dependent moments are small. The derivatives $C_{m_{\dot\theta}}$ and $C_{n_r}(\theta)$ contain a contribution which is directly related to a circular-type motion. This contribution arises from the effect of a circular motion on the aerodynamic roll angle, Φ. In circular motion at finite angle of attack, the aerodynamic roll angle at the fins, Φ_{fins}, differs from the static aerodynamic roll angle by an amount

$$\Delta\Phi = \tan^{-1}\left(\frac{\ell_{cp}\,\dot\theta}{V\cos\theta}\right) \qquad \text{(F-11)}$$

However, for the Aerobee 150A this $\Delta\Phi$ is on the order of one degree at resonance conditions; hence, the contribution of $\Delta\Phi$ to $C_{m_{\dot\theta}}$ and C_{n_r} will be neglected for the present study.

Of greatest significance is the angle of attack dependence of C_{n_r} due to pure circular motion. To see this dependence clearly, it is worthwhile to examine the fin loads resulting from both a planar motion and a lunar circular motion.

Fin Damping for Planar Motion and Lunar Circular Motion. Consider the damping moment produced by the fins of a rocket as a result of body rotations about the center of gravity (Figure 44). For the present example, we assume that the fin aerodynamic section force over the entire span depends only upon the local angle of attack.

For a planar motion we obtain immediately the familiar result

$$(C_{m_q})_{fins} = \frac{\partial C_m}{\partial \frac{q\ell}{V}} = \frac{\ell_T^2 c b}{S \ell^2} (C_{N_\alpha})_{fins} \qquad \text{(F-12)}$$

Next consider the same vehicle in a lunar circular motion with fins (1) and (3) always in the angle of attack plane, and fins (2) and (4) always normal to the angle of attack plane. The angle of attack plane rotation, $\dot{\psi}$, results in a varying local angle of attack along the span of the fins. However, because of symmetry, the (2) and (4) fins cannot contribute a yaw damping moment. The yawing moment produced by the (1) and (3) fins is

$$N_{fins} = (C_n)_{fins} \frac{\rho V^2 S \ell}{2} = -(C_{N_\alpha})_{fins} \xi(y) \frac{\rho V^2 \ell c}{2} \int_{-b/2}^{b/2} dy \qquad \text{(F-13)}$$

where

$$\xi(y) = \dot{\psi} r / V$$

$$r = \ell_T \sin \bar{\alpha} + y \cos \bar{\alpha}$$

and for small $\vec{\alpha}$

$$r \approx \ell_T \vec{\alpha} + y$$

We obtain from equation (F-13) that

$$[\ldots]_{fins} = \frac{\ell_T^2 c b}{S \ell^2} (C_{N_\alpha})_{fins} \vec{\alpha} \qquad \text{(F-14)}$$

Comparison of (F-12) with (F-14) shows that for small $\vec{\alpha}$

$$\ldots = C_{m_q} \qquad \text{(F-15)}$$

However, $\ldots \cos\theta = r/\sin\vec{\alpha} \approx r/\vec{\alpha}$ at small angles of attack;

therefore

$$\left[C_{m_{\ldots}\,fins} \right]_{\text{CIRCULAR MOTION}} = \left[C_{m_q\,fins} \right]_{\text{PLANAR MOTION}}$$

Thus, [illegible] and C_{m_q} are equivalent at small angles of attack, and will have the same angle of attack dependence. This equivalence can be expected to break down at larger angles of attack. The theoretical analyses of Reference 14 show that [illegible] and C_{m_q} can differ by a factor of two at ninety degrees angle of attack.

Complete Circular Motion Equations. Based on the foregoing, the two moment equations can be expressed approximately as

$$I\ddot{\theta} + p\dot{\psi}I_x + I_x\dot{\psi}^2\tan\theta = \frac{\rho V^2 S d}{2}\left[C_{m_{\pi/2}}\cos\theta + C_{m_q}\left(\frac{\dot{\theta}d}{2V}\right)\right] \qquad \text{(F-16)}$$

$$I\ddot{\psi} - pI_x\dot{\theta} + I\dot{\psi}\dot{\theta}\tan\theta = \frac{\rho V^2 S d}{2}\left[C_{n_{\pi/2}}\cos\theta + C_{n_{p_{\pi/2}}}\left(\frac{pd}{2V}\right)\cos\theta + C_{n_r}\left(\frac{rd}{2V}\right)\right] \qquad \text{(F-17)}$$

If we now let the aerodynamic coefficients be constant for a particular range of angle of attack, we can linearize equations (F-16) and (F-17) for near-circular motions by letting

$$\theta = \theta_0 + \Delta\theta$$

$$r = r_0 + \Delta r$$

and introducing the first-order approximations

$$\tan\theta = \tan\theta_0 + \Delta\theta\sec^2\theta_0$$

$$\cos\theta = \cos\theta_0 - \Delta\theta\sin\theta_0$$

It is also convenient to introduce the operator $\mathbb{D} = t^*\frac{d}{dt}(\quad)$, where $t^* = \frac{d}{V}$, and the non-dimensional angular velocities $\hat{p} = pt^*$, $\hat{r} = rt^*$, etc. Further, we let

$$I' = \frac{I}{\rho S d^3}$$

$$I_x' = \frac{I_x}{\rho S d^3}$$

The equations of motion now have the form

$$\left[I D^2 + I \quad \sec^2 \theta_0 + \frac{C_{m_{\pi/2}}}{2} \sin\theta_0 - \frac{C_{m_q}}{4}\right] \Delta\theta$$

$$+ \left[\quad I \quad \tan\theta_0 \right] \Delta\hat{r} \qquad \text{(F-18)}$$

$$= \quad I \quad \tan\theta_0 + \frac{C_{m_{\pi/2}}}{2} \cos\theta_0$$

$$\left[-\hat{p} I_x' - I \quad \tan\theta_0 \right] \Delta + \frac{C_{n_{\pi/2}}}{2} \sin\theta_0 + \frac{C_{n_{p\pi/2}}}{4} \hat{p} \sin\theta \Big] \Delta\theta$$

$$+ \left[\quad - \frac{C_{n_r}}{4} \right] \Delta\hat{r} \qquad \text{(F-19)}$$

$$= \frac{C_{n_r}}{4} \quad + \frac{C_{n_{\pi/2}}}{2} \cos\theta_0 + \frac{C_{n_{p\pi/2}}}{4} \hat{p} \cos\theta_0$$

The steady-state solutions of (F-18) and (F-19), $\Delta\theta = \Delta\dot{\theta} = \Delta\ddot{\theta} = \Delta r = \Delta\dot{r} = 0$, are of primary interest.

From (F-19) we obtain that

$$\hat{r}_0 = \frac{-2 \, C_{n_{\pi/2}} \cos\theta_0 - C_{n_{p\pi/2}} \hat{p} \cos\theta_0}{C_{n_r}} \qquad \text{(F-20)}$$

or that the angle of attack plane rotation, $\dot{\hat{\psi}}$, is

$$\dot{\hat{\psi}} = \frac{-2 \, C_{n_{\pi/2}} - C_{n_{p\pi/2}} \hat{p}}{C_{n_r}} \qquad \text{(F-21)}$$

Likewise, from (F-18) we have that

$$\sin\beta = -\cos\vec{\alpha} = \frac{\frac{C_{m_{\pi/2}}}{2I'} - \rho\dot{\hat{\psi}}\left(\frac{I_x}{I}\right)}{\hat{\psi}^2} \qquad \text{(F-22)}$$

For the special case of lunar circular motion

$$\dot{\hat{\psi}} = \hat{p}/\cos\vec{\alpha}$$

and (F-21) becomes

$$\hat{p} = \frac{-2\,C_{n_{\pi/2}}}{\frac{C_{n_\alpha}}{\cos\vec{\alpha}} + C_{n_{p_{\pi/2}}}}, \quad \text{lunar motion} \qquad \text{(F-23)}$$

and (F-22) becomes

$$\hat{p} = \sqrt{\frac{-C_{m_{\pi/2}}\cos\vec{\alpha}}{2I'}\Big/\left(1-\frac{I_x}{I}\right)}, \quad \text{lunar motion} \qquad \text{(F-24)}$$

By equating (F-23) and (F-24) we find the requirements for lunar circular motion, which is best expressed in terms of the side moment:

$$C_{n_{\pi/2}} = -\frac{1}{2}\left[\frac{C_{n_\alpha}}{\cos\vec{\alpha}} + C_{n_{p_{\pi/2}}}\right]\sqrt{\frac{-C_{m_{\pi/2}}\cos\vec{\alpha}}{2I'}\Big/\left(1-\frac{I_x}{I}\right)} \qquad \text{(F-25)}$$

An immediate consequence of (F-25) is that $C_{n_{\pi/2}}$ will in most cases have to be positive, because $C_{n_2} < 0$ and $|C_{n_2}| > |C_{n_{p_{\pi/2}}}|$. Also, since $I' = I/\rho S d^3$, the $C_{n_{\pi/2}}$ required for lunar circular motion is proportional to the square root of the air density. Thus, the side moment required for circular motion decreases with increasing altitude, and the possibility of a steady-state circular motion occurring becomes more likely as the vehicle ascends.

The lunar motion case is of great interest because under lunar motion conditions we can expect large values for $C_{n_{\pi/2}}$ for certain aerodynamic roll angles. To establish the exact circular motion characteristics with $C_{n_{\pi/2}}$ and $C_{m_{\pi/2}}$ dependent both upon $\vec{\alpha}$ and $\vec{\phi}$, it is most convenient to plot equations (F-23) and (F-24) as functions of $\vec{\alpha}$ and determine the solutions graphically for the various $\vec{\phi}$'s. An analysis of this type is summarized in Figure 45, which is for a Mach number and altitude representative of the nominal Acrobee 150A resonance conditions.

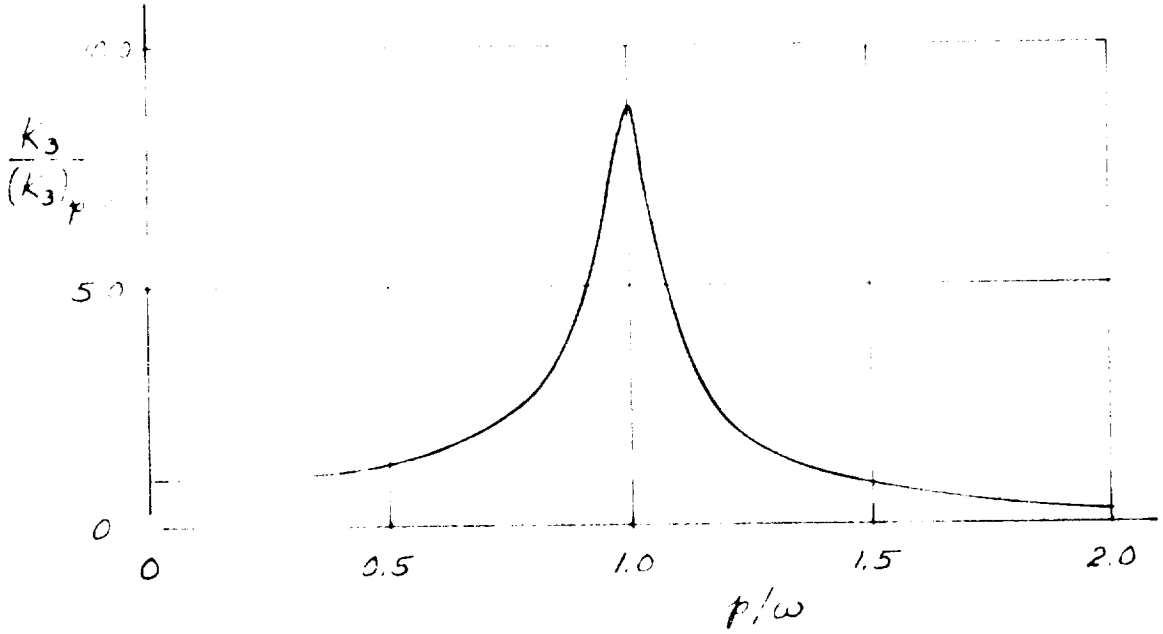

TRIM AMPLIFICATION

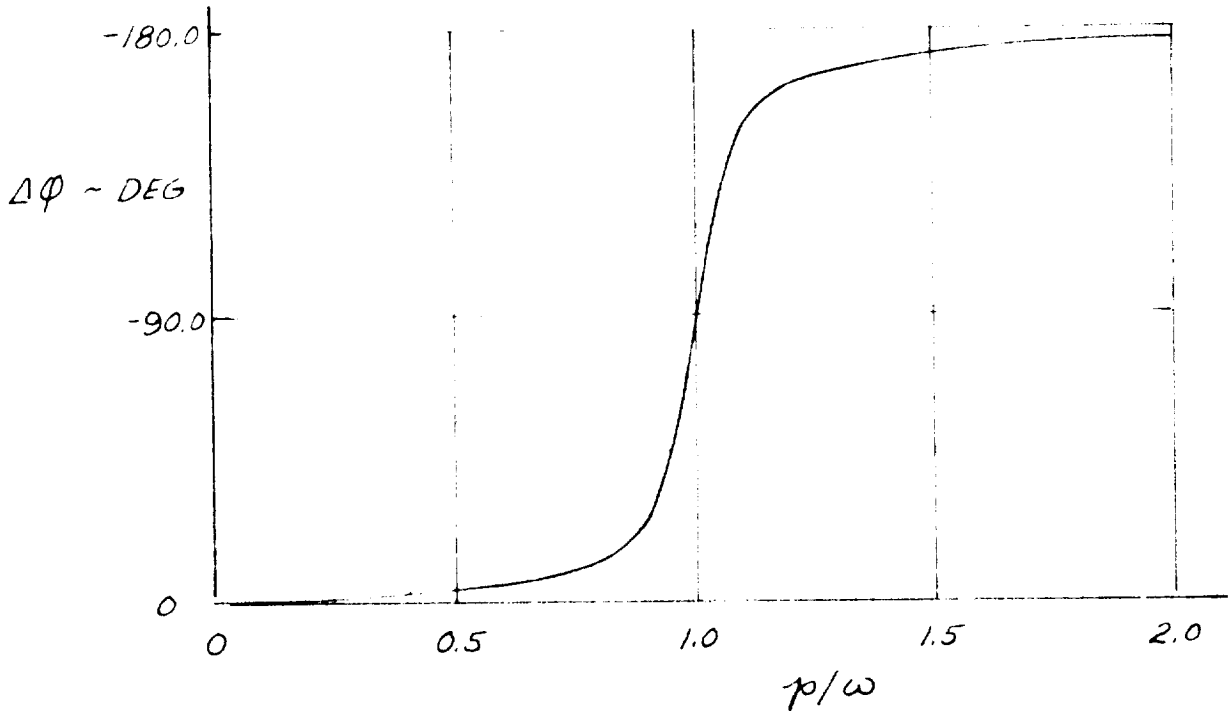

TRIM PHASE ANGLE

FIG 1 TRIM AMPLIFICATION FACTOR AND PHASE ANGLE

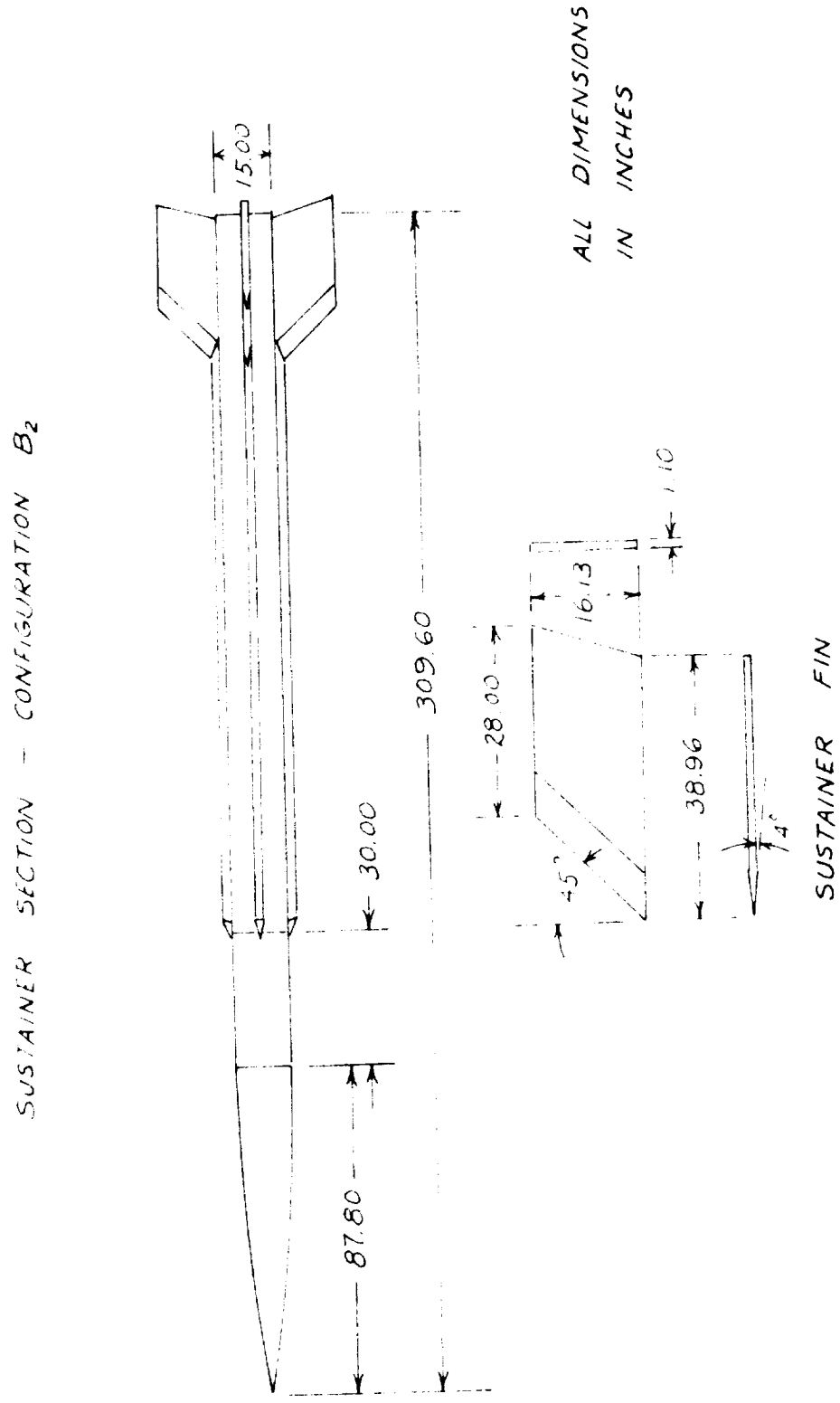

FIG 2 AEROBEE 150A CONFIGURATION

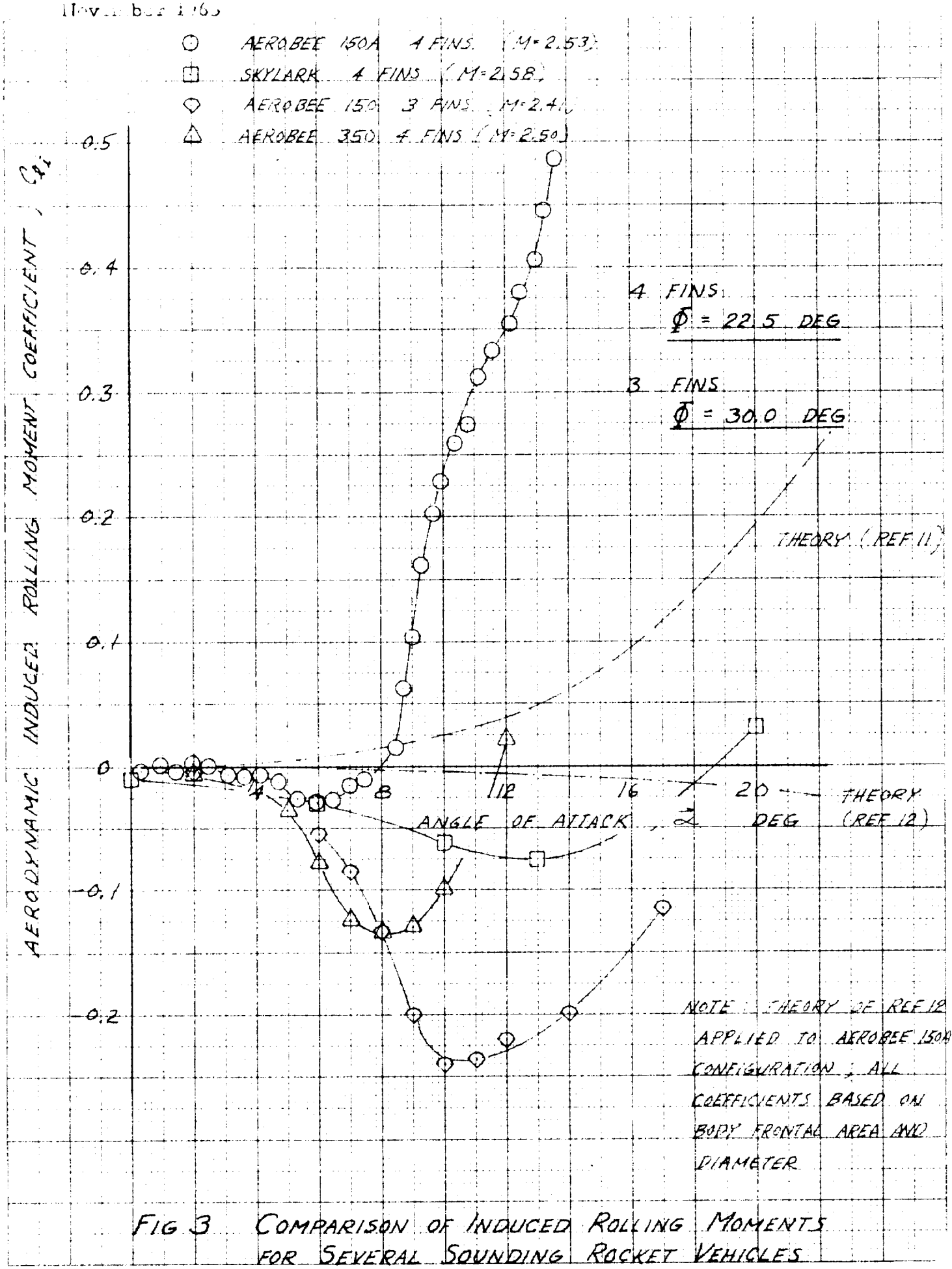

FIG 3 COMPARISON OF INDUCED ROLLING MOMENTS FOR SEVERAL SOUNDING ROCKET VEHICLES

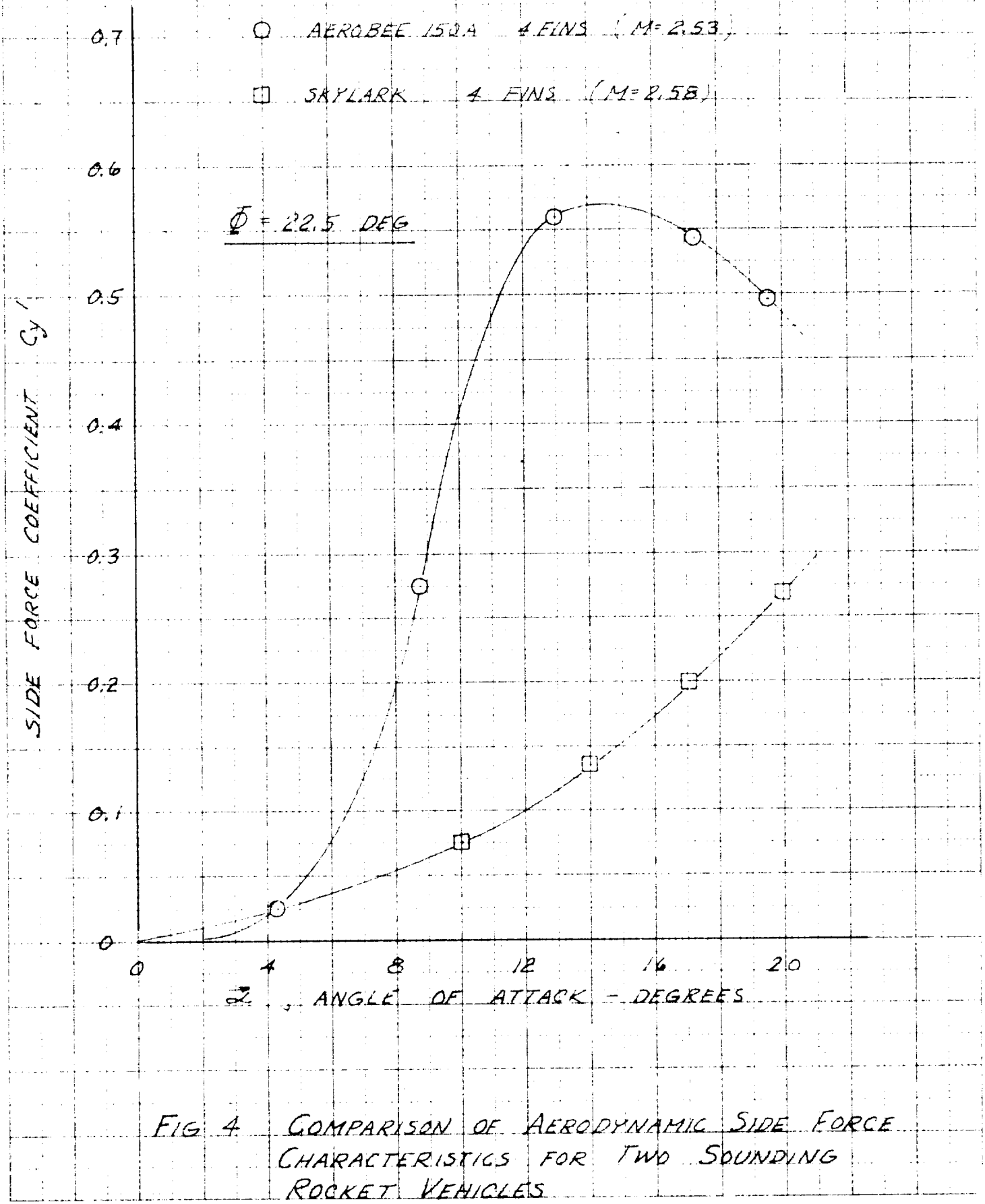

FIG 4 COMPARISON OF AERODYNAMIC SIDE FORCE CHARACTERISTICS FOR TWO SOUNDING ROCKET VEHICLES

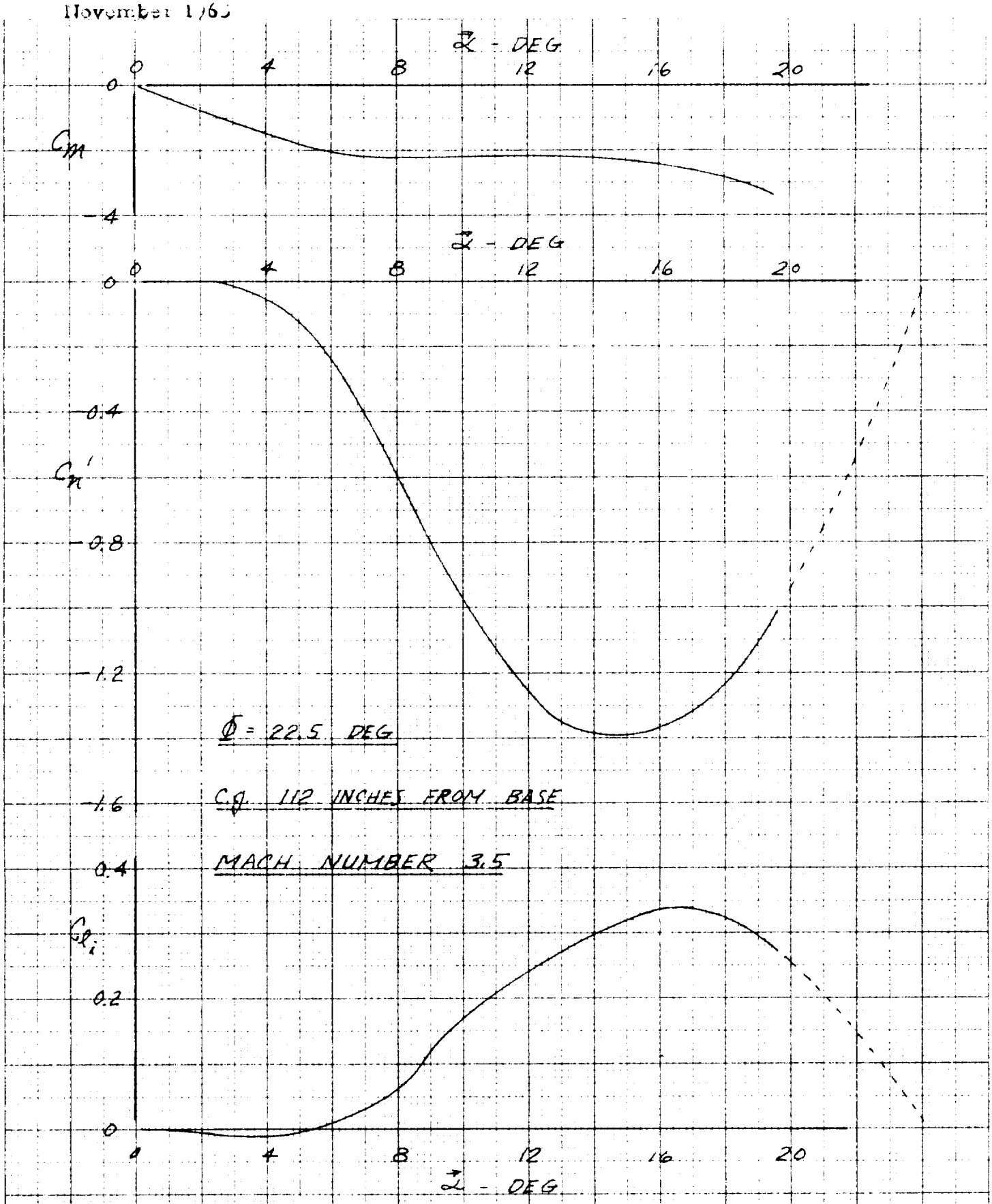

FIG 5 ROLL, PITCH, AND SIDE MOMENT CHARACTERISTICS OF THE AERODEE 150A-B_2 AT NOMINAL RESONANCE CONDITIONS

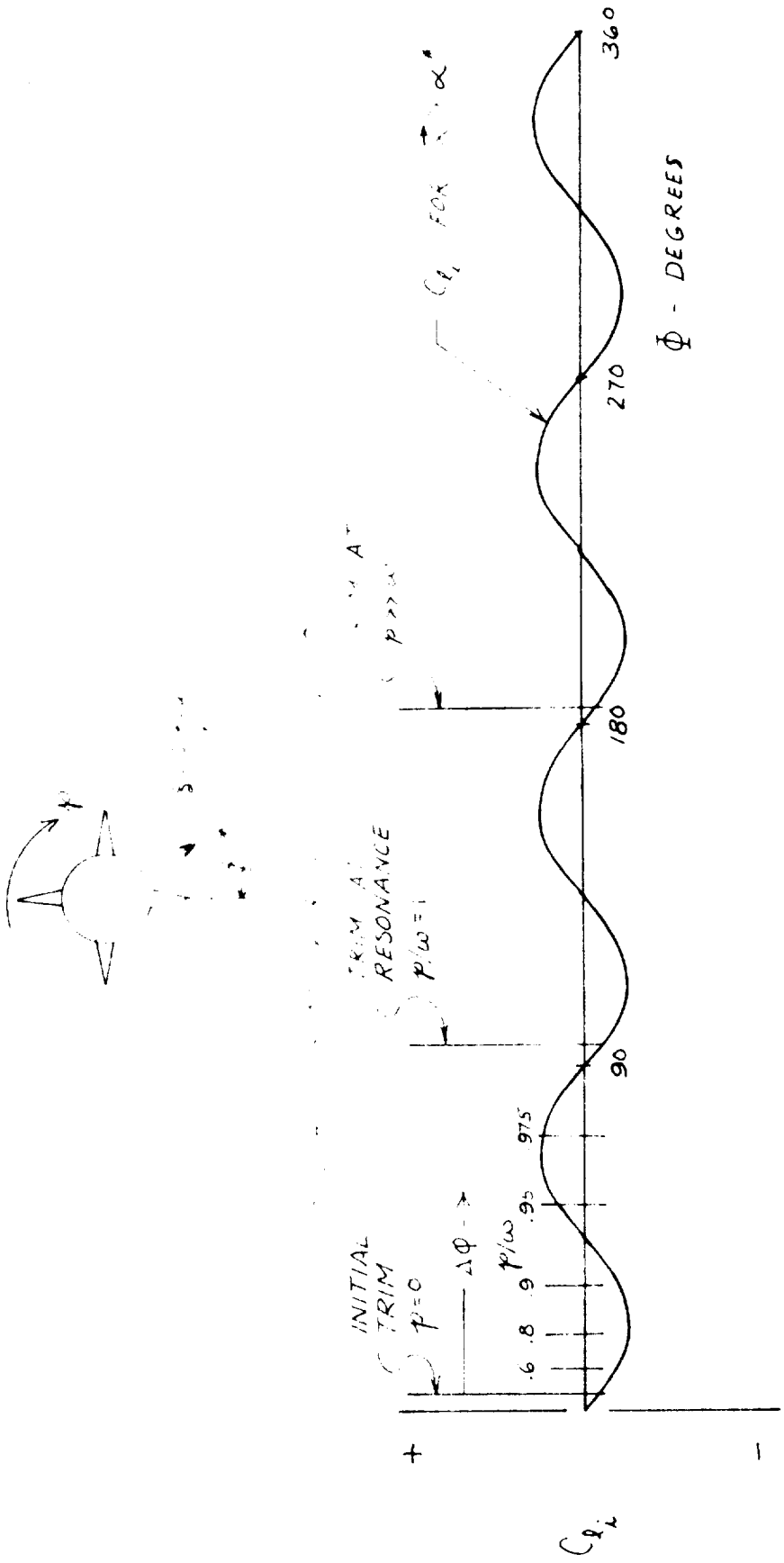

FIG 6 RELATION BETWEEN AERODYNAMIC INDUCED ROLLING MOMENT AND TRIM ORIENTATION

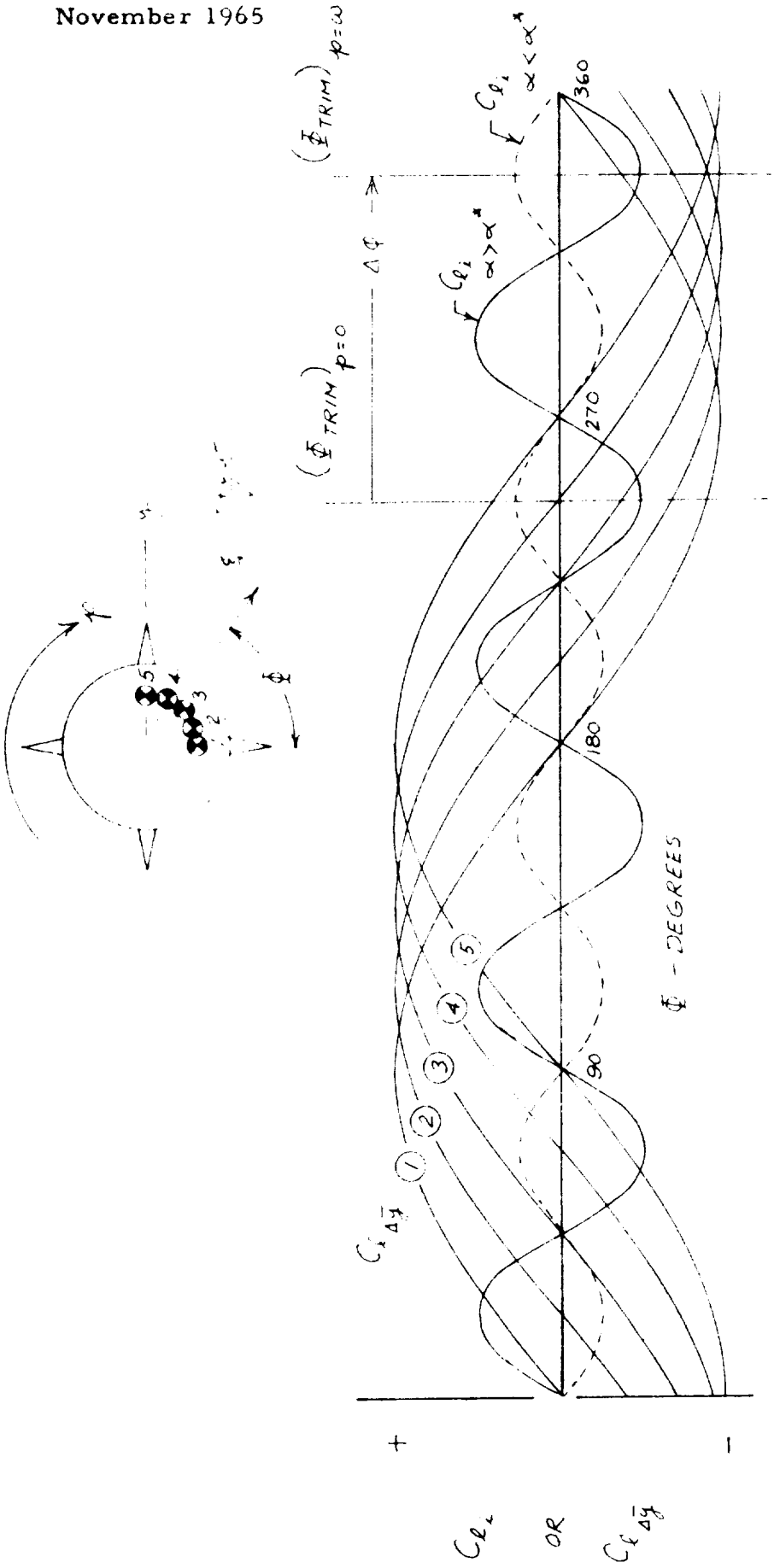

FIG 7 RELATION BETWEEN AERODYNAMIC INDUCED ROLLING MOMENT AND ROLLING MOMENT DUE TO LATERAL ASYMMETRY

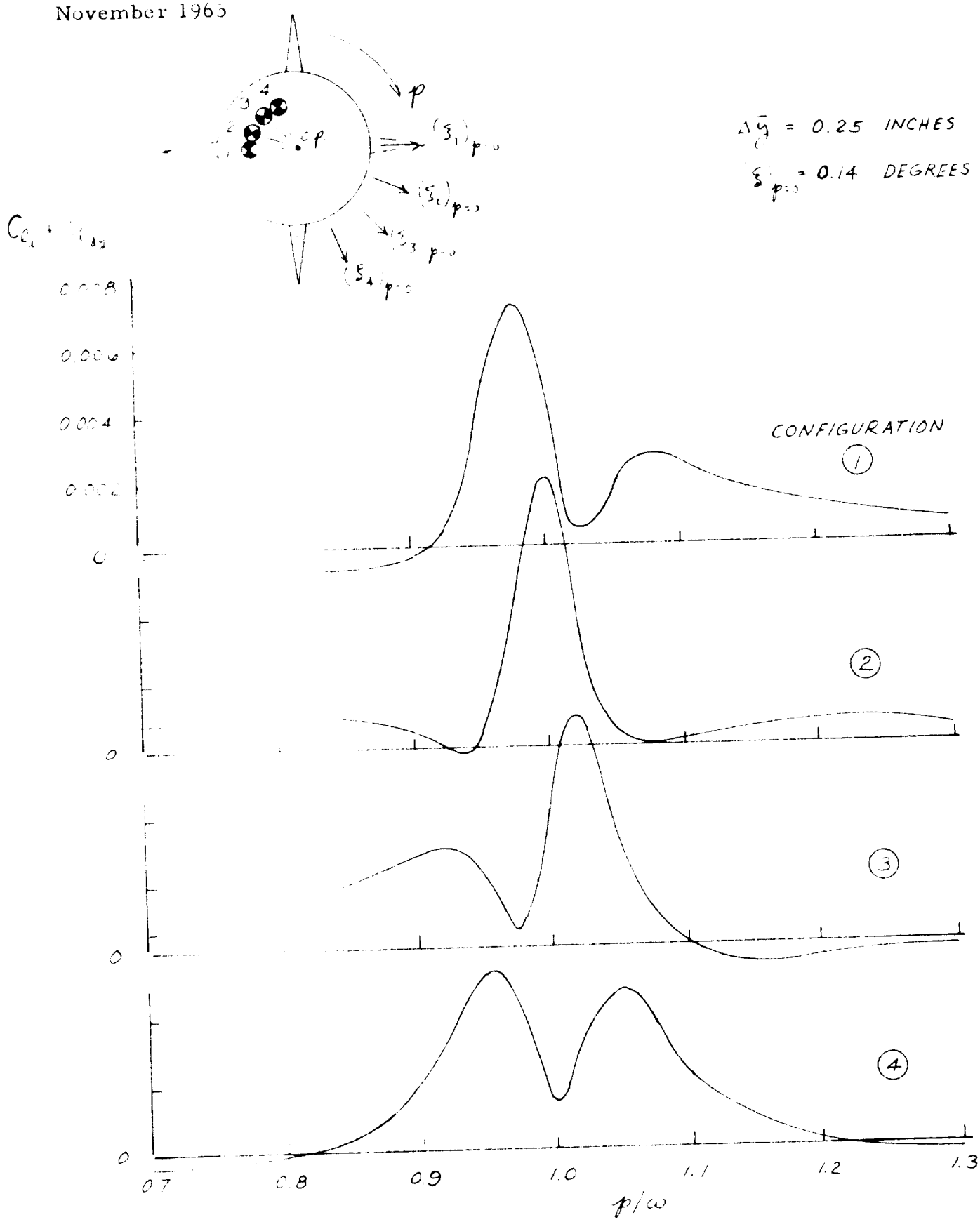

FIG 8 NUMERICAL EVALUATION OF $C_{\ell_z} + C_{\ell_{\Delta\bar{y}}}$ AS A FUNCTION OF p/ω FOR FOUR LATERAL ASYMMETRY CONDITIONS

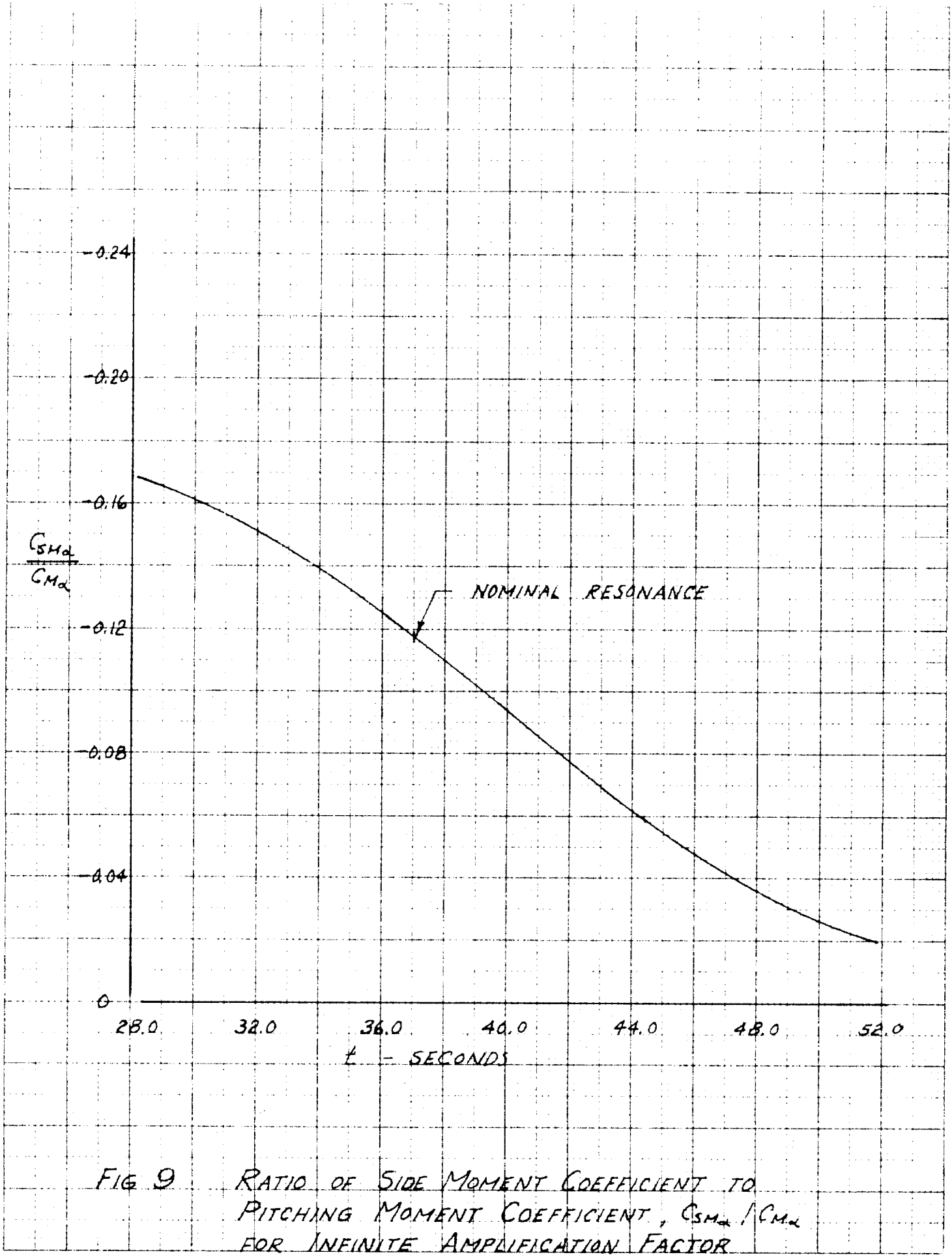

FIG 9 RATIO OF SIDE MOMENT COEFFICIENT TO PITCHING MOMENT COEFFICIENT, $C_{SM_\alpha} / C_{M_\alpha}$ FOR INFINITE AMPLIFICATION FACTOR

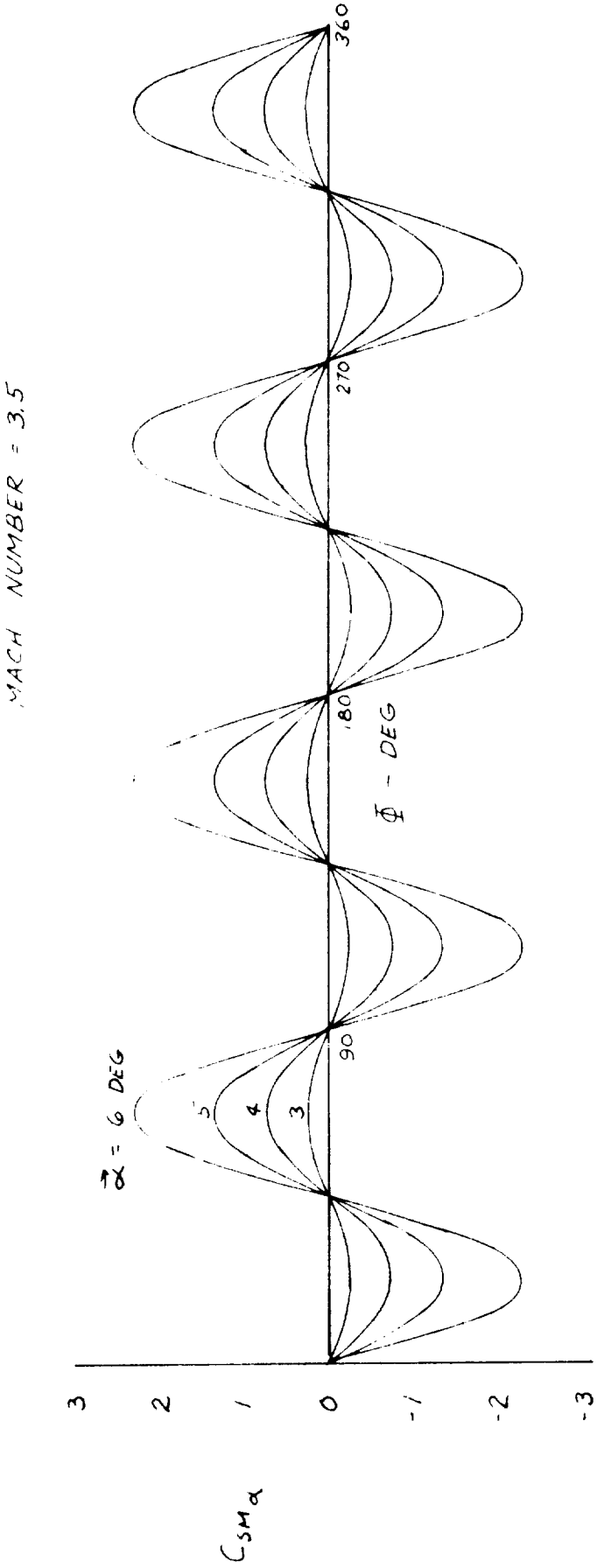

FIG 10 VARIATION OF SIDE MOMENT COEFFICIENT WITH AERODYNAMIC ROLL ANGLE

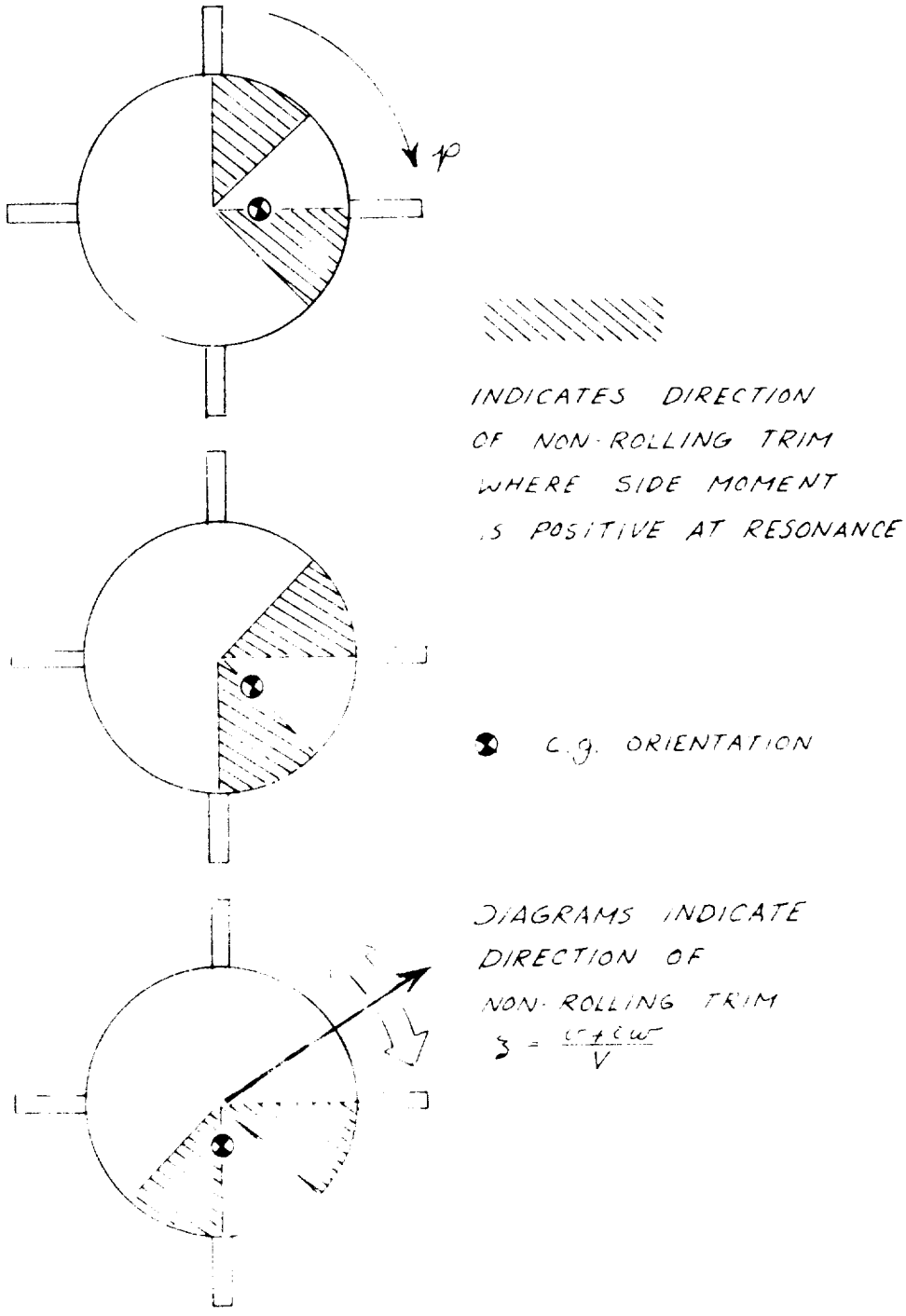

FIG 11 NON-ROLLING TRIM ORIENTATIONS FOR POSITIVE SIDE MOMENT AT RESONANCE AS A FUNCTION OF LATERAL ASYMMETRY ORIENTATION

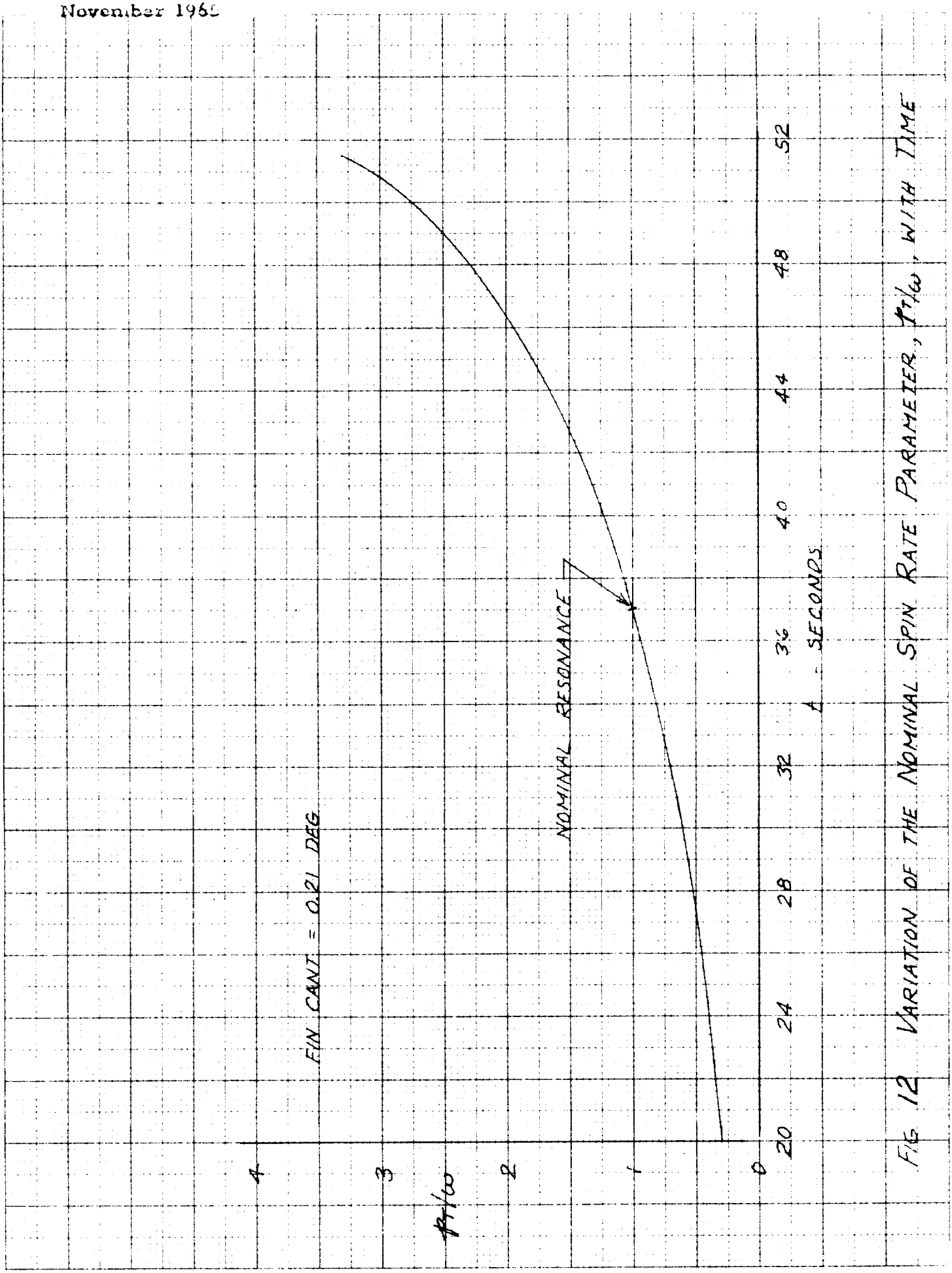

FIG 12 VARIATION OF THE NOMINAL SPIN RATE PARAMETER, p_1/ω, WITH TIME

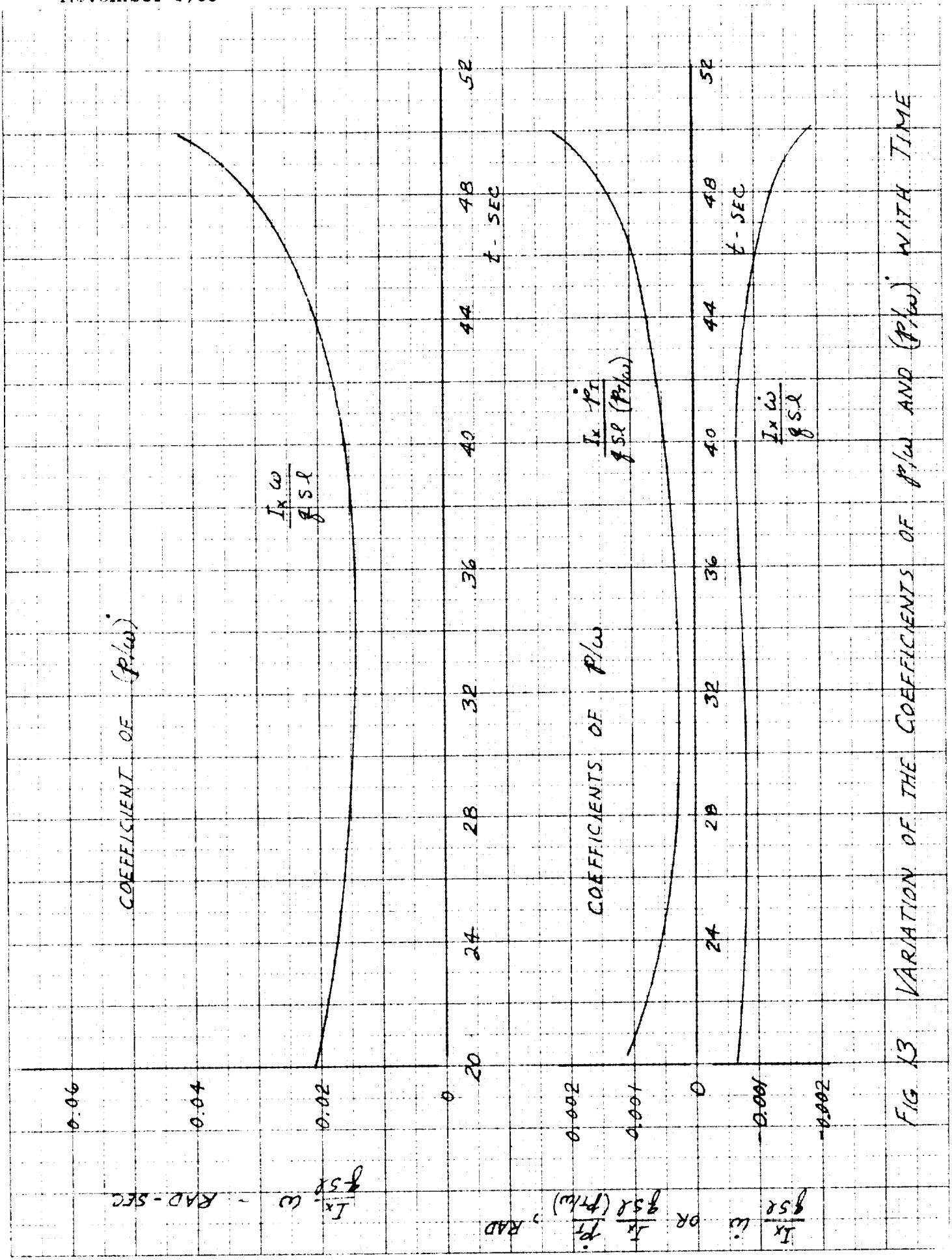

FIG 13 VARIATION OF THE COEFFICIENTS OF p/ω AND $(\dot{p}/\omega)^{\cdot}$ WITH TIME

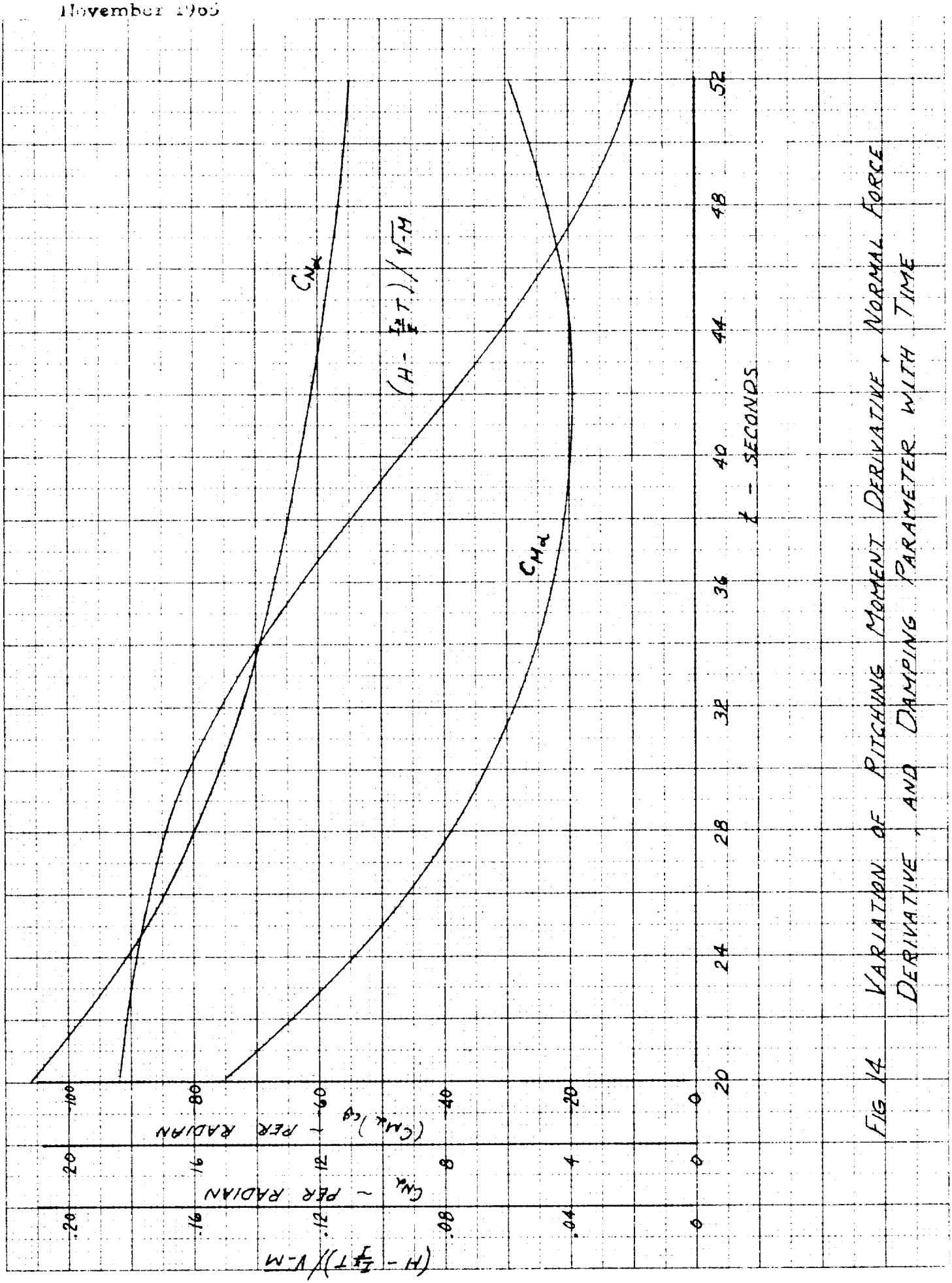

FIG 14 VARIATION OF PITCHING MOMENT DERIVATIVE, NORMAL FORCE DERIVATIVE, AND DAMPING PARAMETER WITH TIME

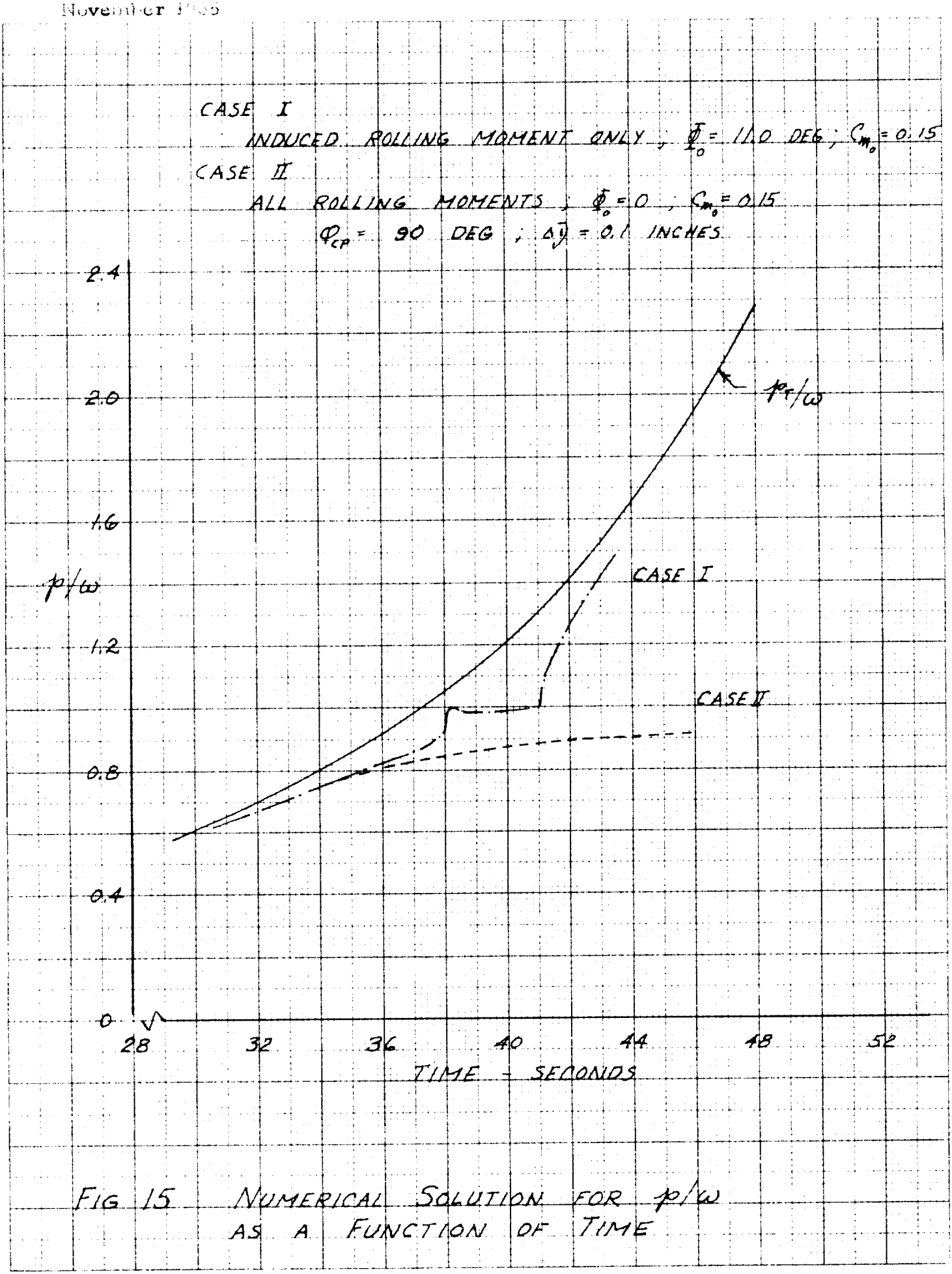

FIG 15 NUMERICAL SOLUTION FOR p/ω AS A FUNCTION OF TIME

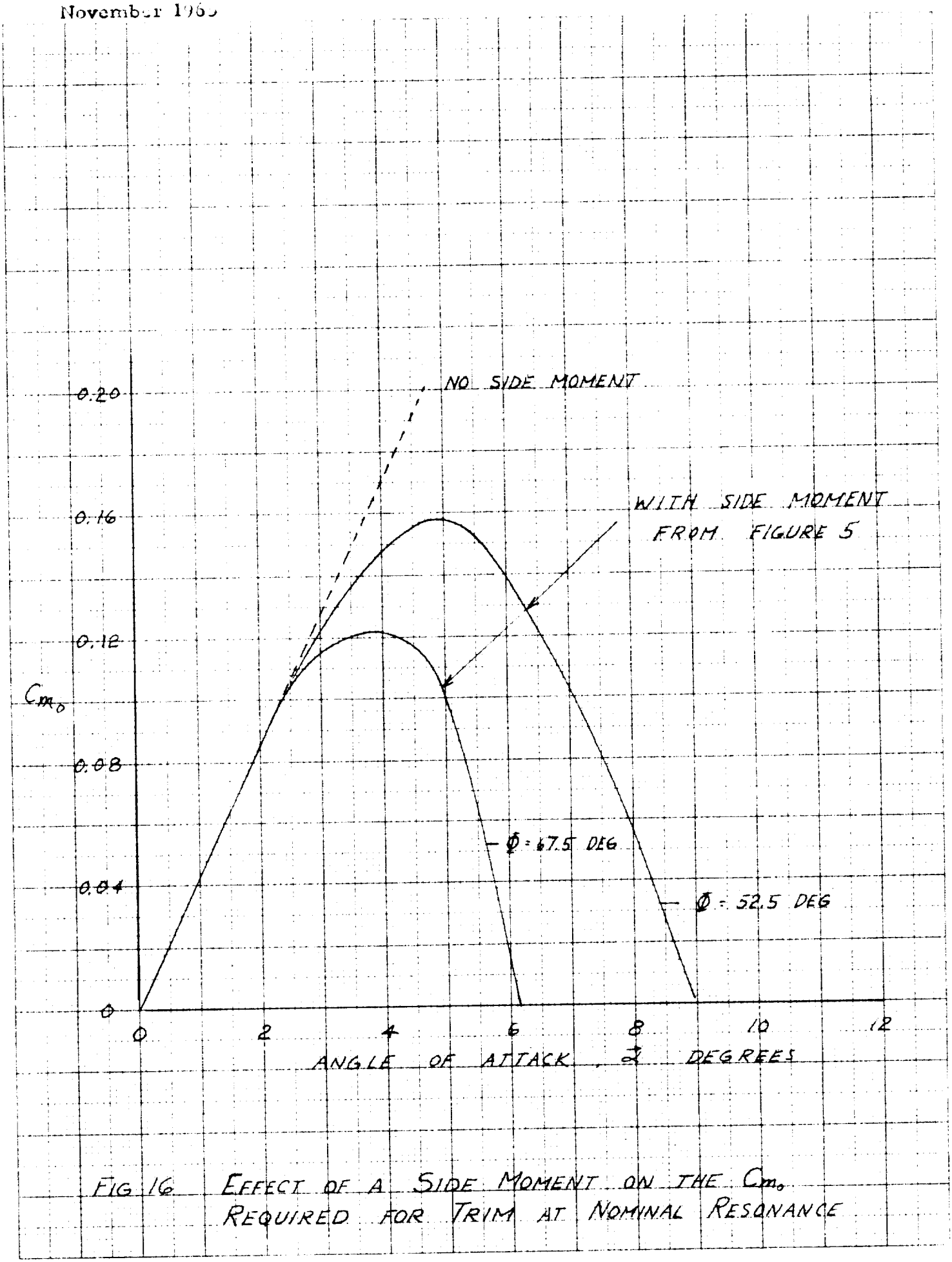

FIG 16 EFFECT OF A SIDE MOMENT ON THE C_{m_0} REQUIRED FOR TRIM AT NOMINAL RESONANCE

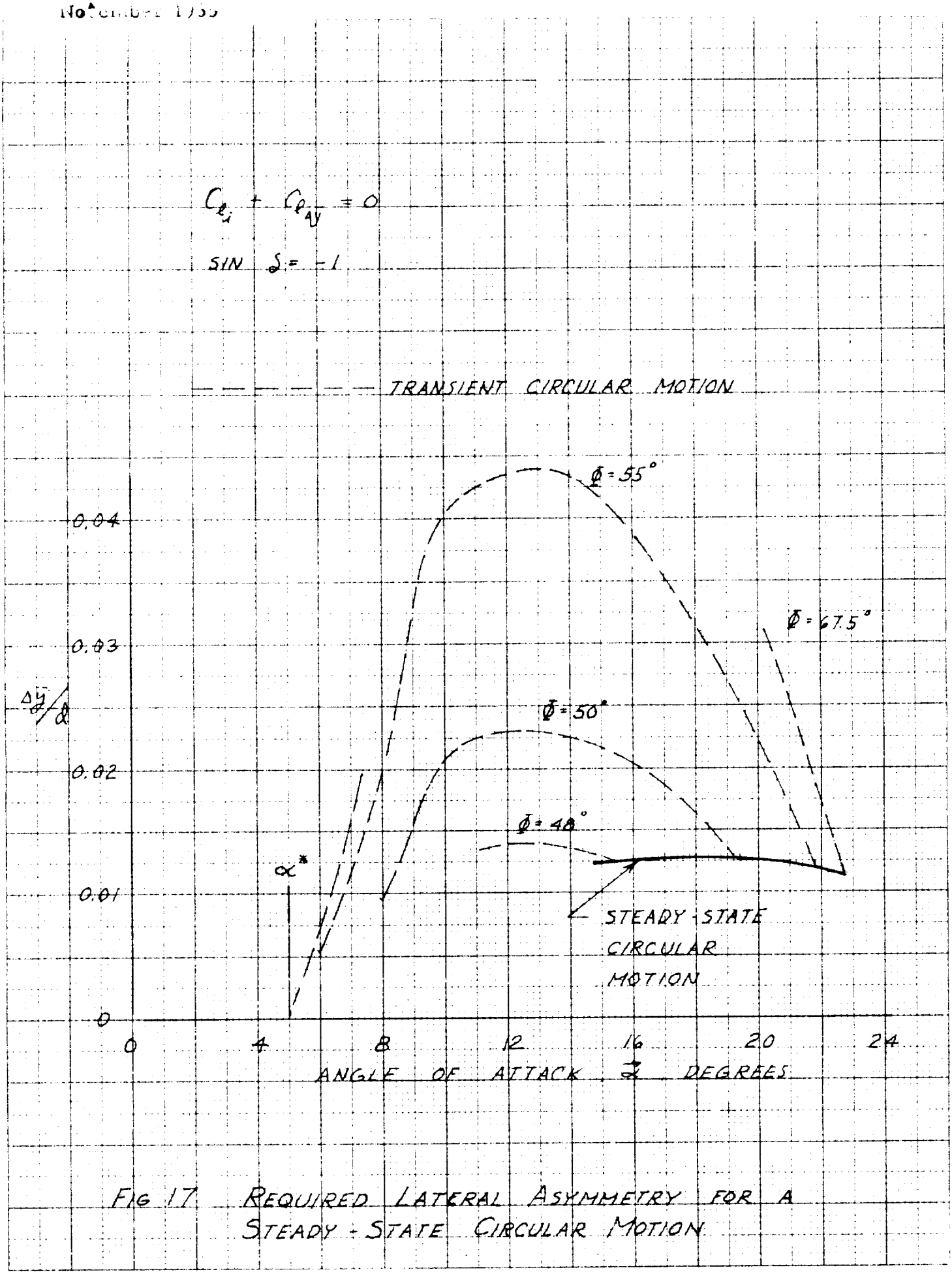

FIG 17 REQUIRED LATERAL ASYMMETRY FOR A STEADY-STATE CIRCULAR MOTION

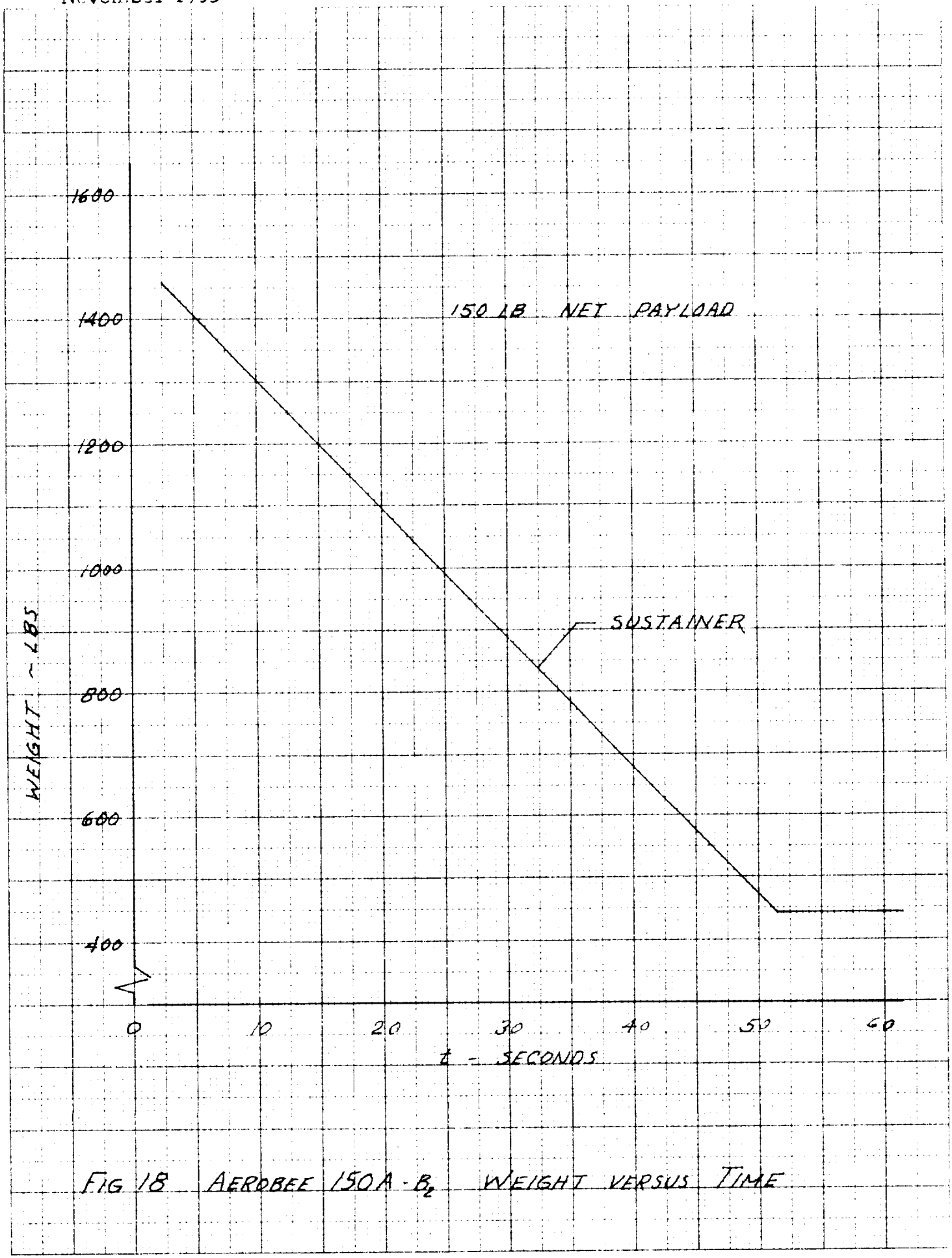

FIG 18 AEROBEE 150A - B_2 WEIGHT VERSUS TIME

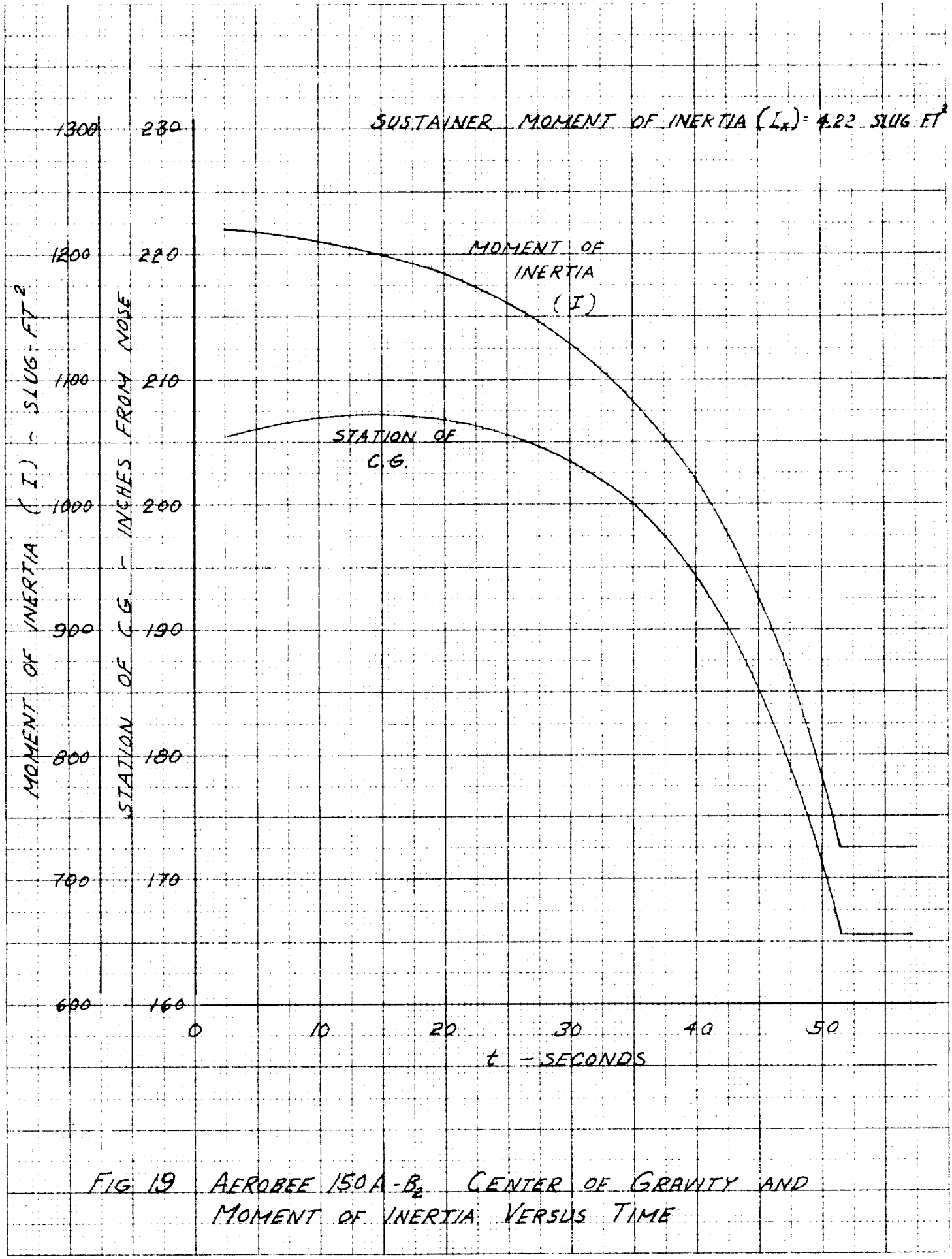

FIG 19 AEROBEE 150A-B_2 CENTER OF GRAVITY AND MOMENT OF INERTIA VERSUS TIME

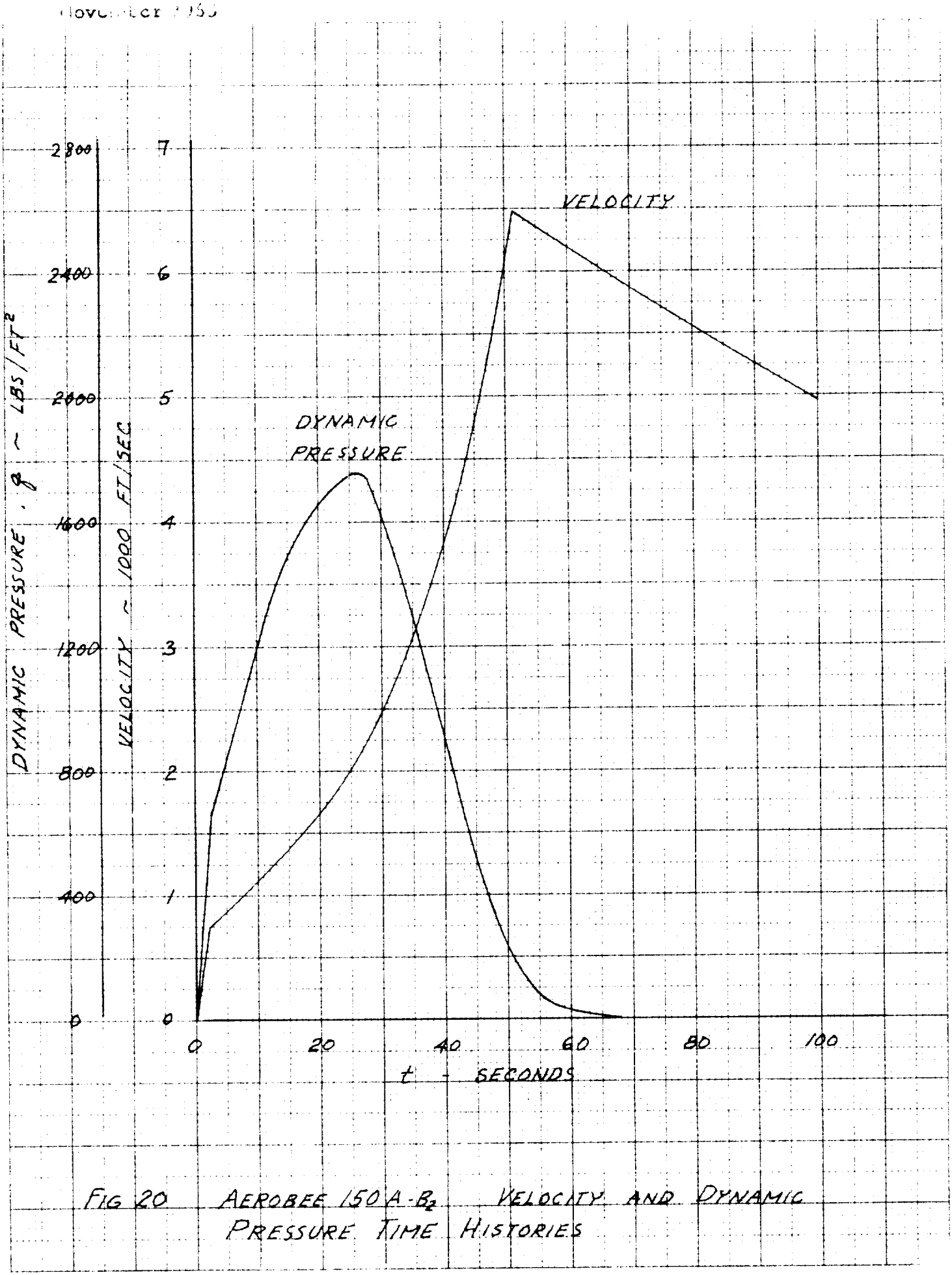

FIG 20 AEROBEE 150 A-B$_2$ VELOCITY AND DYNAMIC PRESSURE TIME HISTORIES

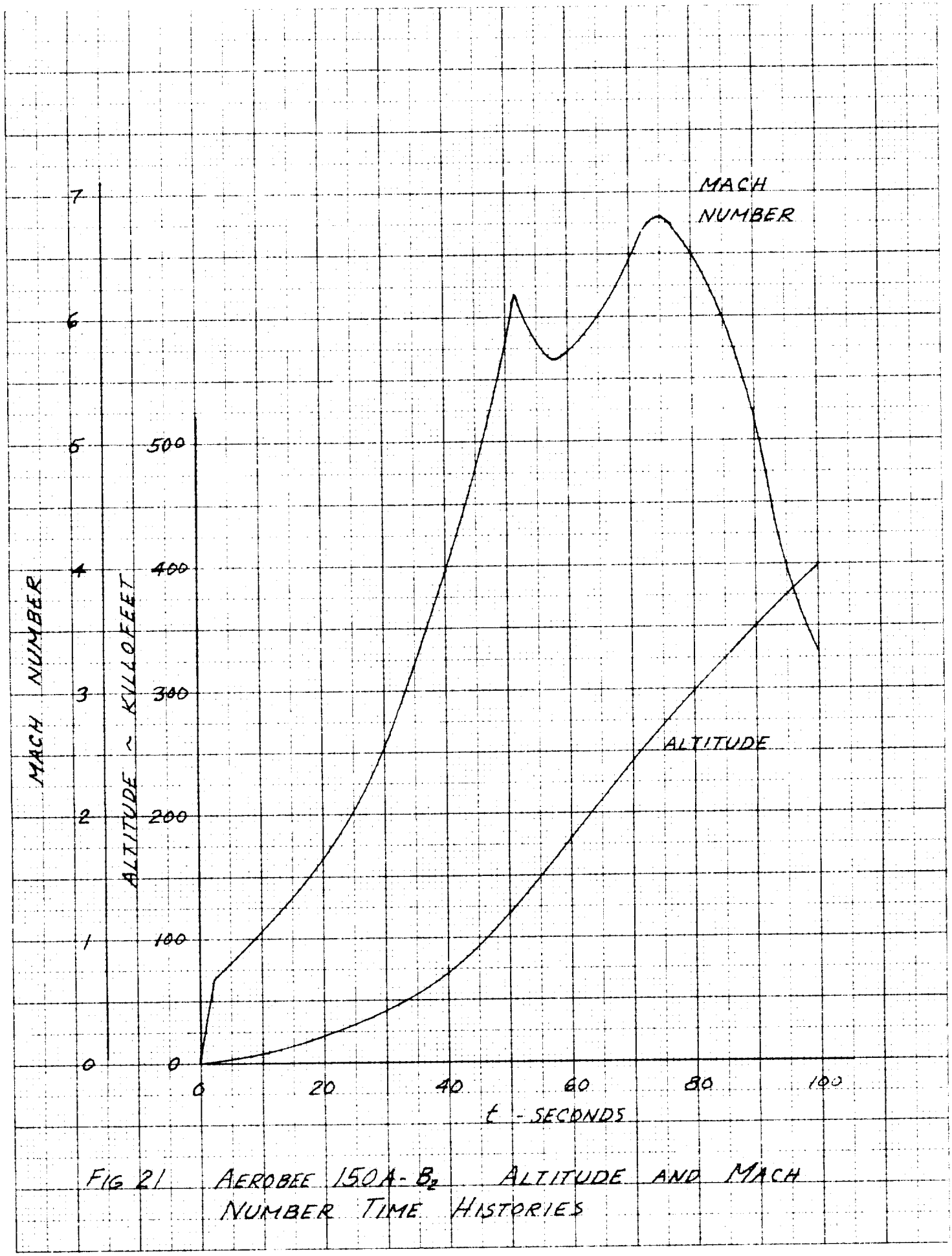

FIG 21 AEROBEE 150A-B_2 ALTITUDE AND MACH NUMBER TIME HISTORIES

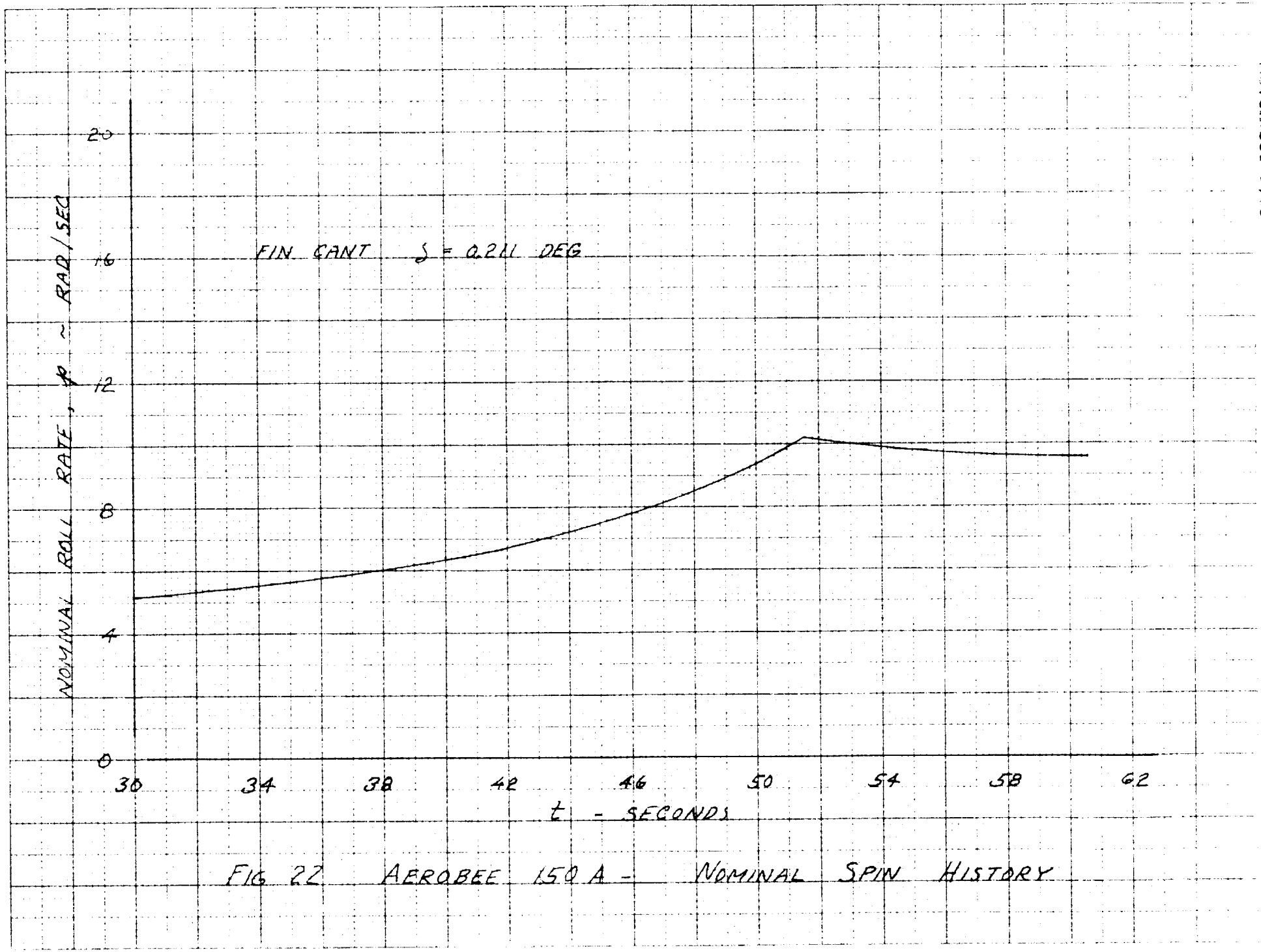

FIG 22 AEROBEE 150 A - NOMINAL SPIN HISTORY

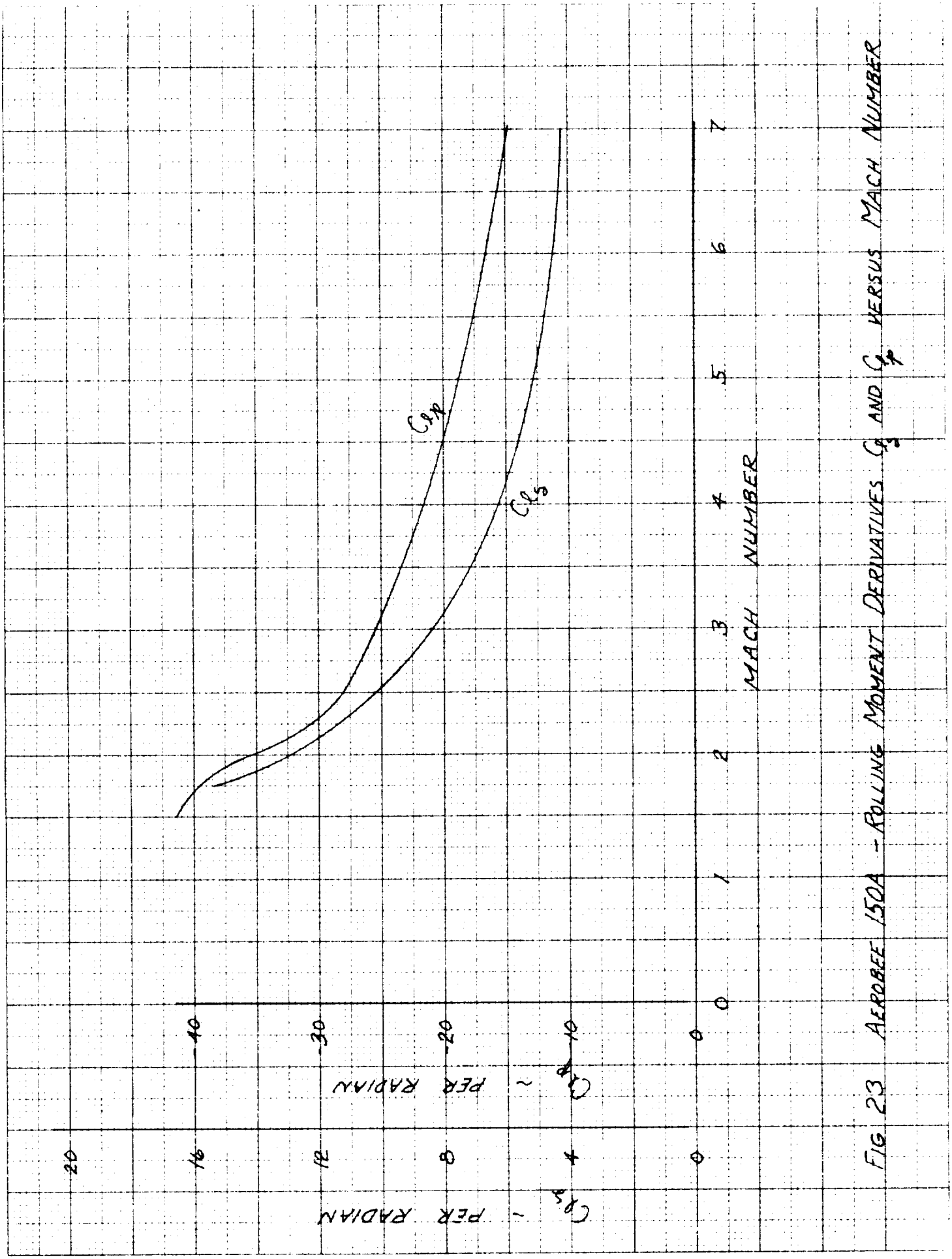

FIG 23 AEROBEE 150A - ROLLING MOMENT DERIVATIVES C_{l_δ} AND C_{l_p} VERSUS MACH NUMBER

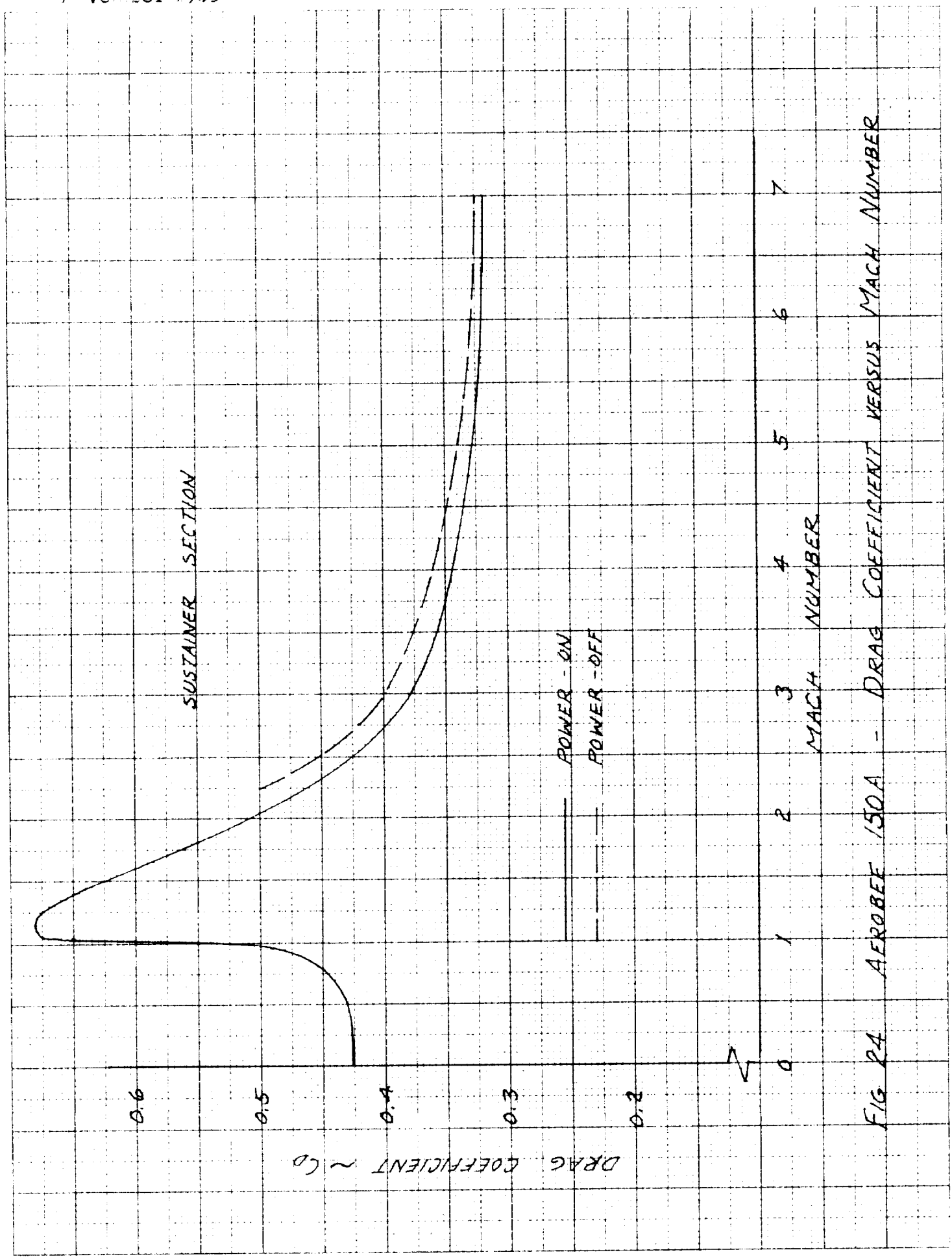

FIG 24 AEROBEE 150A - DRAG COEFFICIENT VERSUS MACH NUMBER

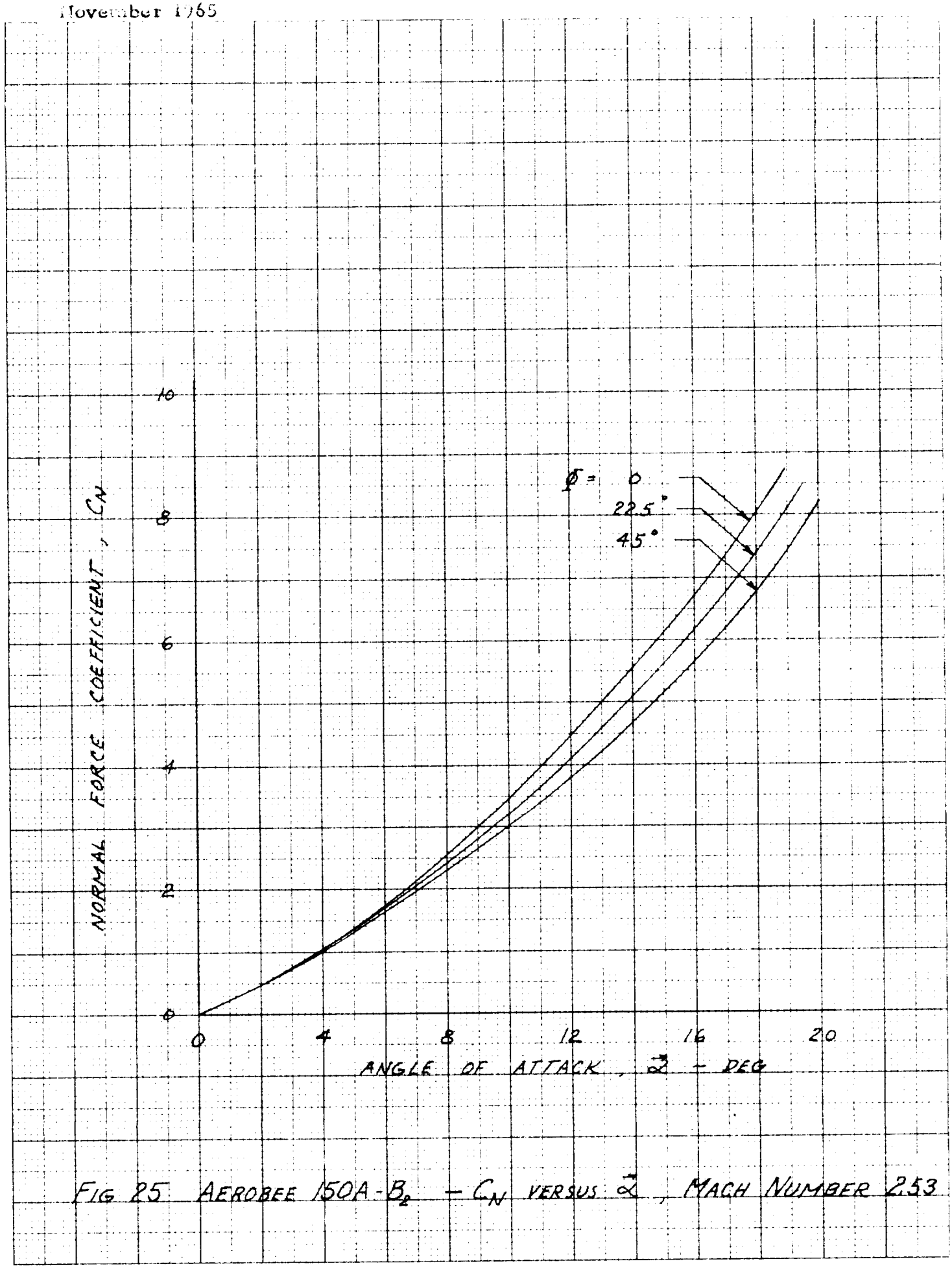

FIG 25 AEROBEE 150A-B_2 - C_N VERSUS α, MACH NUMBER 2.53

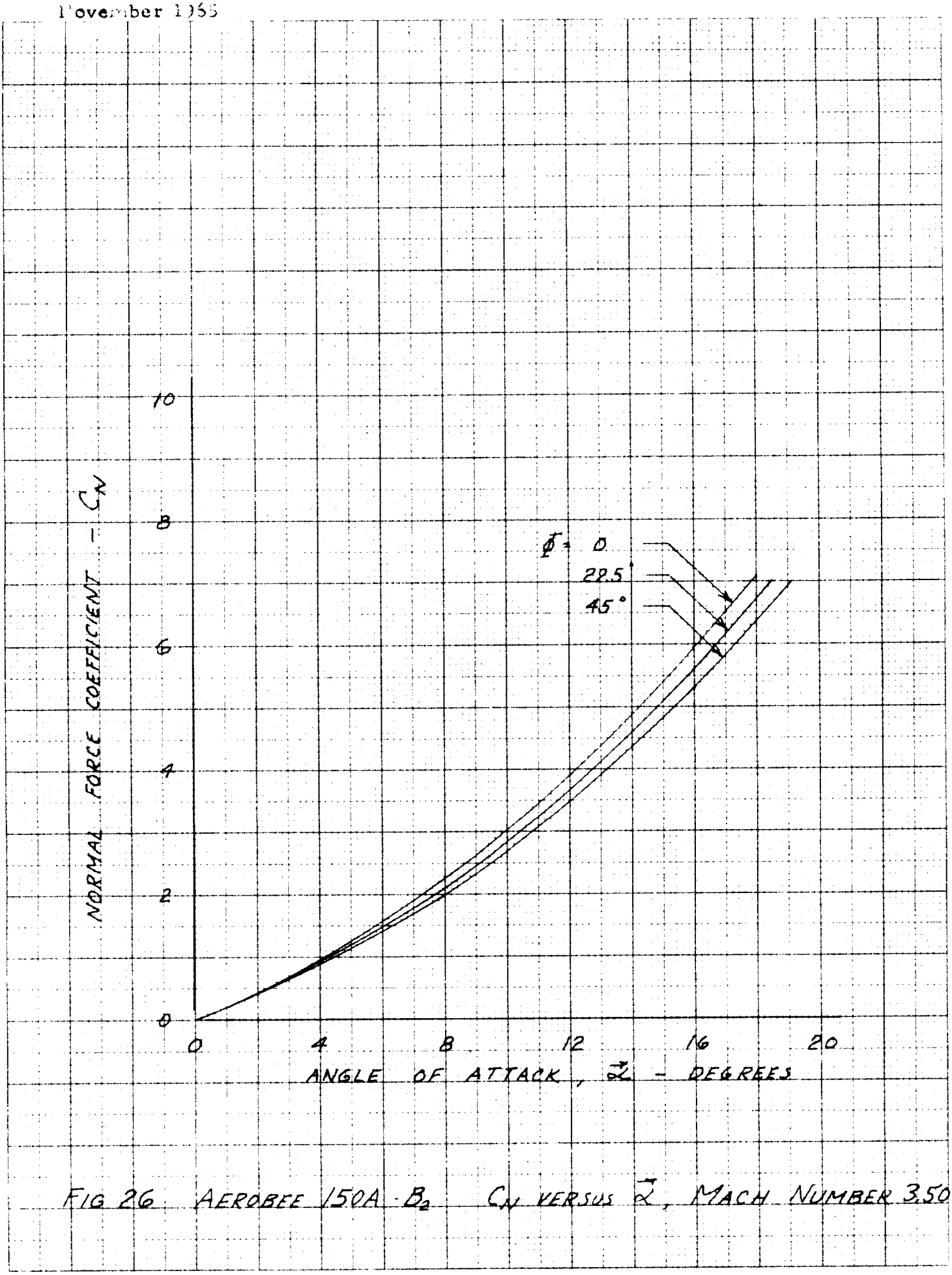

FIG 26 AEROBEE 150A - B_2 C_N VERSUS α, MACH NUMBER 3.50

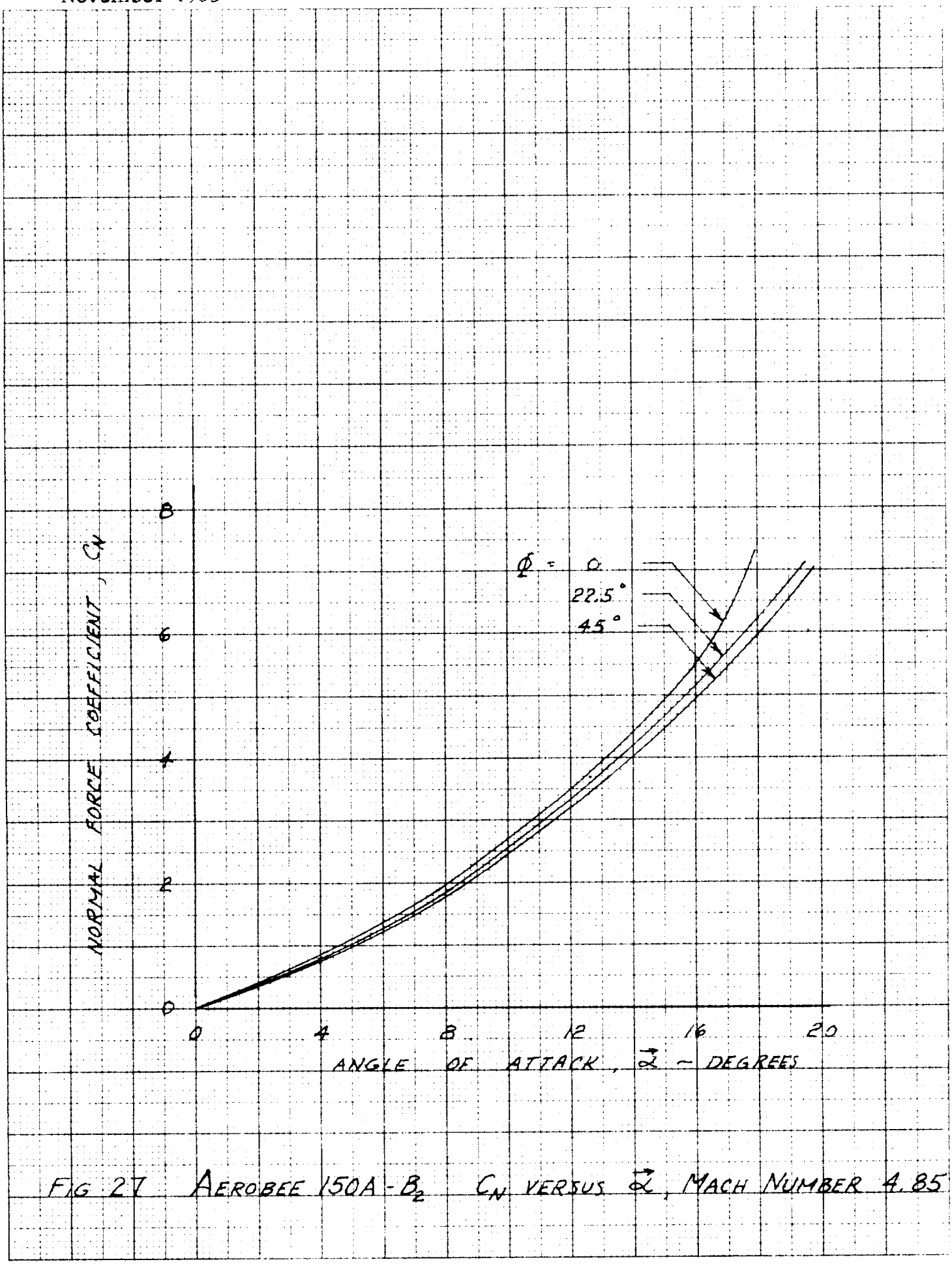

FIG 27 AEROBEE 150A-B_2 C_N VERSUS $\vec{\alpha}$, MACH NUMBER 4.85

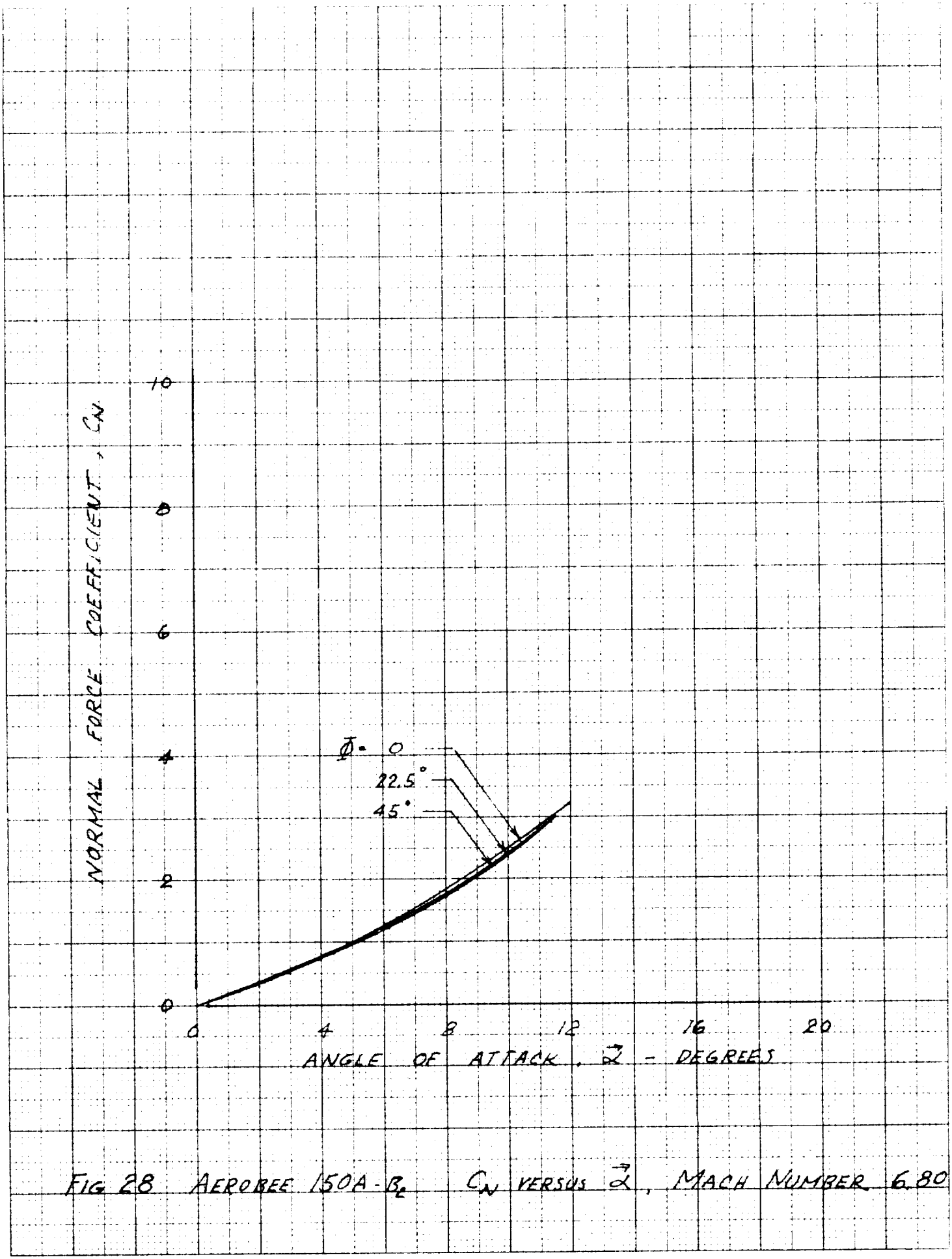

FIG 28 AEROBEE 150A-B_2 C_N VERSUS $\vec{\alpha}$, MACH NUMBER 6.80

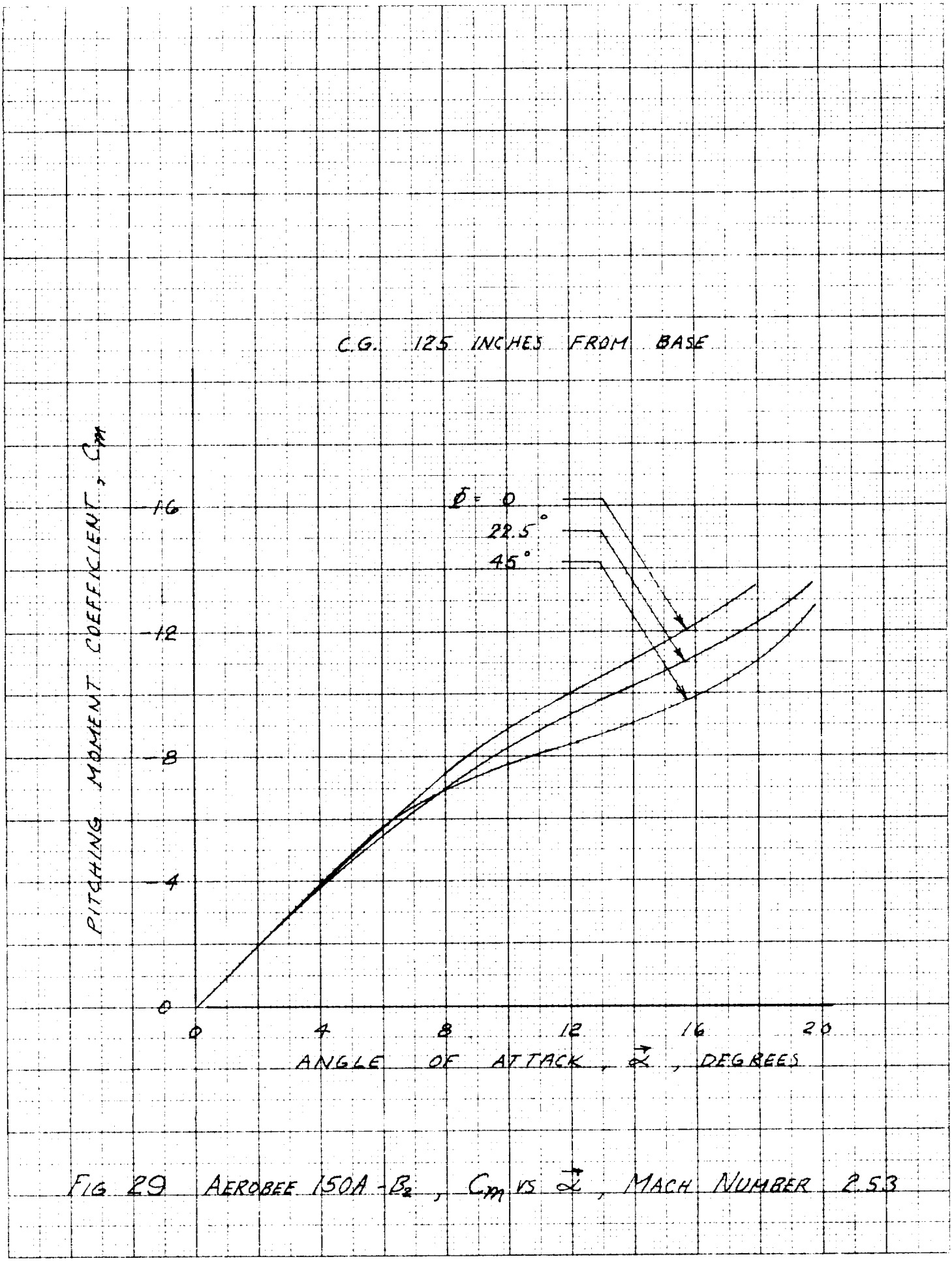

FIG 29 AEROBEE 150A - B_2, C_m VS $\vec{\alpha}$, MACH NUMBER 2.53

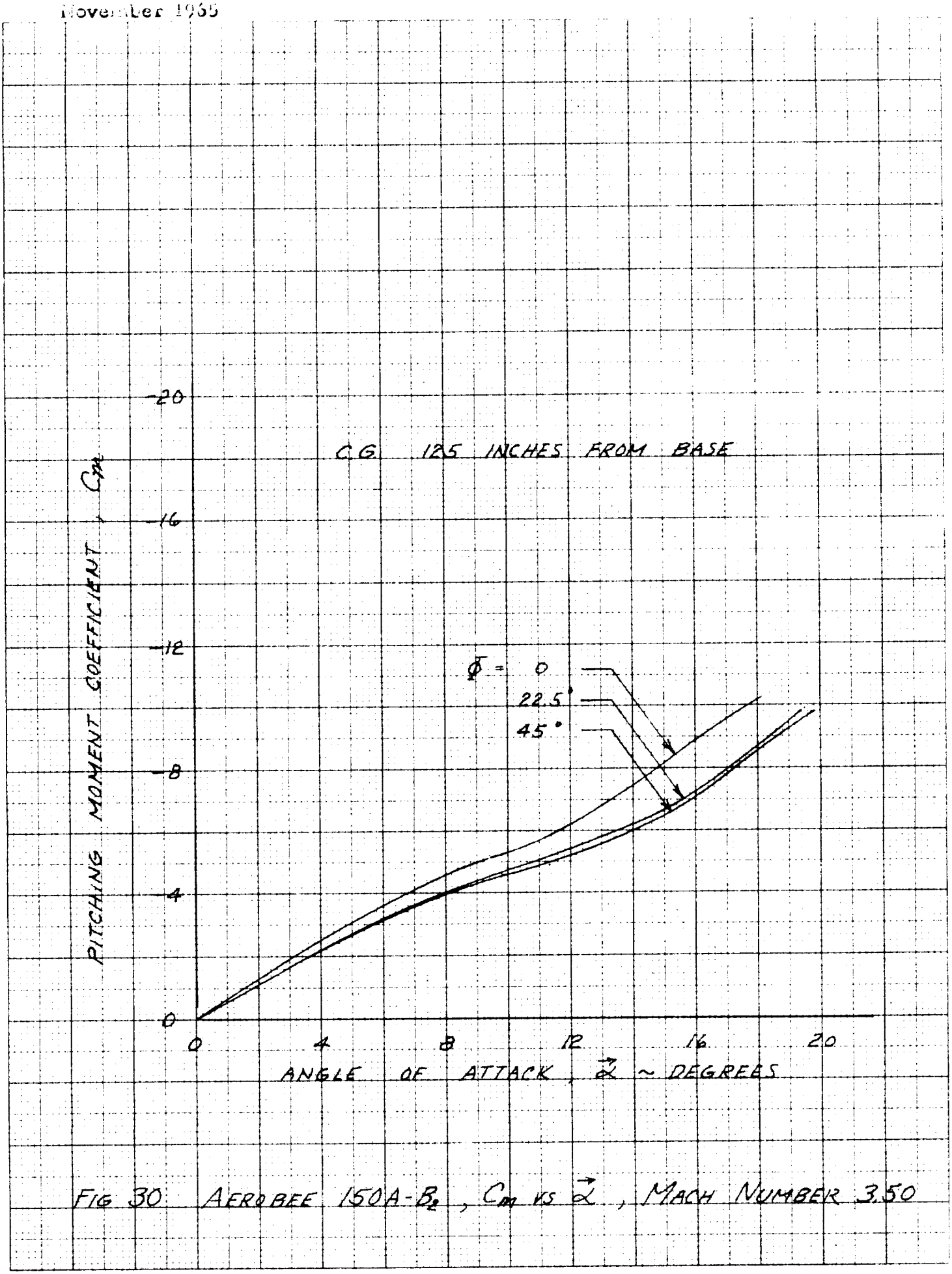

FIG 30 AEROBEE 150A-B_2, C_m VS $\vec{\alpha}$, MACH NUMBER 3.50

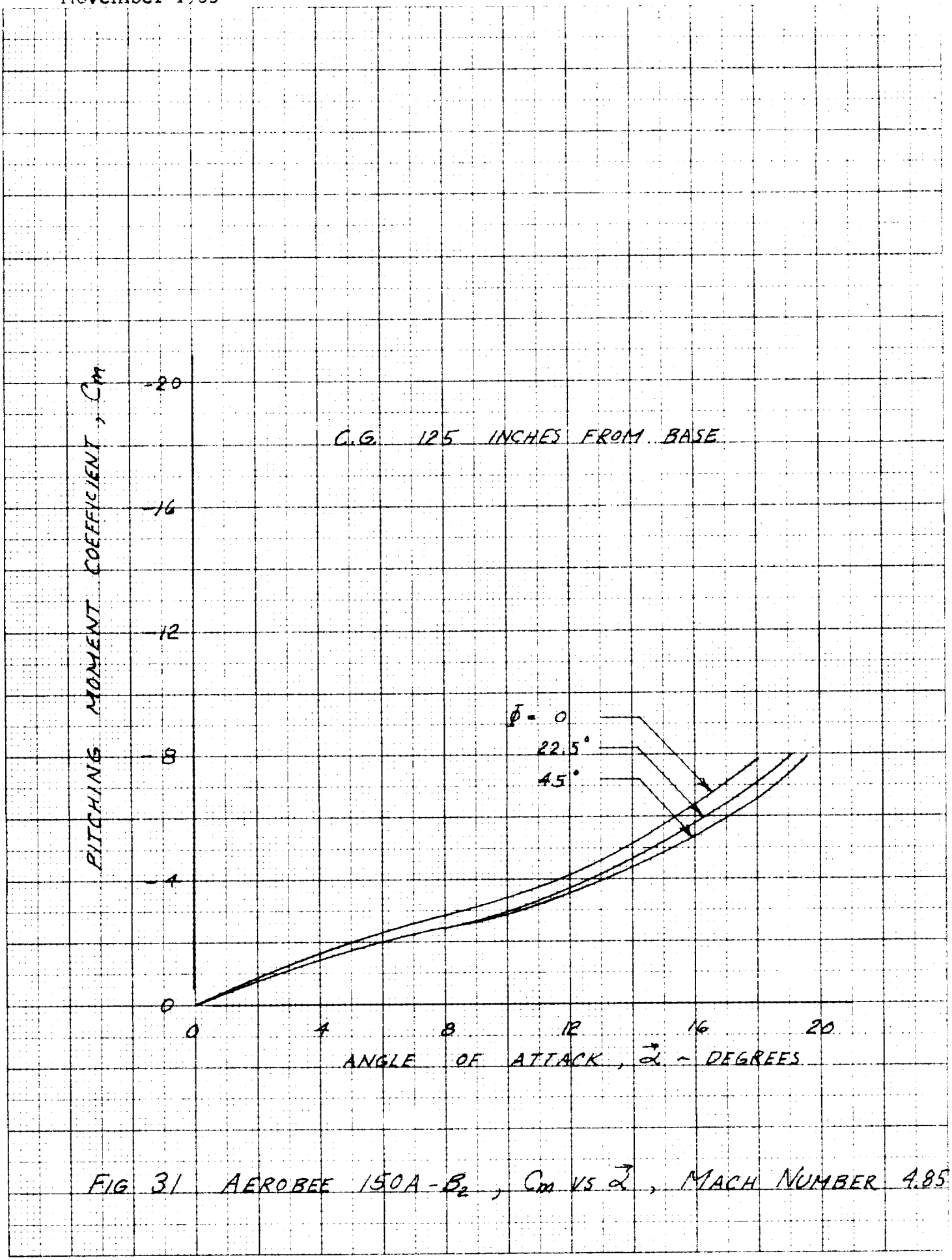

FIG 31 AEROBEE 150A-B_2, C_m VS $\vec{\alpha}$, MACH NUMBER 4.85

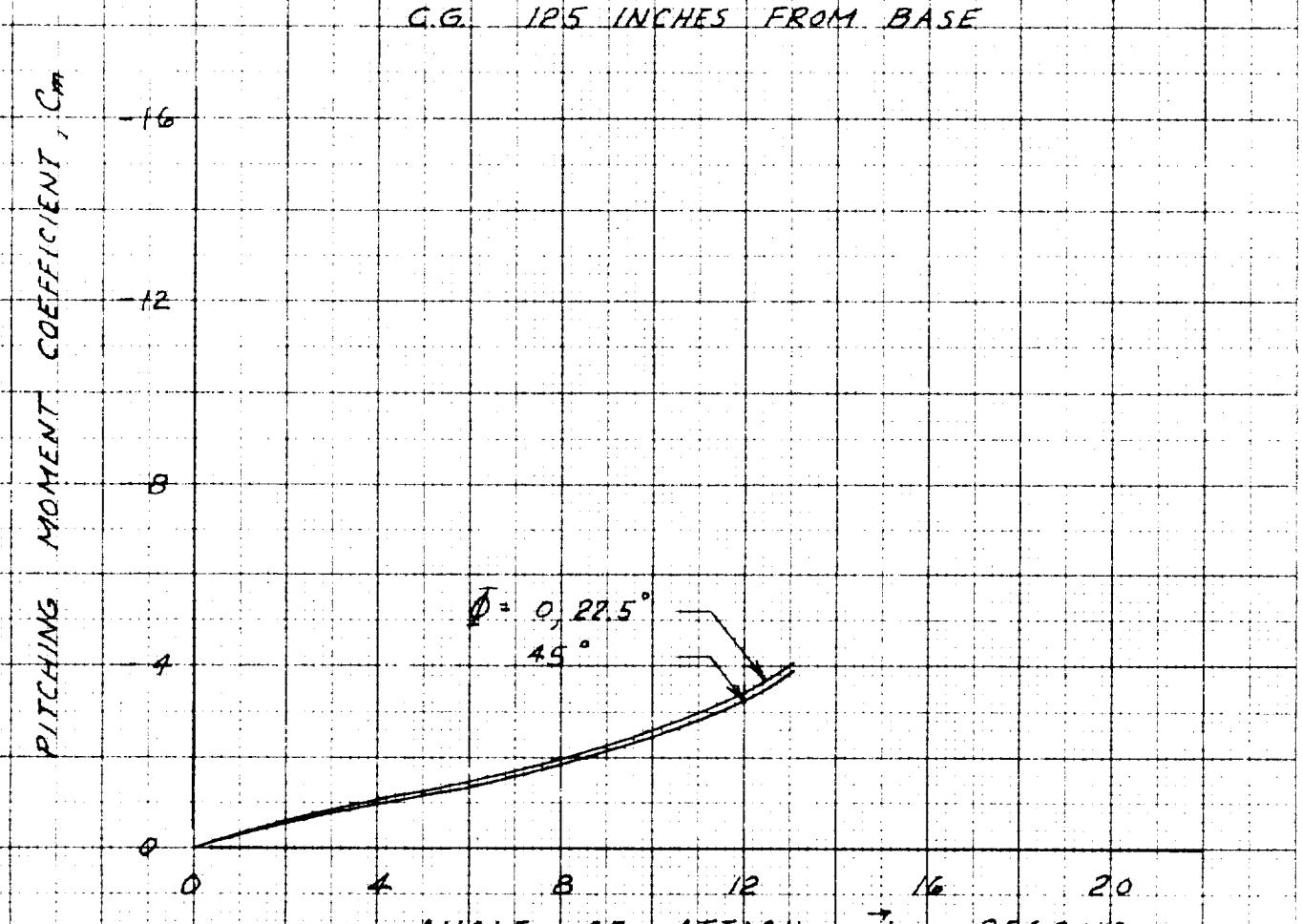

FIG 32 AEROBEE 150A - B_2, C_m VS $\vec{\alpha}$, MACH NUMBER 6.80

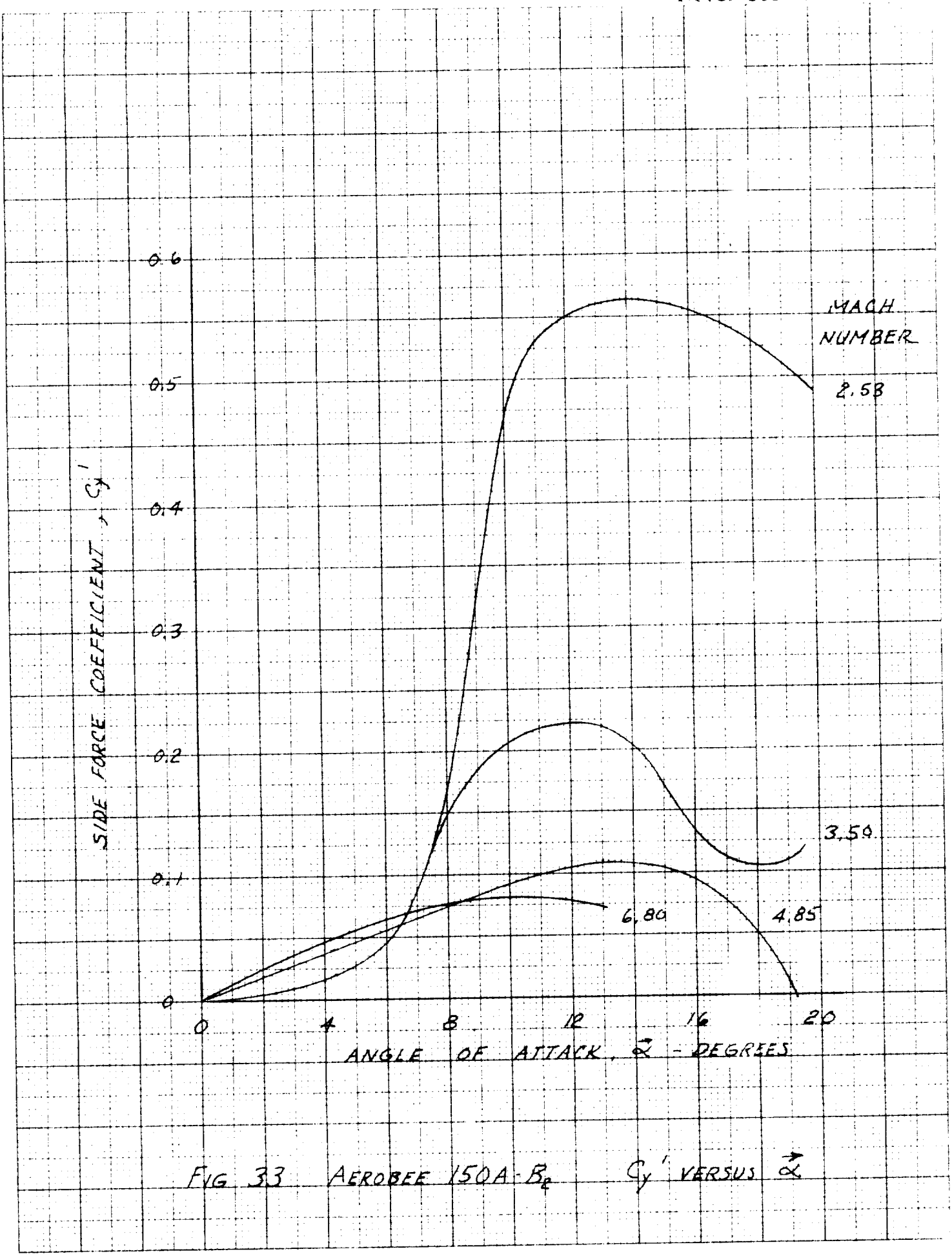

FIG 33 AEROBEE 150A - B_2 $C_{y'}$ VERSUS $\vec{\alpha}$

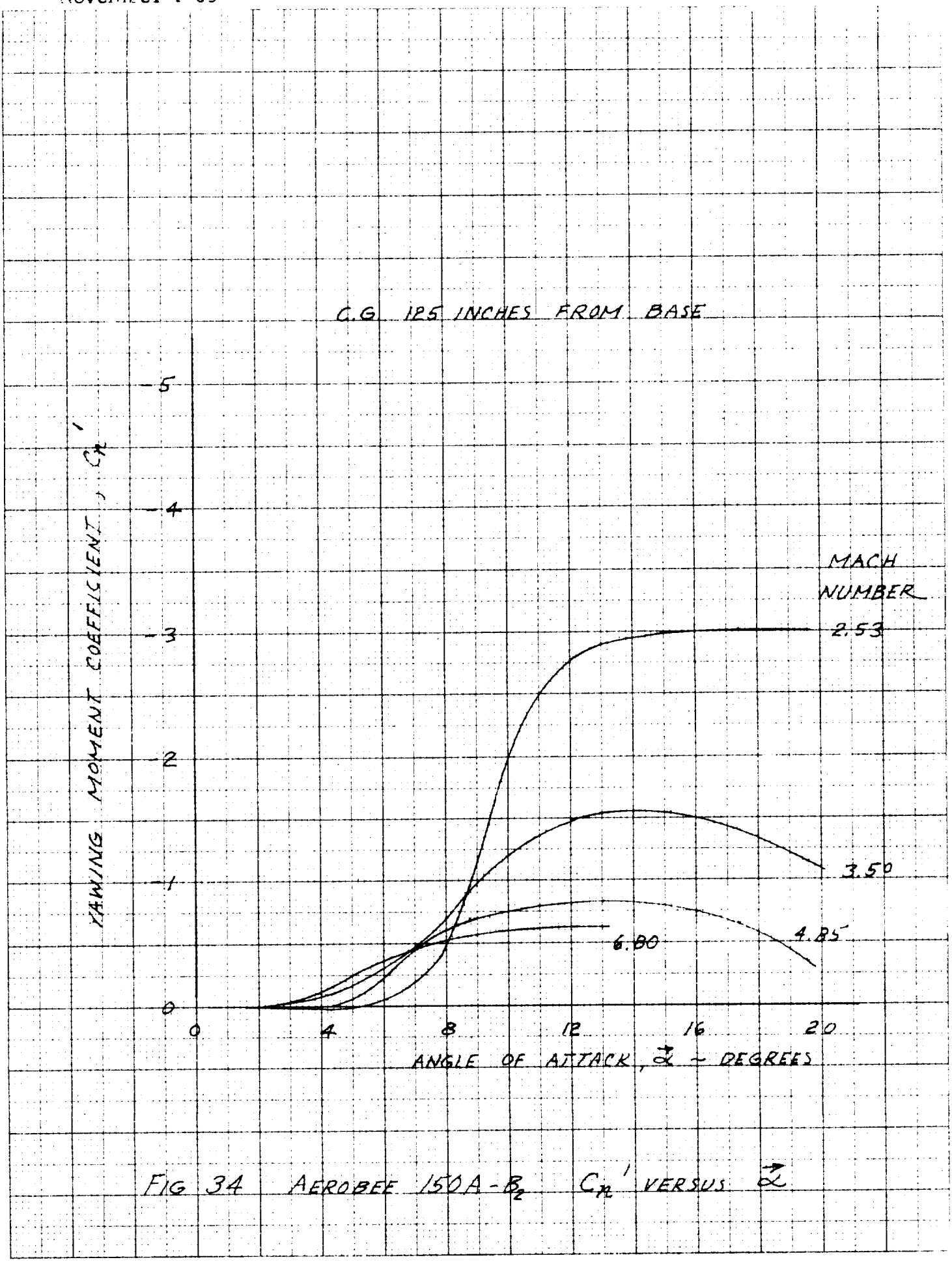

FIG 34 AEROBEE 150A-B_2 $C_{n'}$ VERSUS α

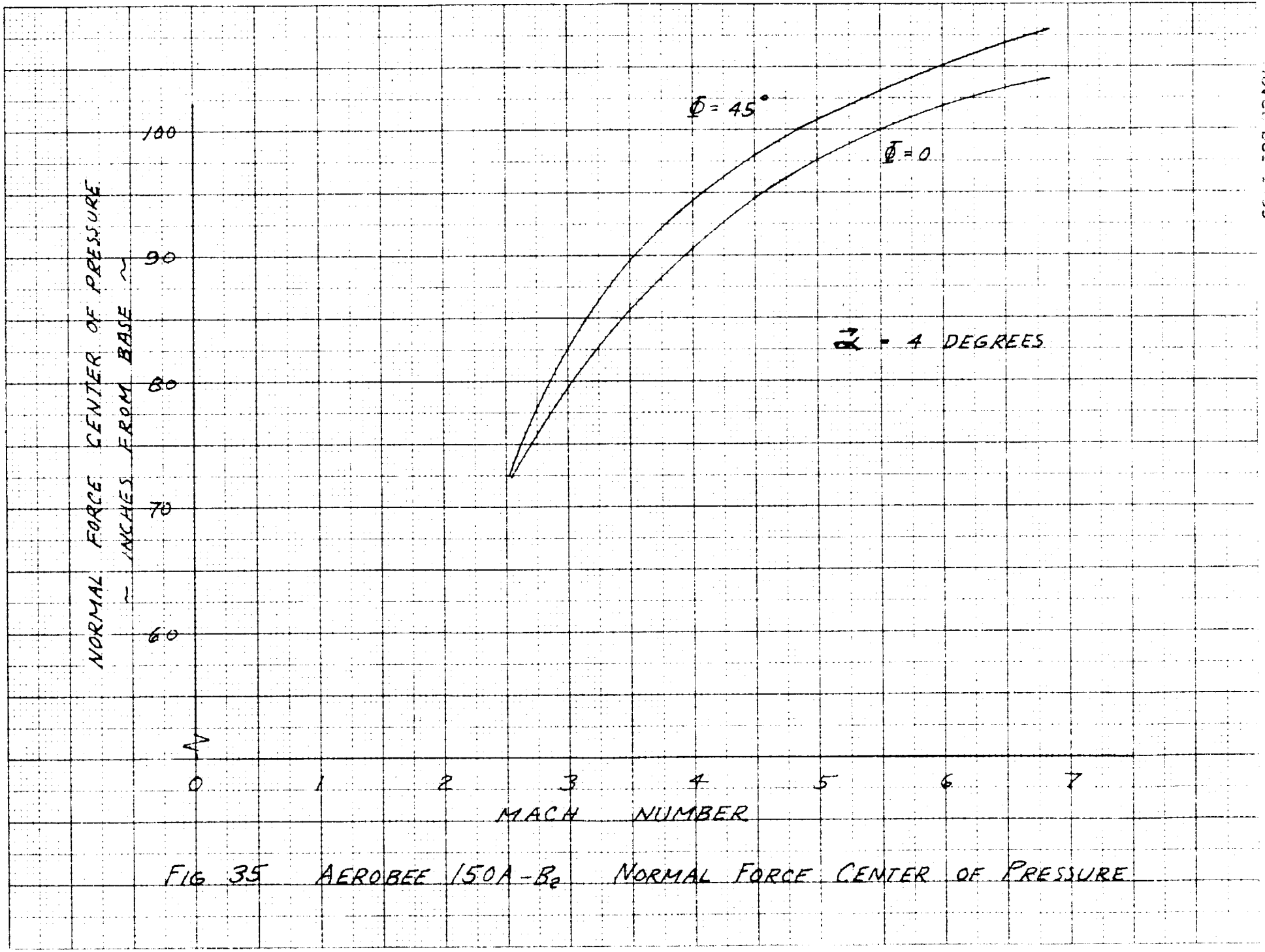

FIG 35 AEROBEE 150A-B_2 NORMAL FORCE CENTER OF PRESSURE

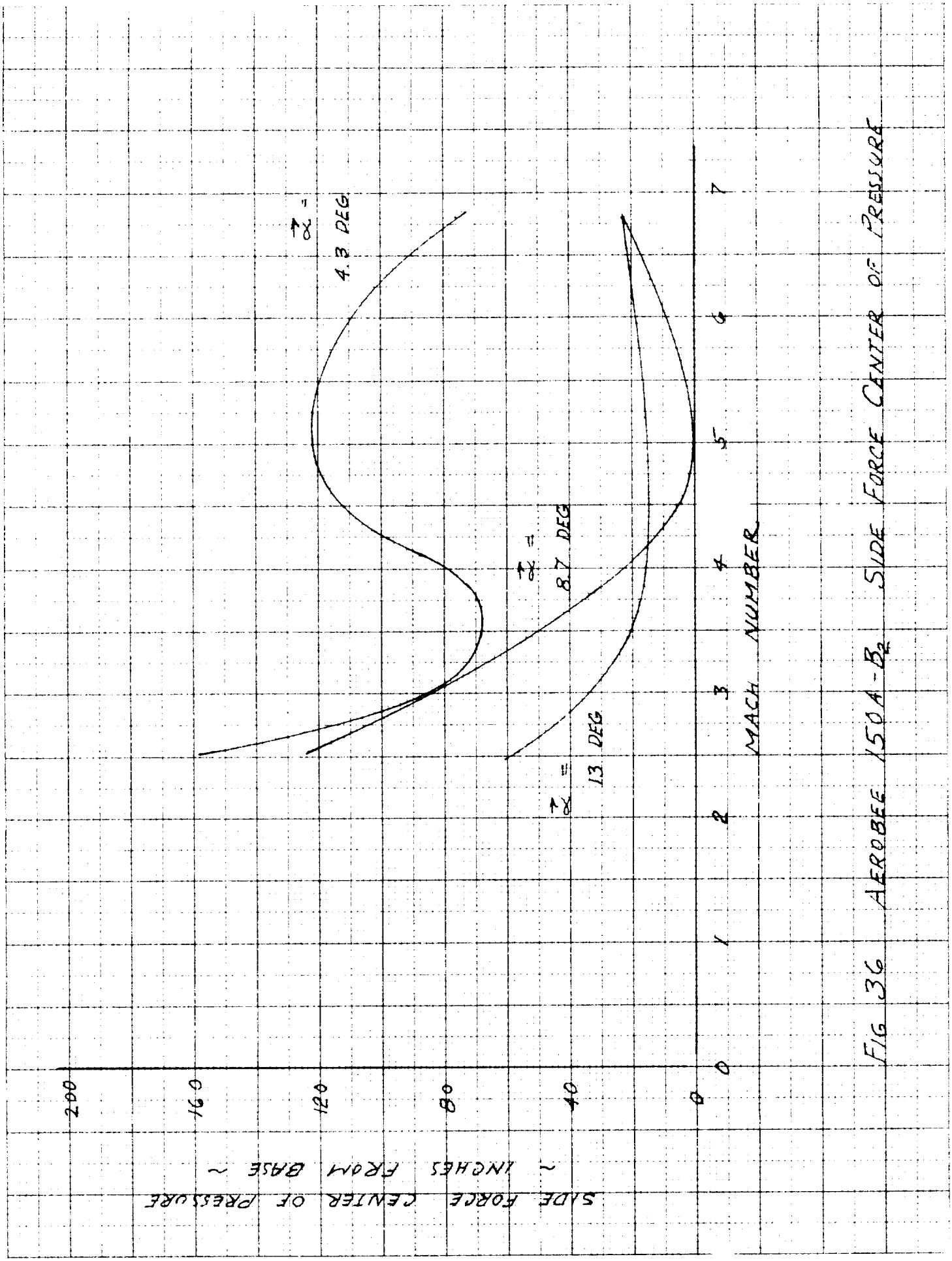

FIG 36 AEROBEE 150A - B_2 SIDE FORCE CENTER OF PRESSURE

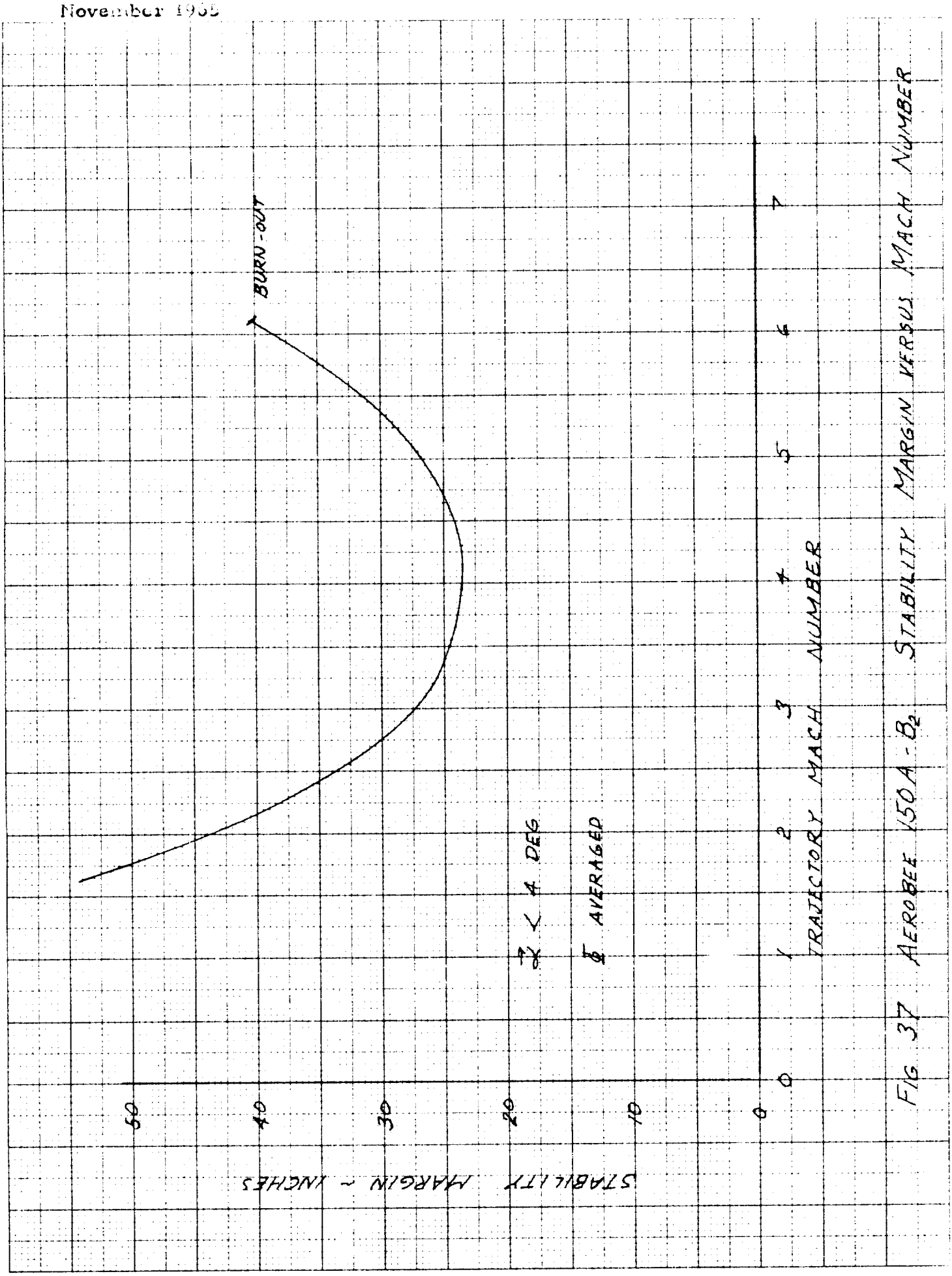

FIG 37 AEROBEE 150A - B_2 STABILITY MARGIN VERSUS MACH NUMBER

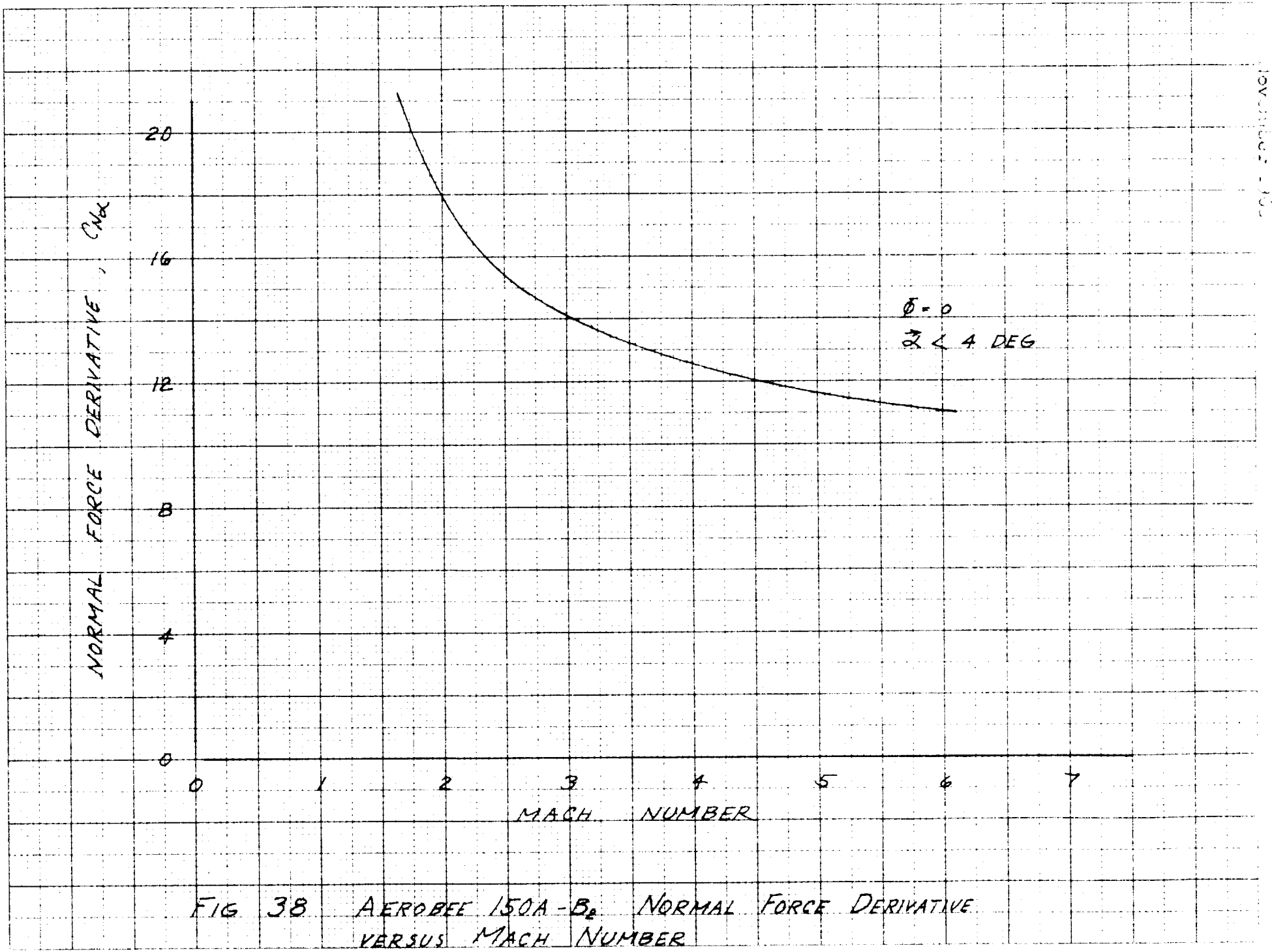

FIG 38 AEROBEE 150A - B_2 NORMAL FORCE DERIVATIVE VERSUS MACH NUMBER

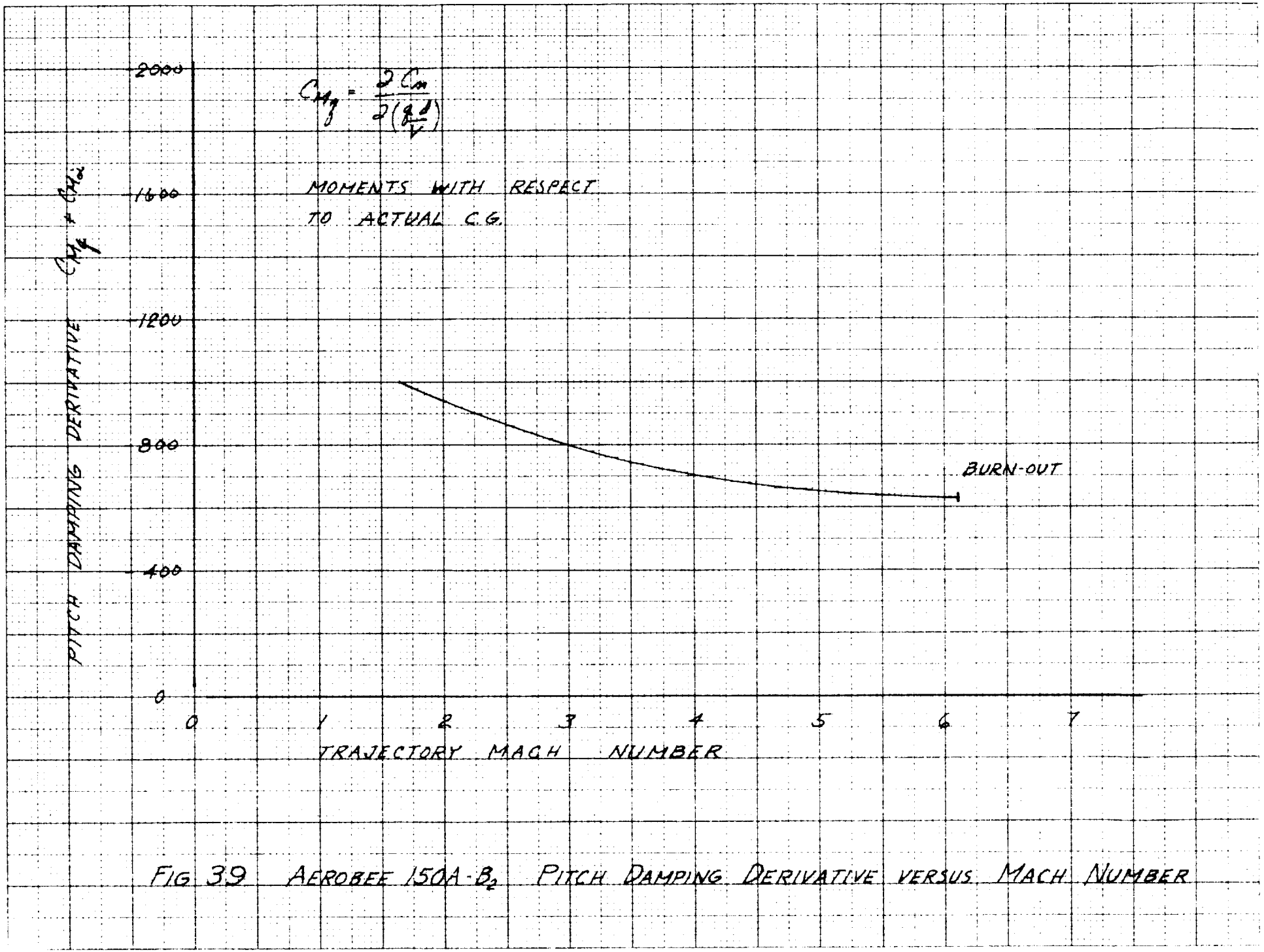

FIG 39 AEROBEE 150A-B_2 PITCH DAMPING DERIVATIVE VERSUS MACH NUMBER

Report 55-7555-7
November 1955

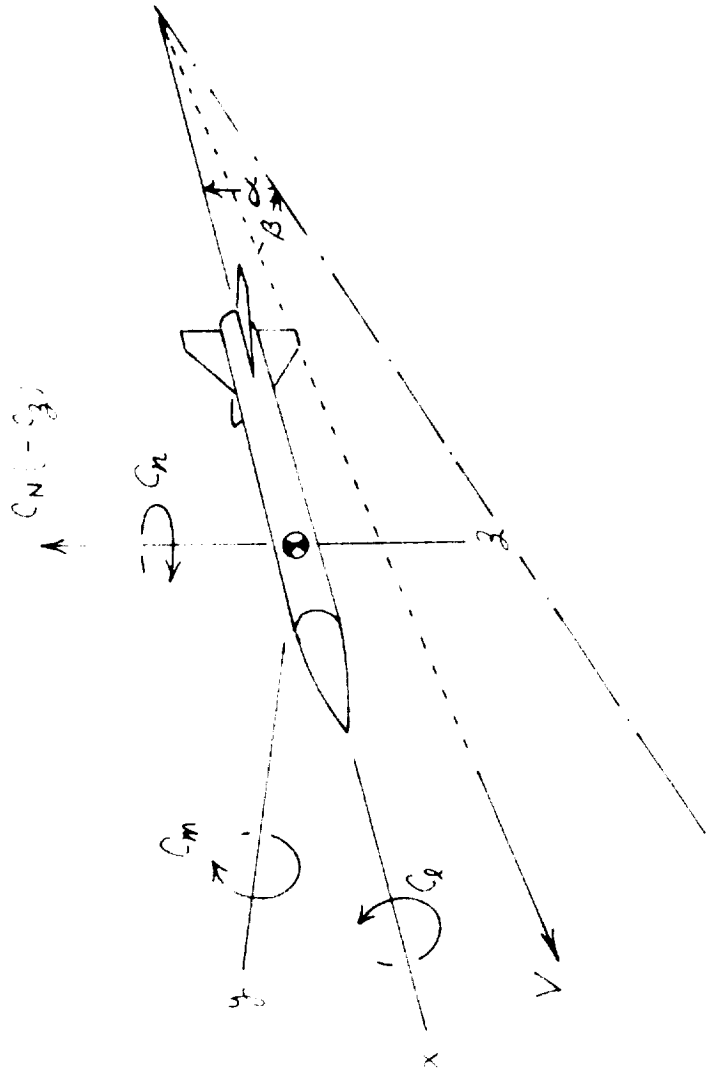

FIG 40 BODY AXES SHOWING DIRECTION AND SENSE OF FORCES AND MOMENTS

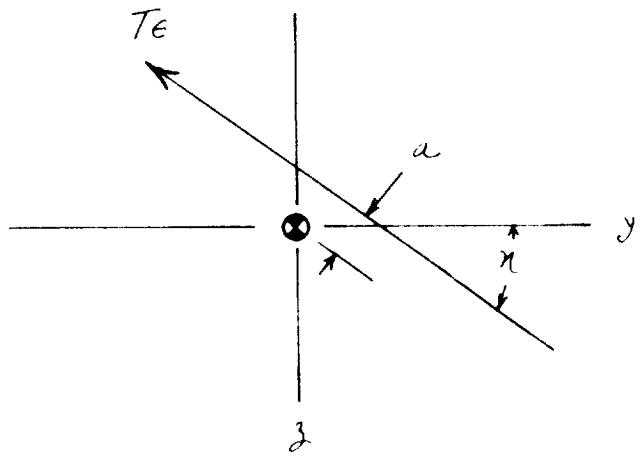

a) THRUST ASYMMETRY

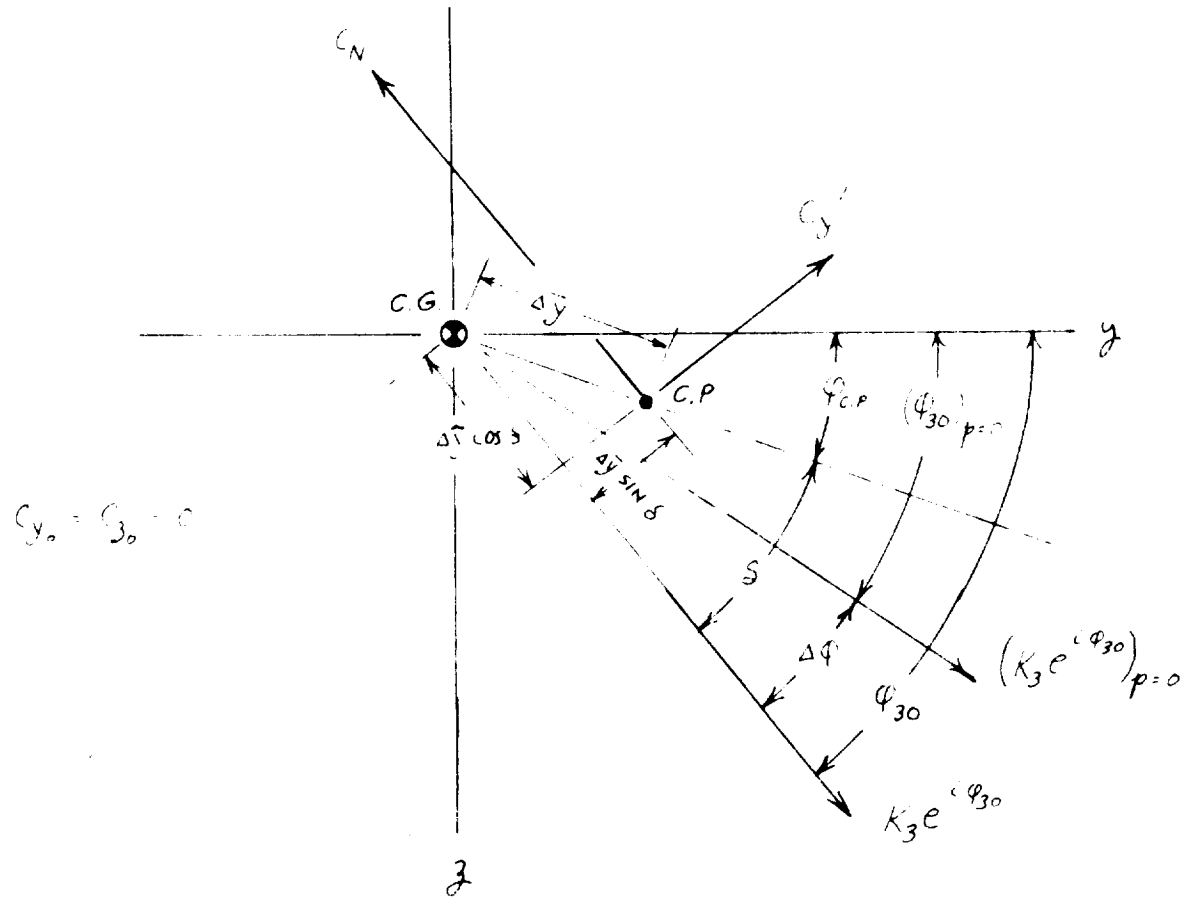

b) AERODYNAMIC ASYMMETRY

FIG 41 NOMENCLATURE FOR ROLLING MOMENTS DUE TO LATERAL ASYMMETRY

X Y Z INERTIAL AXES

x y z FIXED PLANE AXES

BODY-FIXED AXES

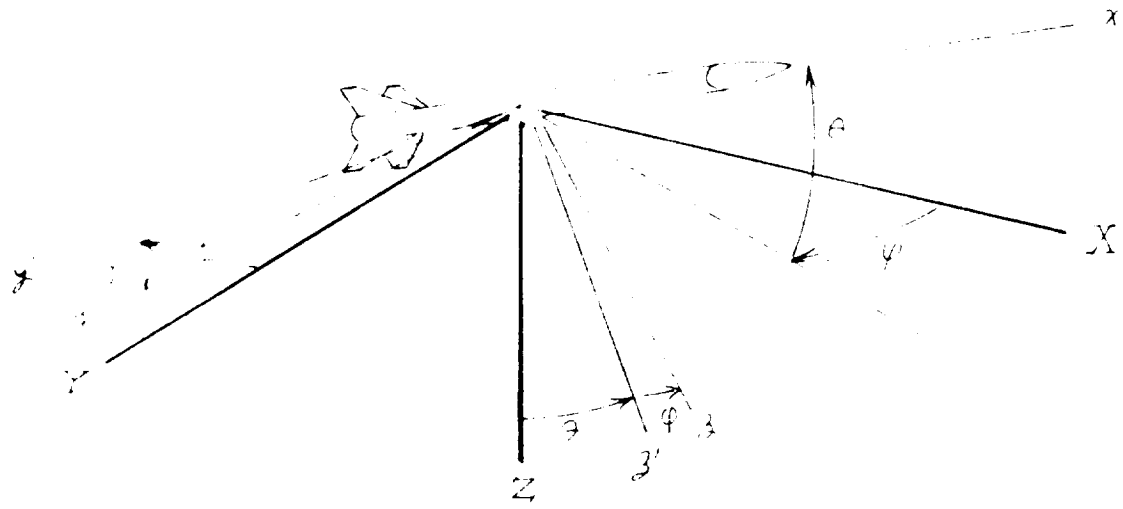

FIG 42 INERTIAL AND FIXED-PLANE AXES

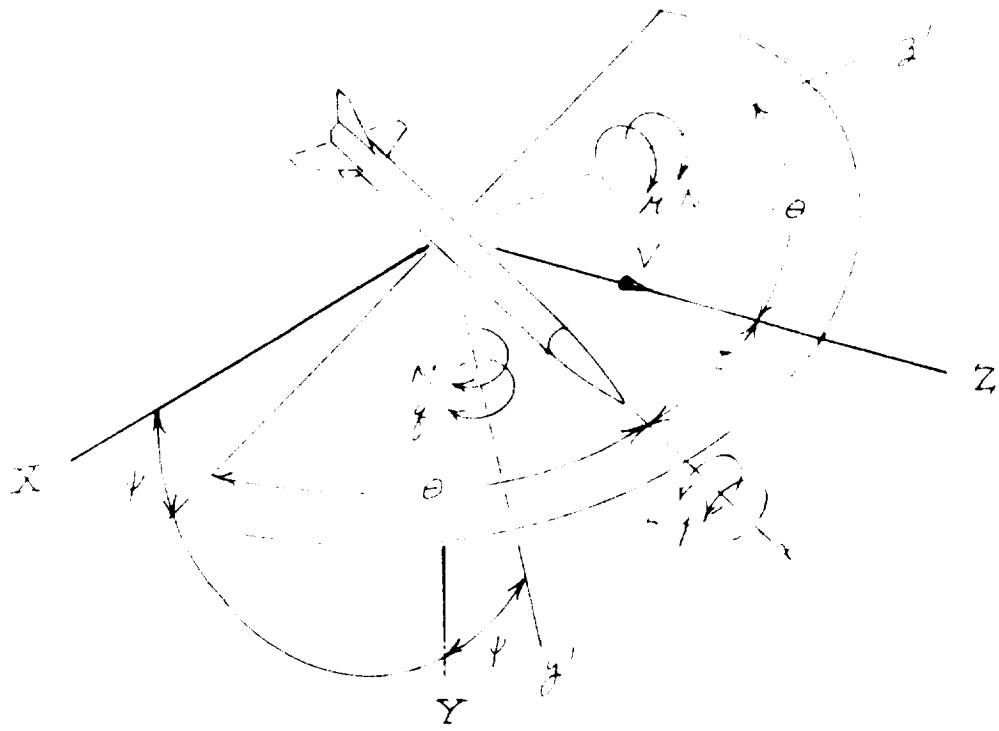

FIG 43 COORDINATE AXES WITH RESPECT TO THE VELOCITY VECTOR

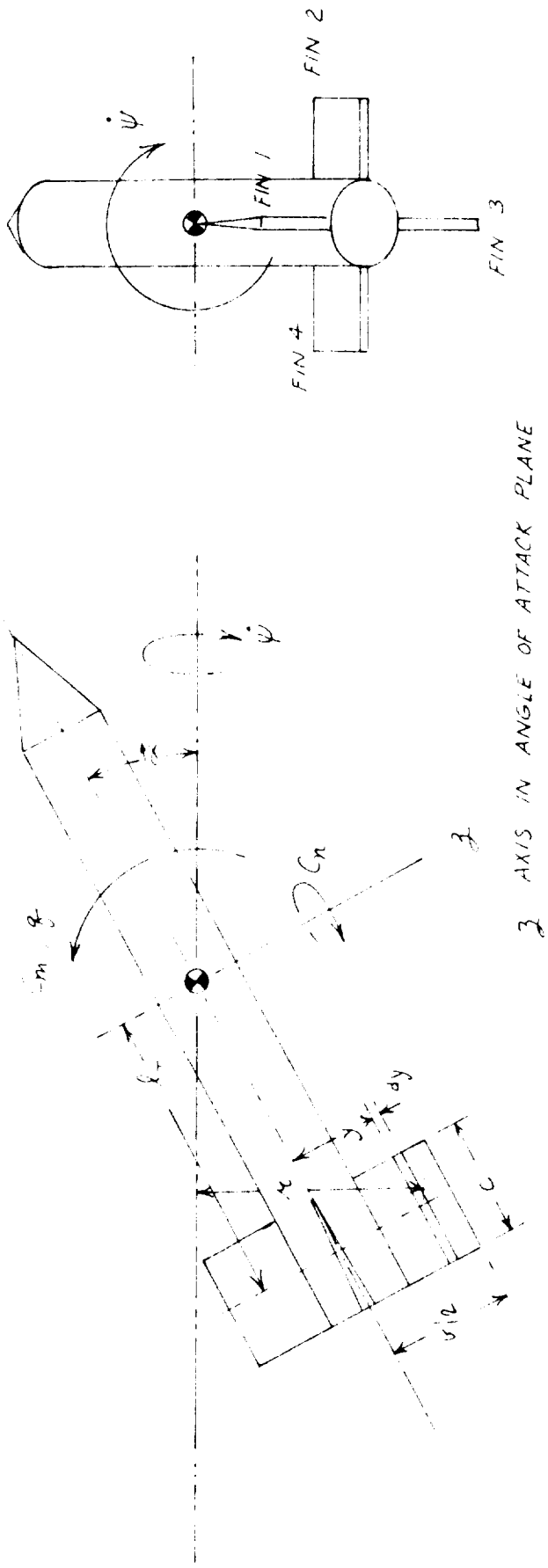

FIG 44 NOMENCLATURE FOR FINNED ROCKET IN CIRCULAR MOTION

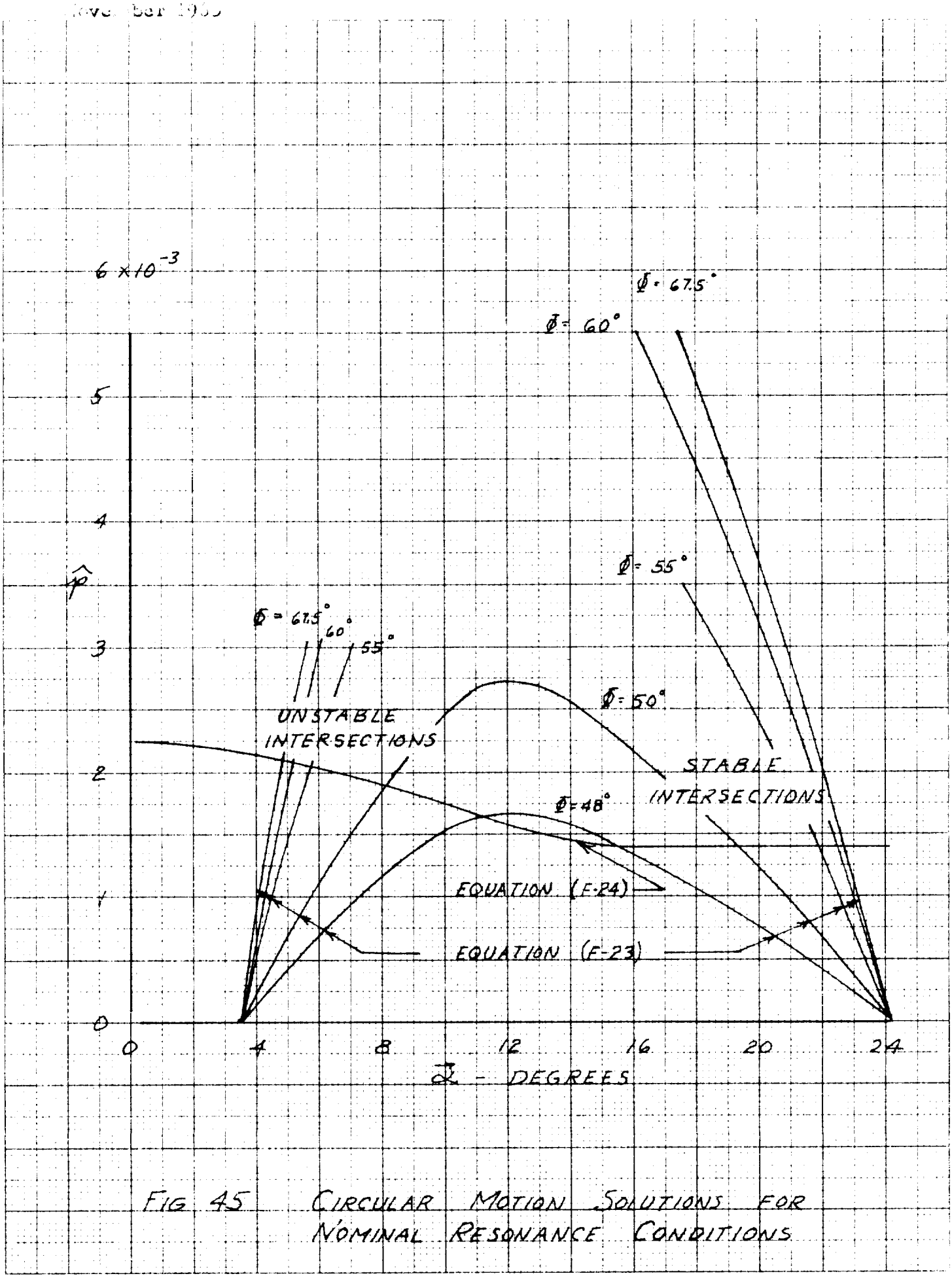

FIG 45 CIRCULAR MOTION SOLUTIONS FOR NOMINAL RESONANCE CONDITIONS